Prediction and Measurement of Power Line Carrier Signal Attenuation and Fluctuation.

Wernich de Villiers

7 November 2001

Supervisor: Professor J.H. Cloete
Co-supervisor: Professor R. Herman

(Thesis presented in partial fulfilment of the requirements for the degree of Master of Engineering at the University of Stellenbosch)

Declaration

I, the undersigned, hereby declare that the work contained in this thesis is my own work and has not previously in its entirety or in part been submitted at any university for a degree.

W de Villiers

Summary

A frequency domain Power Line Carrier (PLC) simulation program, with the ability to simulate signal attenuation including the coupling equipment, was developed. This simulation program was put to the test against the independent program of Professor L.M. Wedepohl and against practical field measurements. The predictions of the two programs were in precise agreement for a wide range of input parameters. Results from the field tests and predictions also showed close agreement.

Further investigations, applying the simulation program, explained how ground conductors and soil resistivity influences PLC signal propagation.

An experiment, which was developed to monitor PLC signal attenuation, was installed on the PLC system between Koeberg power station and Acacia sub-station, both near Cape Town. Data logged continuously over 28 days, indicated measurable and deterministic PLC signal attenuation variations with typical time constants of a few hours. Simulations of the PLC system indicated that the signal amplitude variations were influenced by changes in the height above the ground plane of the phase conductor.

This significant finding creates the possibility to obtain real time knowledge of the sag of an Over Head Transmission Line (OHTL) by exploiting an operational PLC system. The knowledge about real time sag can be used in economical dynamic ampacity control systems. The practical and financial benefits to the electricity supply and distribution industry can be significant.

Opsomming

'n Frekwensie gebied "Power Line Carrier" (PLC) simulasie program wat die sein verswakking en die koppeling verliese kan naboots, is ontwikkel. Die program is getoets teen die onafhanklike program van Professor L.M. Wedepohl asook praktiese metings in die veld. Die vooruitskatings van beide programme is presies die selfde vir 'n wye reeks van parameters. Metings en nabootsings het ook noue ooreenstemming getoon.

Verdere ondersoek, m. b. v. die program, is gedoen ten einde te verduidelik hoe grond-geleiers en grond weerstand die PLC sein se voortplanting beïnvloed.

'n Eksperiment om die PLC sein se verswakking mee te monitor is ontwerp. Die eksperiment was geïnstalleer in die PLC stelsel tussen Koeberg kernkragstasie en Acacia substasie, naby Kaapstad. Die eksperiment was vir 28 dae geaktiveer en die data wat die eksperiment opgelewer het toon meetbare PLC sein verswakking met tyd konstantes van 'n paar uur. Verdere nabootsings het gewys dat die veranderende verswakking in die PLC seinsterkte toegeskryf kan word aan die wisseling in hoogte van die fase geleiers bo die grondvlak.

Hierdie bevinding is van besondere belang aangesien dit die moontlikheid oopmaak om die gemiddelde sak van kraglyne in reële tyd en onder bedryfs toestande te kan meet. Die informasie van die reële sak van kraglyne kan gebruik word in effektiewe stroomdrae-vermoë beheer stelsels. Die praktiese en finansiële voordele wat krag voorsieners en verspreiders hieruit kan put kan aansienlik wees.

Acknowledgements

Soli Deo Gloria

I wish to thank my supervisor, Prof JH Cloete, for his guidance and ever-present optimism as well as Prof R Herman for his assistance and support.

A special word of thanks to Prof LM Wedepohl for his deep insight, advice and continuous involvement.

I would like to thank Eskom and particularly Mr Dave Smith and his team working on PLC systems for their kindness, assistance and advice. Especially Riaan Carstens and Drikus de Wet for the help with the field measurements.

Furthermore I would also like to thank the following people for their support and help.

From University of Stellenbosch:

-Prof HC Reader
-R Urban
-J Greyling

From Eskom:

-Rob Stephen
-Tony Britten
-Graeme Fick
-Mike Korber
-Louis du Plessis
-Frans Venter
-Piet Lubbe
-Roy Hubbard

Special thanks to my family (especially to my Father and Mother), friends and my stunning fiancée, Esre' Meyer, for their continuous love and care.

Table of contents

List of Figures

List of photographs

Chapter 1

Introduction

1.1 Origin of the study

Dynamic ampacity control models were investigated as part of W de Villiers' undergraduate project in 1999 [1]. From that project it was concluded that the real time average height of the phase conductors, which relates to the conductor tension, on an Over Head Transmission Line (OHTL) is the most important parameter in the realization of effective ampacity control.

The idea to estimate the average phase conductor height via an operational Power Line Carrier (PLC) system was proposed by Professor JH Cloete and W de Villiers at Stellenbosch University (SU) in 1999. This concept was investigated in the undergraduate project and it was concluded that further investigations should be done to evaluate its feasibility.

This thesis continues the investigation initiated in the undergraduate project.

1.2 Provisional Patent

A provisional patent in the name of Stellenbosch University (W de Villiers and Professor JH Cloete as the inventors) was taken out (2001) to protect the intellectual property of this work (Appendix A).

1.3 The goals this study aims at

There are two goals for this study.

PLC signal propagation characteristics are dependent on the physical parameters of the transmission line. From [1] it can be learnt that the average height of a transmission line affects the signal attenuation. The sensitivity of this concept has to be investigated on different line designs. The first goal of the study is therefore to develop a comprehensive simulation program to simulate PLC signal attenuation for different conditions. Simulation programs of this nature exist. The purpose in developing this program was to evaluate the assumptions made and to fully understand the theory on which PLC systems function. As part of the accuracy evaluation the simulations were compared to measured end-to-end PLC signal attenuation on an operational OHTL.

The second goal was to design and install an experiment on an operational PLC system in order to observe attenuation variation on a PLC system over a period of time. The attenuation variation of the PLC signals can then be correlated against ambient temperature, wind speed and phase currents which all influences the sag.

1.4 History of the process to identify a practically viable transmission line for the study.

Simulations were initially done on the Droërivier – Muldersvlei and the Bacchus – Proteus 400 kV transmission lines in the Western Cape province. The purpose was to

test the feasibility of doing the experiment on these transmission lines. The additional attenuation introduced by the experiment was calculated on the request of Eskom.

The results of the simulations and calculations were summarized in a report for Eskom. Senior engineers in Eskom (Mr. Dave Smith and Mr. Tony Britten) had several meetings with the author (W de Villiers) about the feasibility of an experiment on the mentioned transmission lines. It was concluded that the loadings of the transmission lines must be included in the evaluation process. It was discovered that the transmission lines, Droërivier – Muldersvlei and Bacchus – Proteus, were operated at approximately only 10% of the maximum design capacity throughout the year.

With Eskom's new criterion, the loading of a transmission line, a visit was paid to national control of Eskom in Simmerpan (Johannesburg) to study the different loadings of transmission lines. An engineer at National control (Mr. L du Plessis) made the loading information of the 400 kV transmission line in the Western Cape region available. From this information it was clear that the 400 kV transmission line between Koeberg power station and Acacia sub-station was carrying the heaviest load, although it was only in the region of 50 - 60% under normal conditions.

This 400 kV OHTL is located relatively close to Stellenbosch, which is convenient.

It was therefore decided to focus the study on the Koeberg - Acacia 400 kV transmission line.

1.5 Layout of the thesis

The Koeberg – Acacia PLC system is described in Chapter 2. The PLC system is comprised primarily of five components namely: OHTL, Coupling Capacitor (CC), Line Trap (LT), Line Matching Equipment (LME), and carrier.

The theory used in the simulation program developed by the author is based on Professor L.M. Wedepohl's work [2] and is described in Chapter 3. The simulation program is Matlab based and simulates the PLC line attenuation from end to end including the losses introduced by the coupling equipment (LT, CC and LMU). The simulation program was tested against Professor Wedepohl's program in Chapter 4 and close agreement was obtained. Simulations for different phase conductor heights and soil resistivity are shown and described.

The simulation program has been expanded (as described in the first part of Chapter 5) to incorporate the resonance effect due to discretely bonded ground conductors.

The first simulations on the Koeberg - Acacia 400 kV transmission system were done assuming steel ground conductors. This was done due to lack of detailed information at the time. When the detailed information was received it was learned that on the Koeberg Acacia line Eskom uses aluminum ground conductors (high corrosion of steel ground conductors at the coast) in the place of the generally used steel ground conductors (inland). The simulations of the PLC signal attenuation for an OHTL with aluminum ground conductors show a noticeable difference compared to an OHTL with steel ground conductors. The magnitude of the difference in the results was unexpected.

The second part in Chapter 5 is focused on explaining the abovementioned phenomenon. The influence due to the variation in soil resitivity on PLC signal attenuation is simulated. Soil resistivity is difficult to measure accurately and is subject to seasonal changes due to e.g. rain.

Chapter 6 describes the design of the experiment. The purpose of this experiment was to incorporate a single outer phase coupling on an operational PLC system and to log the attenuation of that signal over a long period of time.

Field measurements and logged data (via the experiment) are shown and discussed in Chapter 7. The history of the field measurements is also discussed. Initial measurements (Appendix B) indicated faulty PLC equipment and some of the operational PLC components were replaced during the course of the study.

The findings and conclusions are in the Chapter 8 and recommendations are made for further research.

1.6 References:

[1] **W de Villiers**, An investigation into overhead feeder ampacity control, Final year project at University of Stellenbosch, 5 November 1999.
[2] **L.M. Wedepohl**, The Theory of Natural Modes in Multi-Conductor Transmission Systems, unpublished lecture notes, Westband, British Columbia, Canada, 10 January 1999.

Chapter 2

PLC background and description of the operational PLC system between Koeberg power station and Acacia sub-station

2.1 Introduction

In this Chapter the key functions of the different components of a Power Line Carrier (PLC) system will briefly be described. The technical descriptions of the operational PLC communications system between Koeberg power station and Acacia sub-station (Koeberg - Acacia) will also be described.

Figure 2.1 demonstrates the basic layout of a PLC system. A PLC link operates by transmitting signals in the frequency range 50 – 500 kHz over a high voltage line, while the line is carrying the normal 50 Hz current. The PLC signal is not dependent on the 50 Hz current, therefore the PLC system remains operational even if the line is out of commission providing there are no working earths on the line. Through the use of the coupling equipment the PLC signal can be injected and retrieved from the OHTL. PLC transmission constitutes the basic system of communication of many power supply companies. It is typically used for transmitting data, speech and protection.

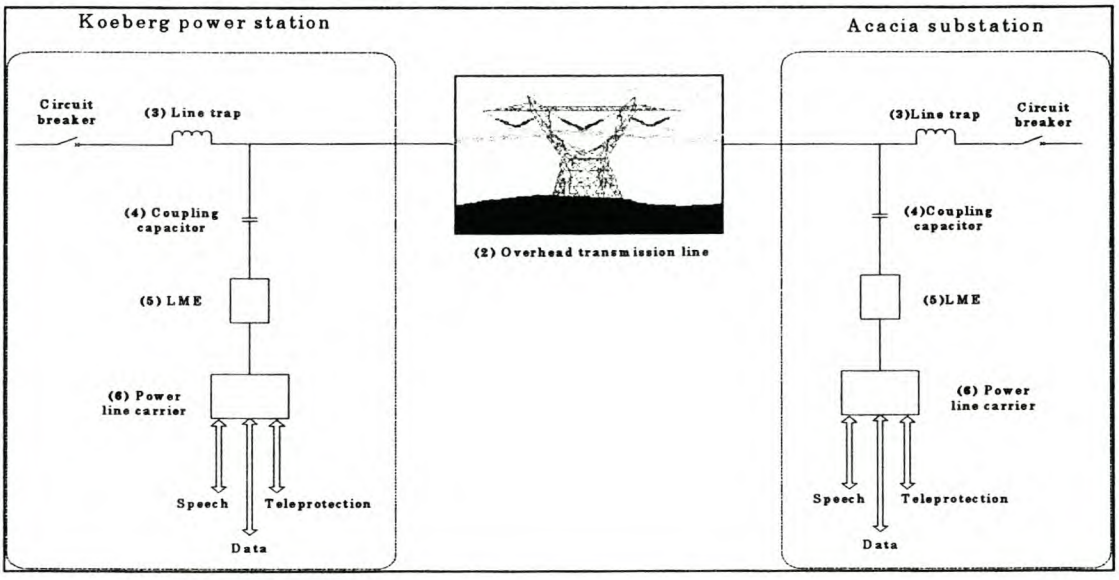

Figure 2.1 PLC system layout (only one phase is shown)

A PLC system consists primarily of five components: transmission line, line trap, coupling capacitor, line matching equipment (LME) and the carrier (a transceiver). In Figure 2.1 a diagram shows one phase of the Koeberg - Acacia PLC system. The five key components are numbered in the diagram (2-6) and are described in the following sections. Each description of the PLC system component is accompanied with the real

values of the Koeberg - Acacia PLC system. In Section 7 the term "coupling configuration" is explained and the coupling configuration is given for Koeberg - Acacia PLC system.

The information that describes the Koeberg - Acacia PLC system was collected from various departments in ESKOM. Some information was retrieved from references [1,2] for the descriptions of the different components.

2.2 The transmission line

2.2.1 The key functions of the physical transmission line in a PLC system.

The transmission line acts like a wave-guide for PLC signals. This can be seen as part of the transmission path where the PLC signals are guided in their propagation. The physical dimensions of the line are thus crucial because they influence the propagation properties of the coupled signal.

In the case of a transmission line there are numerous fixed and also varying parameters. In order to make conclusions on some variable parameters like the average height of the transmission line it is of great importance to understand and describe all the fixed parameters as accurately as possible. In the following section the known fixed parameters of the line will be described.

2.2.2 Description of the Koeberg- Acacia transmission line.

The voltage rating of the line is 400 kV and it is 31.318 km long. A twin "dinosaur" conductor is used. The conductor is classified as Aluminium Conductor Steel Reinforced (ACSR). The main function of the steel in the conductor is to mechanically support the aluminium conductor thus providing tensile strength.

The "Dinosaur" conductor has an overall diameter of 3.556 cm. The conductor comprises 31 strands (24 aluminium strands and 7 steel strands). The diameter of the aluminium strands is 3.95 mm.

The ground conductors of a transmission line are typically made of steel and are generally referred to as the earth wires. Because we are studying a transmission line located in the Western Cape the earth wire is also an ACSR type conductor. Steel conductors rust severely in the harsh environment of the Cape. A "Tiger" type of conductor is used and has the following dimensions: 1.652 cm overall diameter, 18 outer aluminium strands of 2.36 mm diameter.

The average attachment height of a phase conductor is 19.6 m and 25.15 m of an earth conductor. The bundle conductors are separated by 9 m. The earth wires are 8.3 m from the centre of the tower. The two conductors in a bundle conductor are 380 mm apart from each other. These relative dimensions are summarized in Figure 2.2.

The planned average distance between two adjacent towers is 336.7 m. The physical path looking from a distance above the transmission line is shown in Figure 2.3.

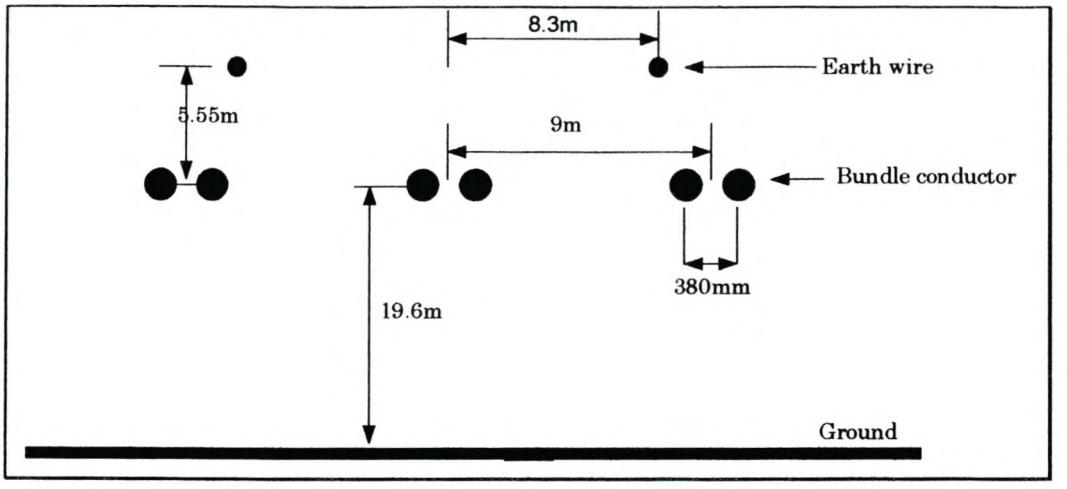

Figure 2.2 Relative dimensions between the phase conductors, ground conductors and the ground plane.

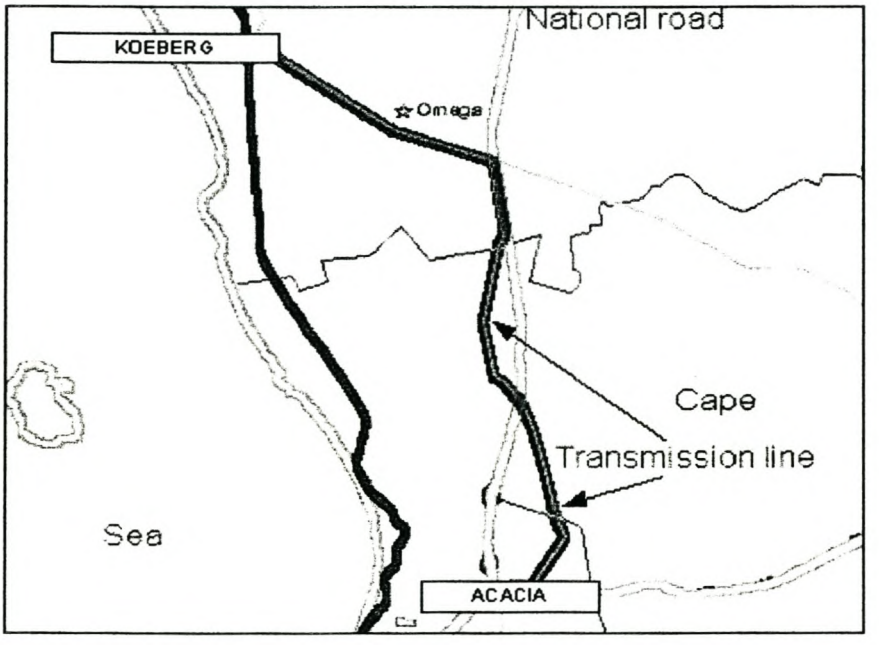

Figure 2.3 Koeberg – Acacia transmission line

Figure 2.4 shows the tower heights above the mean sea level. The towers are numbered from Koeberg power station (tower 1) to Acacia sub-station (tower 94).

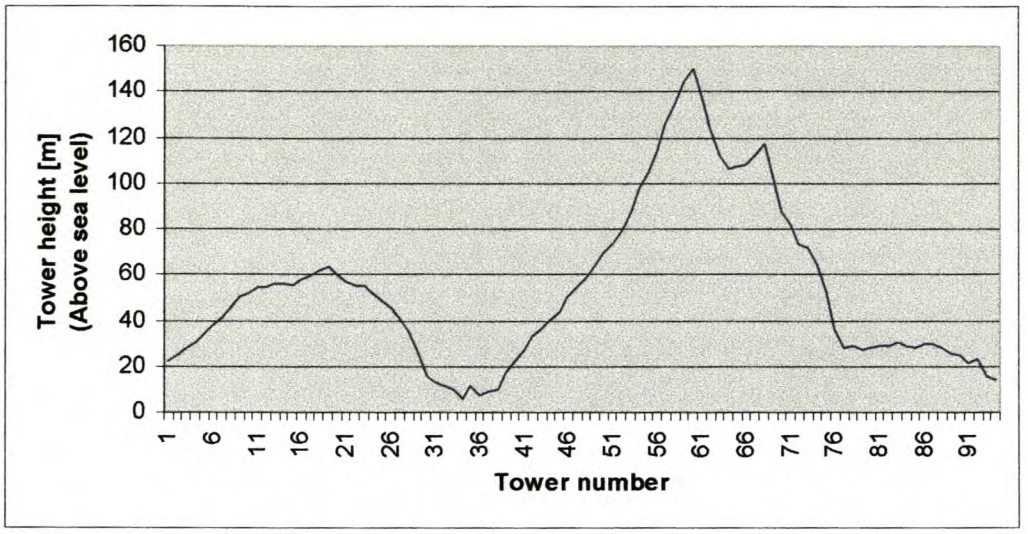

Figure 2.4 Average tower heights above mean sea level

A histogram of the tower spacing, Figure 2.5, indicates that 30 samples of tower spacing is between 330m and 365m.

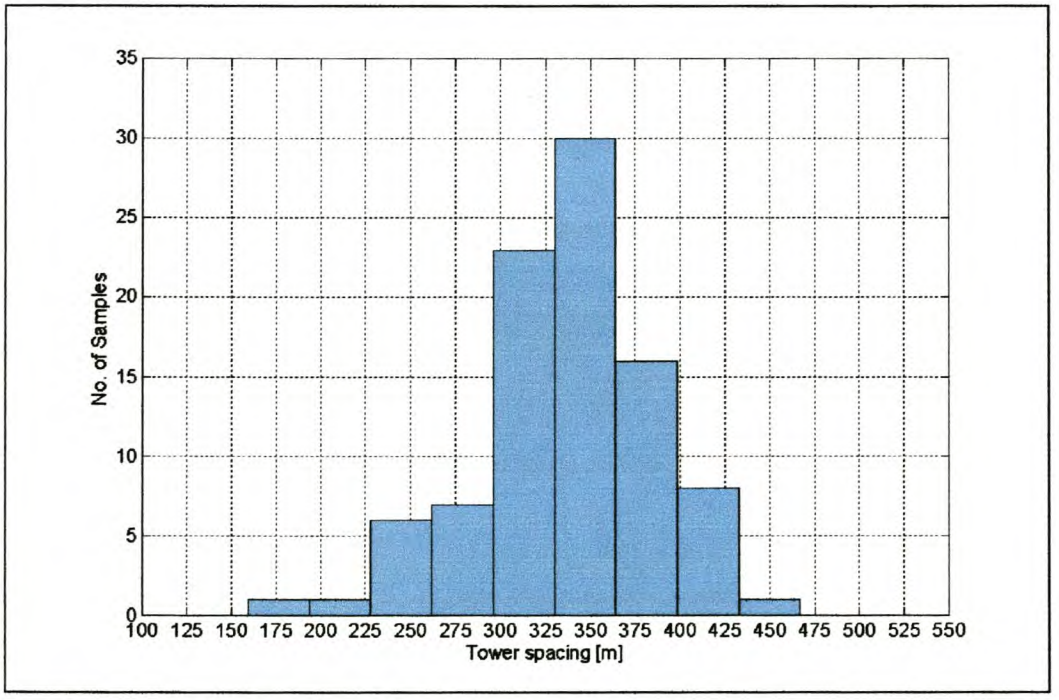

Figure 2.5 Histogram of the tower spacing of the Koeberg-Acacia OHTL.

2.3 The line trap

2.3.1 The main functions of the line trap in the PLC system.

Figure 2.1 shows that there is a line trap at each station. Approaching the station from the OHTL the PLC coupling capacitor junction will first be connected and then the line

trap. The core function of the line trap is to "direct" the PLC signal energy to the OHTL and not to the station itself. In other words for the PLC frequency range, 50 – 500 kHz, the line trap acts like an high impedance and for power frequencies it acts like a low impedance. In Figure 2.6 a model of a typical wide band trap is shown.

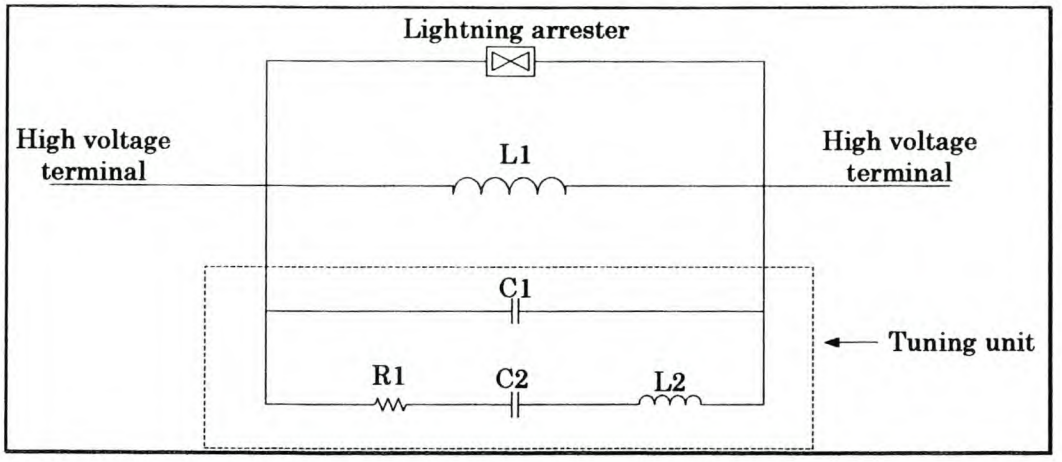

Figure 2.6 Model of a band tuned line trap

The most important function of the lightning arrestor is to protect the tuning unit against high level, rapid rate of rise, surges. The main inductor L1 (Figure 2.6) is the most important component in the line trap. It must be rated to carry full line current and one-second fault currents. Due to these ratings the inductor is physically a very big device. The tuning unit must ensure high impedance over the PLC bandwidth, keeping in mind that the impedance of the station can vary. Generally the impedance of the sub-station is capacitive. If the tuning unit is taken out there is always a chance that the capacitance of the station could equal the inductance of the line trap, thus creating a short circuit for PLC signals. In Chapter 7 measurements of the sudden variations in the PLC signal attenuation indicated a faulty tuning unit.

The model (Figure 2.6) of the line trap will be incorporated in the simulation program (Chapter 3) and the equations describing the line trap will be given and discussed.

2.3.2 Description of the line traps used in the Koeberg-Acacia PLC system.

A band tuned line trap is used. "Heafely" manufactures these line traps and they are rated to withstand 2500 A continuously for 127.2s and asymmetrical peak current 2.55 times the fault current rating of 50 kA (1 sec). The main inductance of the line trap is 0.5 mH. The bandwidth of the line trap is 101-500 kHz. The type of tuning unit is classified as "BW-K" with a colour code of blue / white / green (blue = 101-500 kHz, white = 2500 A and 50 kA and green = 0.5 mH). The arrestor of the line trap is a zinc oxide type. Photograph 2.1 shows two photos of the line trap at Acacia sub-station. The left hand side photo shows the physical size of a line trap. The big round cylinder is the main inductor (L1 in Figure 2.6). The tuning unit and the arrestor are located inside the main inductor, it can be seen in the right hand side photo.

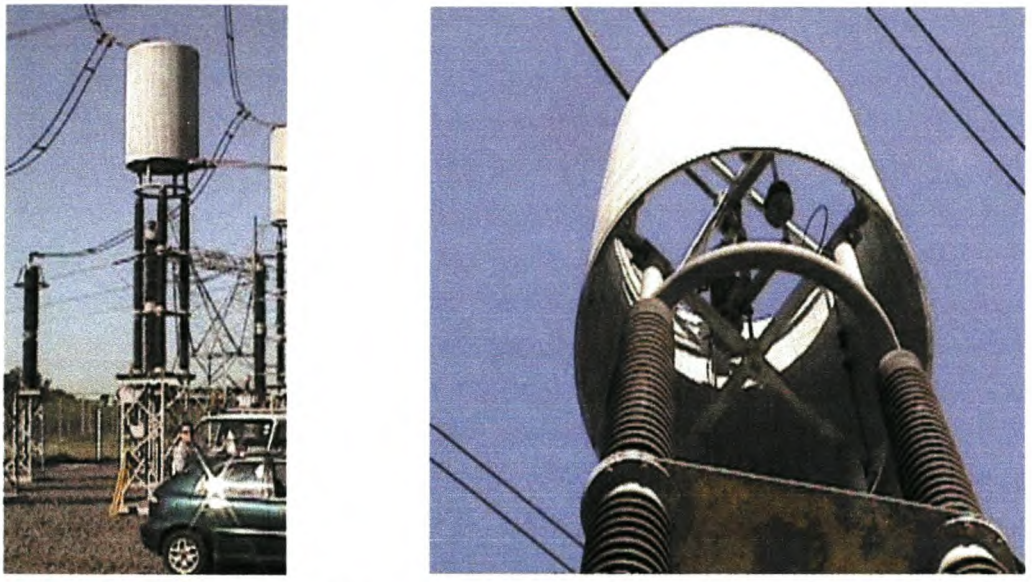

Photograph 2.1 Band tuned line trap (0.5 mH) at Acacia sub-station.

2.4 The capacitor voltage transformer

2.4.1 The core functions of the coupling voltage transformer in the PLC- link.

The core functions of a capacitor voltage transformer (CVT) are to couple PLC signals to the HV power line and to provide a low voltage measurement point of line voltage.

A major requirement of the capacitor is to protect personnel from the high current and voltage power line. This is done by coupling the communications system to the high voltage power line via the coupling capacitor that is designed to withstand the maximum surge that can possibly emanate from the power line.

Figure 2.7 shows a simplified model of a CVT. The intermediate voltage tap is used for line voltage measurements. The low voltage terminal is connected to the LME that will be described in the following section.

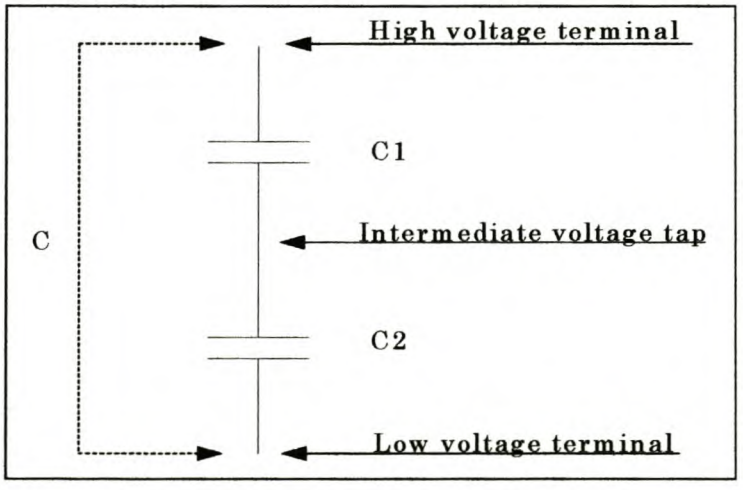

Figure 2.7 Capacitor voltage transformer

2.4.2 Description of the capacitor voltage transformer used in the Koeberg-Acacia PLC system.

The CVT's are manufactured by "ASEA". The total capacitance (C in Figure 2.7) of the CVT is 4600 pf. No more details about the CVT are needed for the purpose of simulating the losses. Photograph 2.2 shows a CVT and LME at Acacia sub-station.

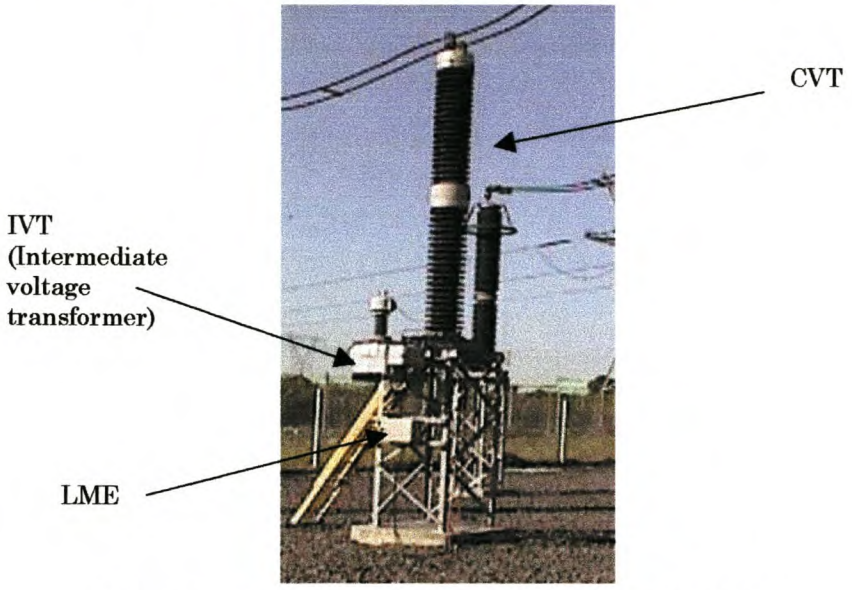

Photograph 2.2 CVT and LME at Acacia sub-station

2.5 The line matching equipment (LME)

2.5.1 The key functions of the line matching equipment in the PLC system.

LME equipment performs two major functions. Firstly it provides a safe connection to the OHTL via the coupling capacitor. Secondly it matches the PLC equipment to the line impedance for optimal power transfer.

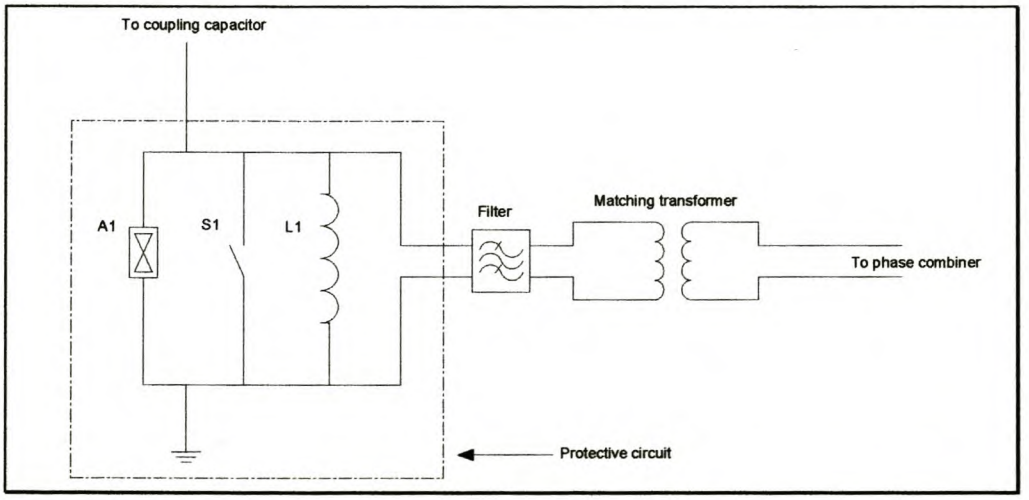

Figure 2.8 Model of LME

The basic structure of the LME is shown in Figure 2.8. The protective circuit comprises of the arrestor (A1), knife switch (S1) and drain coil (L1). The drain coil effectively grounds the lower terminal of the coupling capacitor at power frequencies. For PLC frequencies it provides a high impedance path, thus ensuring that the PLC - signal power is not short circuited to ground.

The line impedance of a twin conductor transmission line is usually of the order of 280 ohms. The impedance of the coaxial cable used by Eskom is 75 ohms. The obvious function of the matching transformer in the LME, Figure 2.8, is thus to match the 75 ohm coaxial cable to the impedance of the transmission line.

Usually the LME contains different types of filters from which the user can choose the best type according to the carrier frequencies and value of the coupling capacitor.

2.5.2 Description of the LME used in the Koeberg-Acacia PLC system.

"Electrisk Bureau" (EB) manufactures the LME. The only adjustments made to the LME by ESKOM were that the arrestors were upgraded to a more conventional type of arrestor, the ABB type RV0.66. The original units (with the old arrestor) used to fail to a short circuit. This was problematic because one generally only noticed that something was wrong when the teleprotection failed to operate after a line fault occurred.

The LME consists of a multiple of configuration options. The "strapping" of the LME is generally used as a term to describe the configuration of the LME. Figure 2.9 demonstrates the LME circuit layout with the different values of the components.

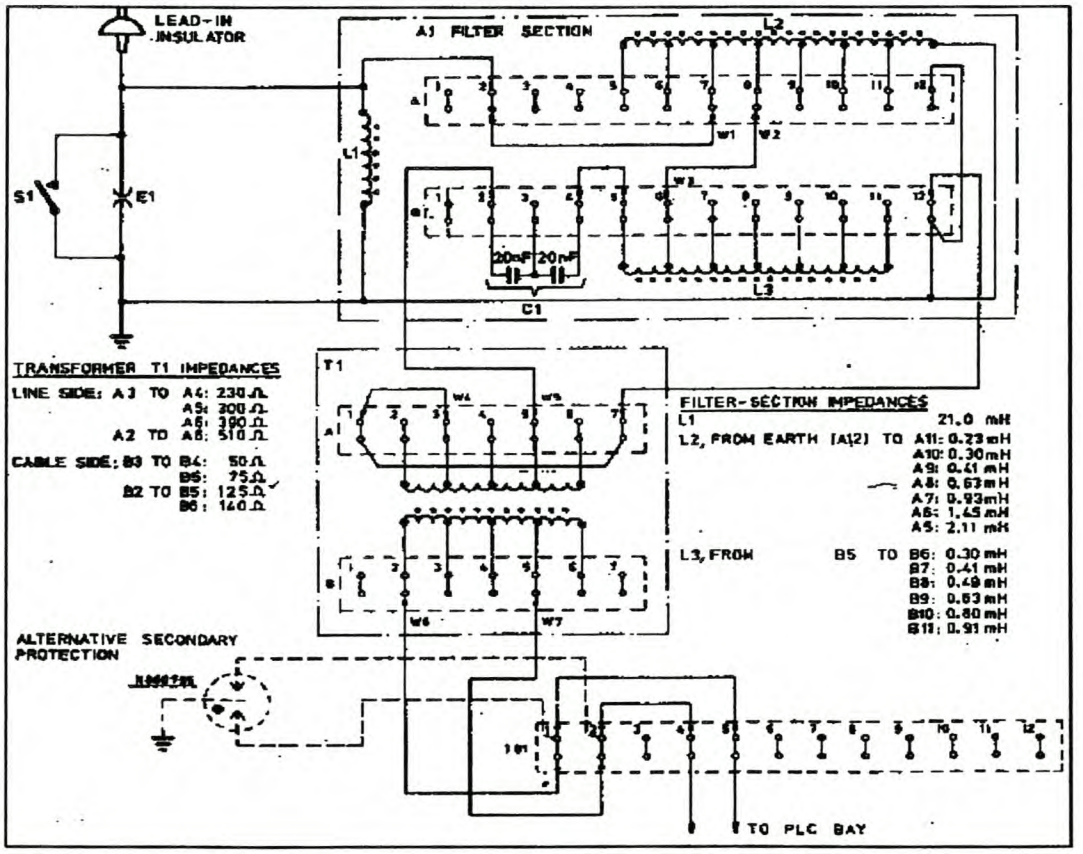

Figure 2.9 LME layout from EB.

The strapping configuration at Acacia sub-station is shown in Figure 2.10.

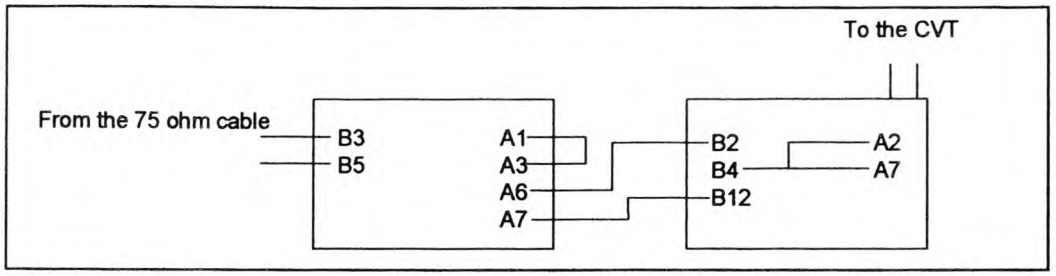

Figure 2.10 LME strapping at Acacia sub-station

Studying the strapping configuration in Figure 2.10 it can be concluded that a basic high pass filter is incorporated in Figure 2.9.

2.6 The carrier

2.6.1 The main function of the carrier

The carrier is the main communication device. All the different signals, for example speech and teleprotection, are transmitted by the local carrier and received at the remote carrier. This is demonstrated in Figure 2.1.

For the purposes of this study the only important parameters of the carrier were the frequency locations of the operational carriers and the power rating of the local carrier.

2.6.2 Description of the carriers used in the Koeberg-Acacia PLC system.

Siemens manufactured the 20-W carriers (SSB Terminal ESB 400, terminal type E401 (Eskom version)) that are used in the PLC system between Koeberg power station and Acacia sub-station.

Currently there are two carriers installed at each side. The operational frequency band of the first carrier is 344 – 352 kHz and 320 – 328 kHz for the second carrier. Each carrier uses adjacent channel operations, which occupies 8 kHz (4 kHz transmitting and 4 kHz receiving).

2.7 Coupling configuration

As mentioned in the introduction, a signal is coupled to the overhead transmission line via coupling equipment.

The term "coupling configuration" is used to specify to which phases the PLC signal is coupled and the relative amplitude and phase voltage relationships of the coupled signals.

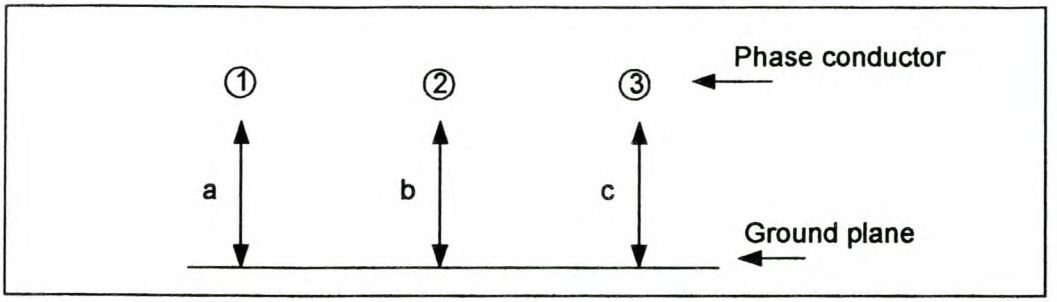

Figure 2.11 Coupling notation (a,b,c)

For the Koeberg-Acacia PLC system, coupling equipment is installed on two phases (phase 1 and 2 in Figure 2.11). The coupling configuration that is used for the active PLC system signals is (1,-1,0) and is a standard coupling configuration in ESKOM.

A phase combiner or symmetrical hybrid is used to couple the signal from the carrier to the two phases. A detailed description of the coupling mechanism will be given in Chapter 6.

2.8 Conclusion

In this Chapter the core functions of the different components in a PLC link were briefly described together with a description of the Koeberg – Acacia PLC system.

The information of all the different components will be used in the simulation program, described in Chapter 3, in order to predict signal attenuation variations on the PLC-link. The accuracy of the results is just as good as the information it is based on and that is why the correctness this information is very important.

It is interesting to note the different manufacturers of the main components identified in the PLC link. This highlights the fact that all the components must be made strictly to the IEC standards or better in order to be compatible.

2.9 References

[1] **D.C. Smith,** *PLC system engineering and practical application,* unpublished lecture notes, University Stellenbosch, 1999.
[2] **CIGRE study committee 35,** *Guide on power line carrier,* Paris meeting in 1979.

Chapter 3

The PLC simulation program

3.1 Introduction

The motivation to develop a simulation program was primarily to fully understand the theory of modal propagation and PLC concepts. University of Stellenbosch (US) does not have the source code of Professor Wedepohl's program and that limits the flexibility of the program (for research purposes). Therefore a secondary motivation for developing a local simulation program is to make customized simulations as demonstrated in Chapter 5.

This Chapter will describe the basic structure, assumptions and formulas of the simulation program.

Figure 3.1 shows the eleven steps taken in the development of the simulation program. In the first step the line and coupling parameters are specified. Chapter 2 discussed all the parameters required for the simulation program. In steps 2 to 5 the impedance and admittance matrices are formulated. A few assumptions are made and motivated in these steps. The motivations will be described together with the relevant formulas in Section 3.2. The transmission line attenuation is calculated in steps 6 to 8 and is described in Section 3.3. The attenuation introduced by the coupling equipment is calculated in step 9 (Section 3.4). In Section 3.4 the term "coupling equipment" is used as the combination of the LME, LT and the coupling capacitor as described in Chapter 2. It can specify which parameters to vary (step 10) in the simulation program for a specific investigation. Finally the attenuation is displayed in step 11.

Professor L.M. Wedepohl developed a simulation program that is based on Fortran [1]. In Chapter 4 the author's simulation program is tested against Prof L.M. Wedepohl's program (using the Acacia-Koeberg PLC system data) and in Chapter 5 the influences of the ground conductor and the soil resistivity are investigated by using the simulation program.

A more detailed description of concepts, formulas and assumptions used (in particular the Matlab environment) in the simulation program are given in [2].

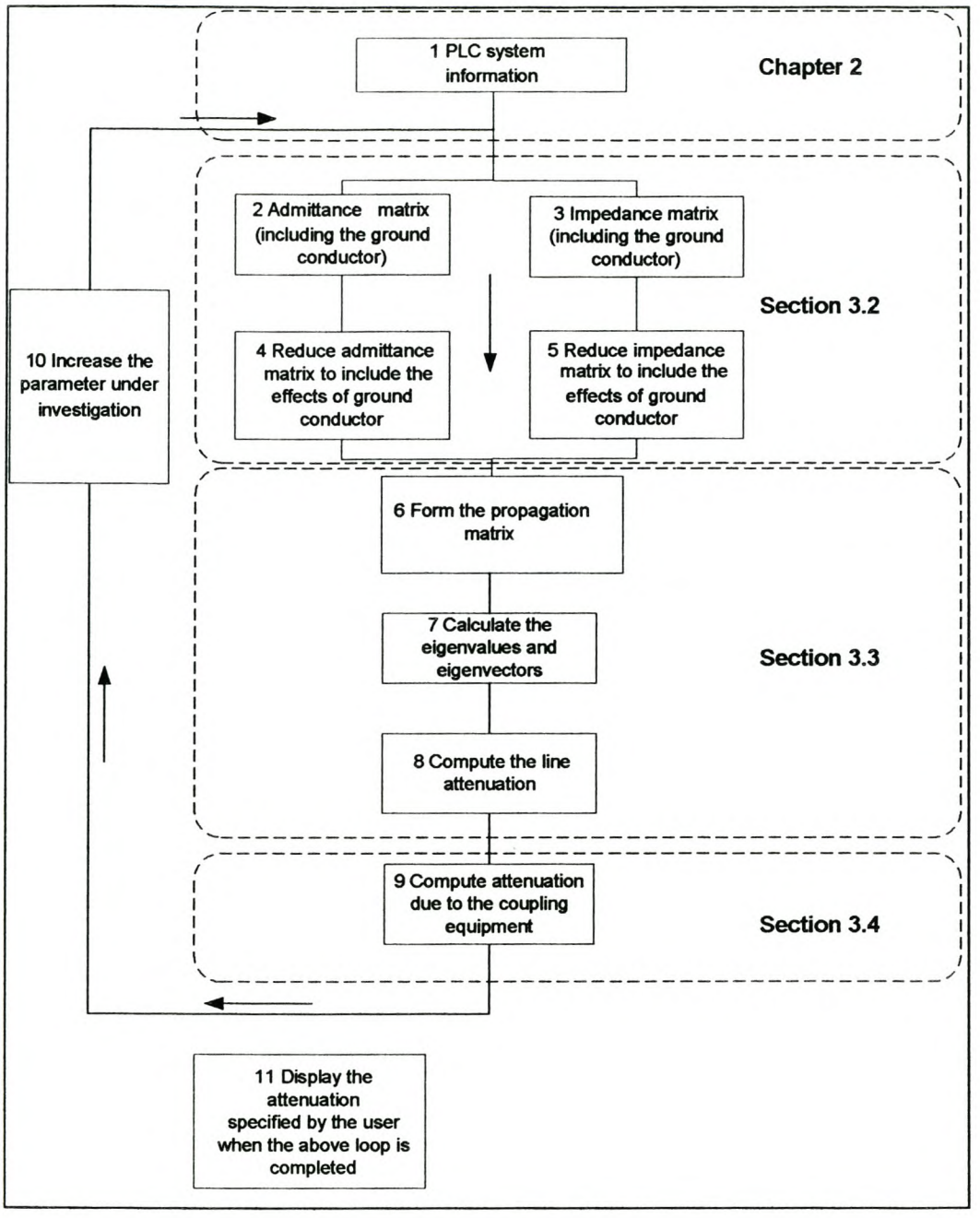

Figure 3.1 Layout of the simulation program

3.2 Formulation of the impedance and admittance matrices.

The basic impedance matrix [1] of an OHTL is:

$$Z = [R_i] + [\mathrm{R}_e] + j([X_i] + [X_e] + [X_v]) \tag{3.1}$$

where

$[R_i] + j[X_i]$ = Internal impedance matrix
$[R_e] + j[X_e]$ = Matrix of the earth correction impedances
$j[X_v]$ = Matrix of the self and mutual impedances

The internal impedance will be thoroughly discussed due to its great importance. The discussion is based on correspondence between Prof L.M. Wedepohl and W de Villiers.

3.2.1 Calculation of the internal impedance

The following discussion will describe the impedance calculations of a solid cylindrical conductor. The formula developed (solid cylindrical conductor) will be expanded to describe the internal impedance of a stranded conductor (Figure 2.1).

The impedance of a solid conductor at low frequencies, is

$$Z_{dc} = R_{dc} = \frac{\rho}{\pi r^2}\ \Omega\mathrm{m}^{-1} \tag{3.2}$$

and at high frequencies

$$Z = \frac{\rho}{2\pi r d_e} \tag{3.3}$$

where

$$d_e = \sqrt{\frac{\rho}{j\omega\mu}} \tag{3.4}$$

and: ρ = resistivity of the conductor
ω = angular frequency
μ = permeability
r = outer radius of the conductor

The formula for high frequencies can easily be interpreted. The current is flowing in a very thin annulus of radius r and thickness d_e (depth of the penetration) so that the area is $2\pi r d_e$. A function must be chosen to combine the properties of Eqns. 3.2 and 3.3 in order to formulate a general formula for the internal impedance of a solid conductor.

The function $\coth(x)$ has attractive properties for the abovementioned task. If x tends to infinity $\coth(x)$ tends to unity and if x tends to zero $\coth(x)$ tend to $1/x$. Using $\coth(x)$, the following approximation for the conductor impedance can be derived:

$$Z = \frac{\rho}{2\pi r d_e}\coth\left(\frac{K_1 r}{d_e}\right) + K_2 \tag{3.5}$$

The values of K1 and K2 are described in the discussion to follow. The following characteristics can be noted of eqn. 3.5.

$$\omega \longrightarrow \infty, Z \longrightarrow \frac{\rho}{2\pi r d_e} + K_2 \approx \frac{\rho}{2\pi r d_e} \tag{3.6}$$

and

$$\omega \longrightarrow 0, Z \longrightarrow \left(\frac{\rho}{2\pi r d_e}\right)\left(\frac{d_e}{K_1 r}\right) + K_2 = \frac{\rho}{2\pi K_1 r^2} + K_2 \tag{3.7}$$

Noting that as ω tends to infinity, d_e (the depth of the penetration) tends to zero and the argument of $\coth(\ )$ tends to infinity, i.e. $\coth(\ )$ tends to unity (eqn 3.6). A similar explanation can be given for the behaviour of eqn. 3.7.

The complete approximation of the impedance can be found by applying the following constraints

1. Eqn 3.7 must be equal to the d.c. resistance (eqn. 3.2).
2. The value of the derivative of the low frequency approximation with respect to the angular frequency must equal the derivative of the exact Bessel function. K1 = 0.777 [3].

This leads to the complete approximation:

$$Z = \frac{\rho}{2\pi r d_e}\coth\left(\frac{0.777 r}{d_e}\right) + 0.3565\left(\frac{\rho}{\pi r^2}\right) \tag{3.8}$$

Eqn. 3.8 describes the approximation of the impedance of a solid conductor. The impedance for a stranded conductor can be found by changing the DC resistance (eqn. 3.2) to

$$R_{dc} = \frac{\rho}{N\pi(r_s)^2} \tag{3.9}$$

where

N = total number of effective conductor strands
r_s = radius of each strand

and the impedance at high frequency (eqn. 3.3) to

$$Z = \frac{K\rho}{r_s(n+2)\pi d_e} \tag{3.10}$$

where

K = factor due to the conductor stranding
n = number of the outer strands

Following the same process as described for the solid conductor the impedance for a stranded conductor can now be calculated as:

$$Z_{strand} = \frac{K\rho}{r_s(n+2)\pi d_e}\coth\left(\frac{0.777r}{d_e}\right) + K_2$$
$$K_2 = \frac{\rho}{N\pi(r_s)^2} - \left(\frac{K\rho}{r_s(n+2)\pi d_e}\right)\left(\frac{0.777r}{d_e}\right)^{-1} \quad (3.11)$$

3.2.2 Calculation of the earth correction, self and mutual impedances

One of the first versions of the simulation program [4] used the numerical expansions given in [3] to calculate the earth correction factors. The method used was cumbersome. The Carson's integral [1] is given in eqn. 3.12.

$$Z_{carson} = \frac{j\omega\mu_0}{2\pi}\left[\left(\log_e\left(\frac{D_{ij}}{d_{ij}}\right)\right) + 2\int_0^\infty \frac{e^{-\alpha\cos(\theta_{ij})\cos(\alpha\sin(\theta_{ij}))}d\alpha}{\alpha+\sqrt{\alpha^2+jr_{ij}^{\,2}}}\right] \quad (3.12)$$
$$Z_{carson} = [R_e] + j([X_e]+[X_v])$$

All the parameters are described in [1,3,5] separately and are therefore not repeated. In [1] an approximation called the Gary – Dubanton formula is used for the Carson's earth correction factors that is uncomplicated, efficient and numerically stable. The formula is shown in eqn. 3.13.

$$Z_{GD} = \frac{j\omega\mu}{2\pi}\log_e\left(\frac{D'_{ij}}{d_{ij}}\right) \quad (3.13)$$

In [2] the assumption (eqn. 3.13) was tested against Carson's formula (eqn. 3.12) and indicates close correlations at low frequencies and a little deviation at higher frequencies (approximately 1 – 8 % deviation). It can be noted that the self and mutual impedances are included with the earth correction factors in Eqns. 3.12 and 3.13.

Another assumption is that the ground consists of a single layer. In [6] the Carson's formula (eqn. 3.12) was expanded to include a multi-stranded ground plane. From [6] the following conclusions were made

1) For stratified cases, considerable differences from the homogeneous cases occurred when the earth layer resistivity differ by a factor of 10.
2) At very high frequencies, when the return current is confined to the first earth layer, the homogeneous approach produces accurate results.

The PLC system operates in the 50 – 500 kHz range and for this bandwidth the return current is mostly confined to the upper part of the soil. It can be concluded that the effect of stratified ground will not influence the impedance matrix dramatically and therefore it is not included in the simulation program.

3.2.3 Calculation of the admittance matrix

The calculation of the admittance matrix is much simpler than the impedance matrix. Eqn. 3.14 shows the admittance matrix as in [1].

$$[Y^{-1}] = \frac{1}{j2\pi\varepsilon_0\omega}\log_e\left(\frac{D_{ij}}{d_{ij}}\right) \tag{3.14}$$

3.2.4 Incorporation of the bundle conductors in the model

A valid question, at this stage, is: how is a model of the bundle conductors built in the formulas? There are two strategies that can be followed.

1) Calculate the propagation modes for all the single conductors and thereby model the conductors separately.
2) Treat the bundle conductor as a single-phase conductor in the simulation program.

In Prof L.M. Wedepohl's simulation programs as well as in the simulation program described in this Chapter the second strategy was used. In order to do so one needs a formula that relates the bundle conductor to a single conductor. The formula given in [7] was used in the simulation program and is shown in eqn 3.15.

$$r_{equiv} = \sqrt[N_s]{N_s r A^{N-1}} \tag{3.15}$$

where
N_s = number of sub-conductors in the bundle
r = radius of the sub-conductors
A = radius of the bundle

r_{equiv} is used instead of the overall radius in the impedance formulas.

3.2.5 Reduction of the impedance and admittance matrices

The impedance matrix and admittance matrices (Eqns. 3.1 and 3.14) have the order p + q, where p is the number of bundle conductors and q the number of the ground conductors.

It will now be discussed how the admittance and impedance matrices are reduced to order p including some effects due to the ground conductor.

In order to reduce the impedance and admittance matrix the voltage of the ground conductor is set to zero. It is proven in [8] that this is a valid assumption except for the frequency (and close neighbouring frequencies) for which the nominal inter-tower separation is a half-wave length. At these frequencies the reflection coefficient for PLC signals is high and therefore it can influence the attenuation of the different natural modes severely. Usually this effect is not included in simulation programs. A sub-model is developed in the simulation program (based on the theory given in [8]) to investigate this effect when required. The results of the different modal attenuations including this effect are shown in Chapter 5.

In the following discussion it is assumed that the ground conductor is at zero potential throughout the transmission line. Equation 3.16 relates the series voltage drop with the current.

$$\begin{aligned} V &= ZI \\ I &= (Z^{-1})V \end{aligned} \tag{3.16}$$

The last q rows of the inverted impedance matrix (Z^{-1}) are disregarded because the last q voltages of V are zero (the voltages of the ground conductor). The reduced Z^{-1} matrix can then be re-inverted to form the impedance matrix. By ignoring the last q rows of Y, the size of the admittance matrix is also reduced.

3.3 Formulation of the line attenuation.

Once the impedance and the admittance matrices are computed the propagation matrix can be formulated as eqn 3.17 demonstrates:

$$[\mathrm{P}] = ZY \tag{3.17}$$

The eigenvectors (M) and eigenvalues (λ) of P must be computed. Eqn 3.18 shows the relationship between the eigenvalues, eigenvector and propagation matrix.

$$\begin{bmatrix} \lambda_1 & & \\ & \ddots & \\ & & \lambda_n \end{bmatrix} = [M]^{-1}[\mathrm{P}][M] \tag{3.18}$$

Due to the great importance of the eigenvalues and eigenvectors in modal propagation some background on this topic will briefly be given [9].

Eigenvalues have their greatest importance in dynamic systems. The solution is changing with time growing or decaying or oscillating. Almost all vectors, when multiplied by A, change direction. Certain exceptional vectors M are in the same direction as the product of A times M. Those are the "eigenvectors." The basic equation is:

$$AM = \lambda M \tag{3.19}$$

The eigenvalues λ tells whether the special vector M is stretched or shrunk or reversed or left unchanged- when it is multiplied by A.

Thus a physical interpretation of this powerful formulation can be interpreted as follows. The eigenvectors contain the direction of the vectors or the fixed "physical part" of the solution. This statement can be explained in terms of the natural modes in a multi-conductor system. The modal matrix of the system relates to the eigenvectors and is approximately fixed because of physical laws. The eigenvalues of the solution affect the dynamical characteristics of the different modes (eigenvectors) describing the system. Thus the attenuation and phase retardation of modes are associated with the eigenvalues.

The eigenvalues (M) of a flat 3 phase horizontal line, as described in Chapter 2, are commonly approximated by the so-called Clark's matrix [5]:

$$M = \begin{bmatrix} -\frac{1}{2} & 1 & 1 \\ 1 & 0 & 1 \\ -\frac{1}{2} & -1 & 1 \end{bmatrix} \tag{3.20}$$

The three columns of M describe the natural modes on a PLC system. In the simulation program the Clark assumption is not used because it is only valid for flat horizontal transmission lines and therefore it would limit the simulation program to one type of transmission line.

The eigenvalues and eigenvectors are calculated with the process of repeated squares. The process is thoroughly described in [1] and the implementation of the process in Matlab is shown in [2]. Attenuation and phase retardation of different modes can be extracted from the eigenvalues by using eqn. 3.21.

$$\sqrt{\lambda_i} = \alpha_i + j\beta_i \tag{3.21}$$

where

α_i = attenuation coefficient per unit length of the i-th mode

β_i = the phase shift coefficient

The two-port theory will now be introduced in the following discussion to calculate the PLC signal attenuation.

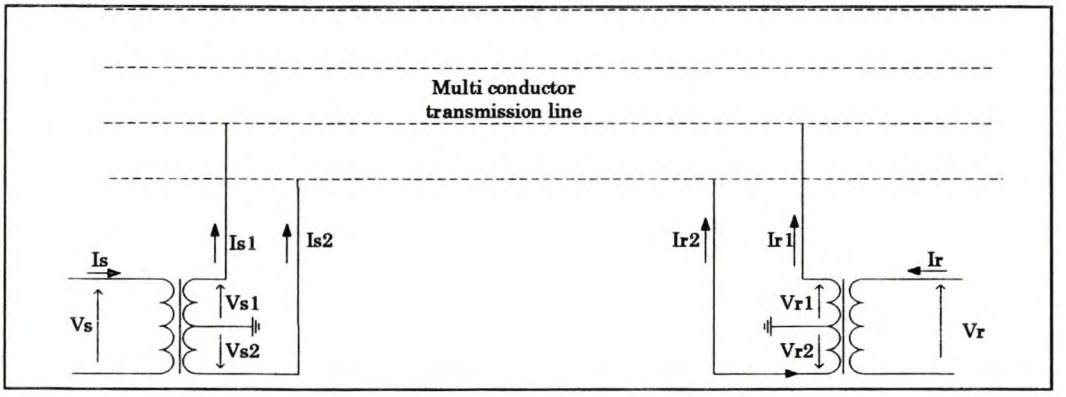

Figure 3.2 Coupling to a multi conductor system

In [10] the relationship between send voltage, V_s, and the received voltage, V_r, is shown (eqn. 3.22 and Figure 3.2).

$$\begin{bmatrix} I_s \\ I_r \end{bmatrix} = \begin{bmatrix} A & -B \\ -B & A \end{bmatrix} \begin{bmatrix} V_s \\ V_r \end{bmatrix}$$
$$\begin{bmatrix} V_s \\ V_r \end{bmatrix} = \begin{bmatrix} C & D \\ D & C \end{bmatrix} \begin{bmatrix} I_s \\ I_r \end{bmatrix} \tag{3.22}$$

where

$$A = Y_0 \coth(\psi l)$$
$$B = Y_0 \operatorname{cosech}(\psi l)$$
$$C = \coth(\psi l) Z_0$$
$$D = \operatorname{cosech}(\psi l) Z_0$$

and the propagation-coefficient ψ matrix equals $M(\sqrt{\lambda})M^{-1}$.

Different coupling configurations can be incorporated by changing A and B in eqn. 3.22 as shown in eqn. 3.23.

$$A' = n_t \cdot A \cdot n$$
$$B' = n_t \cdot B \cdot n \tag{3.23}$$

where n_t is the transposed of n which describes the coupling configuration.

The attenuation of the transmission line can now be calculated as shown in eqn. 3.24 [11].

$$Att_{line} = 20\log_{10}\left(\left|\frac{(A+Y)(Y+Y_{in})}{2BY}\right|\right) \tag{3.24}$$

3.4 Incorporation of the coupling and line-trap loss

Eqn. 3.24 can be expanded to include the attenuation of the coupling equipment. A model of the coupling equipment and line trap are shown in Figure 3.3 [1,11].

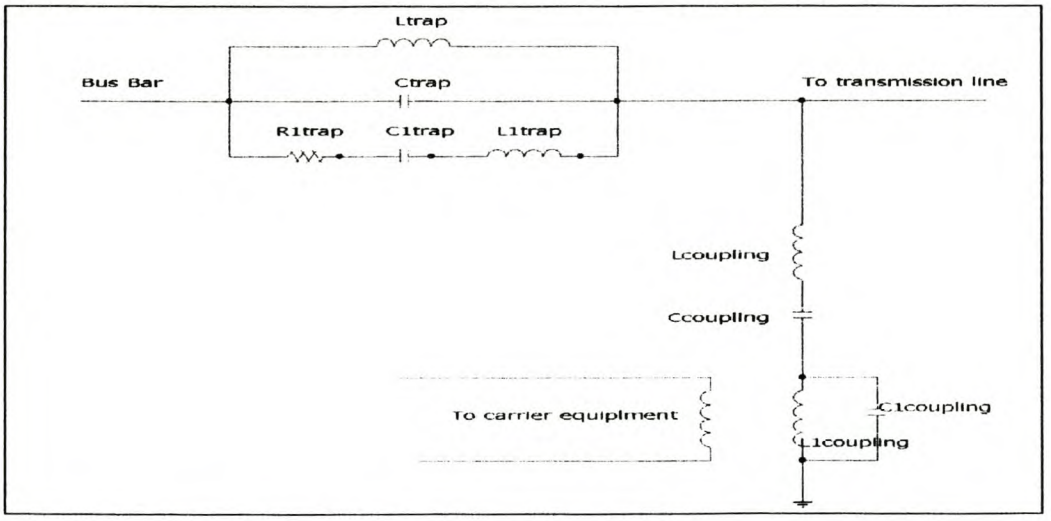

Figure 3.3 Layout of the model for the PLC coupling system

The following parameters must first be obtained for the insertion loss calculation:

1) The inductance of the line trap, *Ltrap* at carrier frequencies.
2) The series resistance in the tuning unit, *R1trap*.
3) The capacitance of the coupling equipment, *Ccoupling*.

4) The centre frequency, defined in the equation below:

$$f_0 = \sqrt{Upperfrequency \times Lowerfrequency} \tag{3.25}$$

All the above parameters can be retrieved from the information given in Chapter 2 for the Koeberg-Acacia PLC system. In order to calculate the other parameters required by the simulation program Eqns. 3.26 to 3.31 can be used. L_{trap} and ω_0 are known and C_{trap} (eqn. 3.26) can be calculated as:

$$C_{trap} = \frac{1}{\omega_0^{\,2} L_{trap}} \tag{3.26}$$

The resistance of the tuning unit is generally known. Figure 2.4 shows the tuning unit section of the line trap. The capacitance and the inductance of the tuning unit can be calculated as:

$$Ll_{trap} = C_{trap} \times R^2 \tag{3.27}$$

$$Cl_{trap} = \frac{L_{trap}}{R^2} \tag{3.28}$$

The coupling equipment parameters described in Eqns. 3.29 to 3.31 are formulated for maximised bandwidth for the given value of the coupling capacitor.

$$L_{coupling} = \frac{1}{w_0^{\,2} C_{coupling}} \tag{3.29}$$

$$Cl_{coupling} = \frac{L_{coupling}}{R^2} \tag{3.30}$$

$$Ll_{coupling} = C_{coupling} \times R^2 \tag{3.31}$$

All the component values that describe the line trap and the coupling equipment can now be calculated. The following discussion will describe how the coupling loss is incorporated in eqn. 3.32.

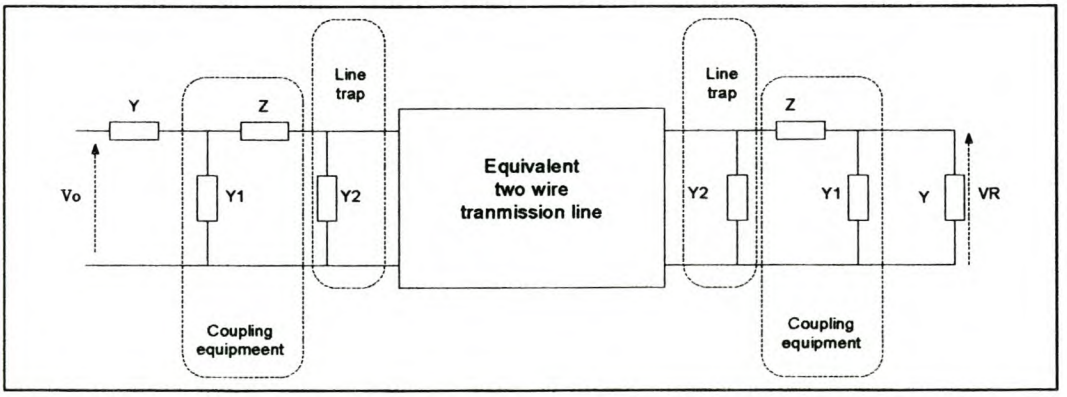

Figure 3.4 PLC model including the coupling equipment

In Figure 3.4 the symbols used have the following meaning:

Y	=	the series admittance of the signal generator (for Eskom's system it is the line side admittance of the matching transformer, Subsection 2.5.2)
Z	=	series element of the coupling unit
Y1	=	shunt element of the coupling unit
Y2	=	the admittance of the line trap

The above parameters can be calculated by using Eqns. 3.26 to 3.31 to describe the parameters in Figure 3.3. As mentioned before, the equations describing the coupling equipment are derived for maximum bandwidth. In Subsection 2.5.2 the LME is described. From the strapping formation (Figure 2.8) and the LME circuit diagram in Figure 2.7 the exact values of ***Z***, ***Y***, ***Y1*** and ***Y2*** can be found for the Koeberg-Acacia system. The simulation proved that there is not a big difference in the attenuation if the exact parameters are used in eqn. 3.32 compared to the optimized parameter according to Eqns. 3.29 to 3.31.

The attenuation of the PLC system can then be described in eqn. 3.32 as

$$Att_{Total} = \frac{\left(A' + Y_R'\right)\left(1 + Z\left(Y_1 + Y\right)\right)\left(1 + Z\left(Y_2 + Y_S'\right)\left(Y + Y_S\right)\right)}{2B'Y} \tag{3.32}$$

where

$$Y_R' = Y_2 + \frac{\left(Y_1 + Y\right)}{1 + Z\left(Y_1 + Y\right)}$$

$$Y_S' = A - \frac{B^2}{A + Y_R'}$$

3.5 Conclusion

The goal with the simulation program was to go through the learning process in order to understand the concepts of a PLC system and the theory of modal propagation. All the references stated were used in building up theory and knowledge in order to develop the simulation program. The author also had the privilege to discuss some issues about the simulation with Prof L.M Wedepohl. In the following Chapter a thorough comparison is made to show the strong correlation between Prof L.M. Wedepohl's and W de Villiers' simulation programs.

3.6 References

[1] **L.M. Wedepohl,** *The Theory of Natural Modes in Multi-Conductor Transmission Systems*, unpublished lecture notes, Westband, British Columbia, Canada, 10 January 1999.

[2] **W de Villiers,** Supplementary work on Professor Martin Wedepohl's Class notes, University of Stellenbosch, unpublished report, 25 October 2000.

[3] **L.M. Wedepohl,** *"Calculation of electrical parameters for short and long polyphase transmission line"*, IEE proceedings, Volume 111, No. 12, December 1964, pp. 2051-2059.

[4] **W de Villiers**, An investigation into overhead feeder ampacity control, Final year project at University of Stellenbosch, 5 November 1999.

[5] **F.Eggimann,W.Senn** and **K. Morf** , "The Transmission Characteristics of High – Voltage Lines at Carrier Frequencies ", Brown Boveri Review 8-77, pp. 449-459.

[6] **L.M. Wedepohl and R.G. Wasley,** *"Wave propagation in multi-conductor overhead lines, calculations of series impedance for a multi-layer earth"*, IEE proceedings, Volume 113, No. 4, April 1966, pp. 627-632.
[7] **H.W. Dommel**, *"Overhead line parameters from handbook formulas and computer programs"*, IEEE Transactions on power Apparatus and Systems, Vol. PAS-104, No.2, 2 February 1985, pp. 366-372.
[8] **L.M. Wedepohl**, *"Wave propagation in polyphase transmission systems – Resonance effect due to discretely bonded earth wires"*, IEE proceedings, Volume 112, No. 11, December 1965, pp. 2113-2119.
[9] **G. Strang**, Introduction to Linear Algebra, 1993, Wellesley-Cambrige Press, ISBN 0-9614088-5-5, Chapter 6, pp. 237 – 302.
[10] **L.M. Wedepohl,** "Electrical characteristics of polyphase transmission systems with special reference to boundary-value calculation at power-line carrier frequencies", IEE proceedings, Volume 112, No. 11, December 1965, pp. 2103-2112.
[11] **L.M. Wedepohl,** *"Propagation of carrier signals in homogeneous, non-homogeneous and mixed multi-conductor system"*, IEE proceedings, Volume 115, No. 1, January 1968, pp. 179-186.

Chapter 4

Results of the PLC simulation program

4.1 Introduction

The simulation program was developed to fully understand the theory of modal propagation, PLC concepts and to realize customized PLC investigations.

4.4.1 Testing the simulation program against Professor Wedepohl's program.

The locally developed simulation program was tested against Professor Wedepohl's program and the results are shown in this Chapter. It will be shown that the two simulation programs produce essentially the same results. Prof L.M. Wedepohl and W. De Villiers had numerous discussions using the E-Mail communication medium in order to explain some of the initial differences between the two programs. There were changes made in both W. De Villiers and Prof L.M. Wedepohl's original programs in order to produce the results demonstrated in this Chapter. The two simulation programs were developed independently from each other on different computer programming language platforms, De Villiers' in Matlab and Wedepohl's in Fortran.

4.4.2 Simulations of the experiment to observe attenuation variation due to change in average conductor heights.

Simulations were done to detect attenuation variations in the PLC coupling band for different average conductor heights. For the Koeberg-Acacia transmission line configuration, it can be seen that the attenuation of the PLC signal (single phase coupling on the outer phase) is sensitive to the average height of the phase conductors.

4.2 Comparison between programs, including the standing wave effect.

Because a relatively short line is simulated (Koeberg – Acacia) the standing wave effect can be clearly noticed. The distance of successive peaks of the standing wave occurring in Figure 4.1 will be discussed.

The phase shift of a travelling wave, in radians, is $\omega l / c$. By equating the phase shift of a travelling wave to $\pi / 2$ (Eqn 4.1), the frequency difference between the successive peaks and troughs of a standing wave can be calculated.

$$\frac{\pi}{2} = \frac{\omega l}{c} \tag{4.1}$$

where c = speed of light
ω = angular frequency
l = length of the line.

In this study the length of the transmission line is 31.3 km and the phase velocities of the travelling waves on a differential coupled PLC system are close to the speed of light, 3×10^8 m/sec. The calculation shows that the frequency difference between peaks must be 4.8 kHz. It can be observed that the frequency distance between the neighbouring

peaks is approximately 4.8 kHz, see Figure 4.1. The peaks are not exactly 4.8 kHz because the attenuation of the standard coupling configuration is the result of a combination of the different attenuations of the natural modes, which propagate at slightly different phase velocities. The least attenuated mode, (1,-2,1) – mode 1, has a propagation speed close to the speed of light. Three quarters of the signal power for the standard coupling configuration (1,-1,0) is embedded in mode 1 (Chapter 6 will show the formulation to calculate the power distribution) and therefore the successive peaks occurs close to 4.8 kHz. The dotted line represents Professor Wedepohl's program and the solid line the De Villiers program.

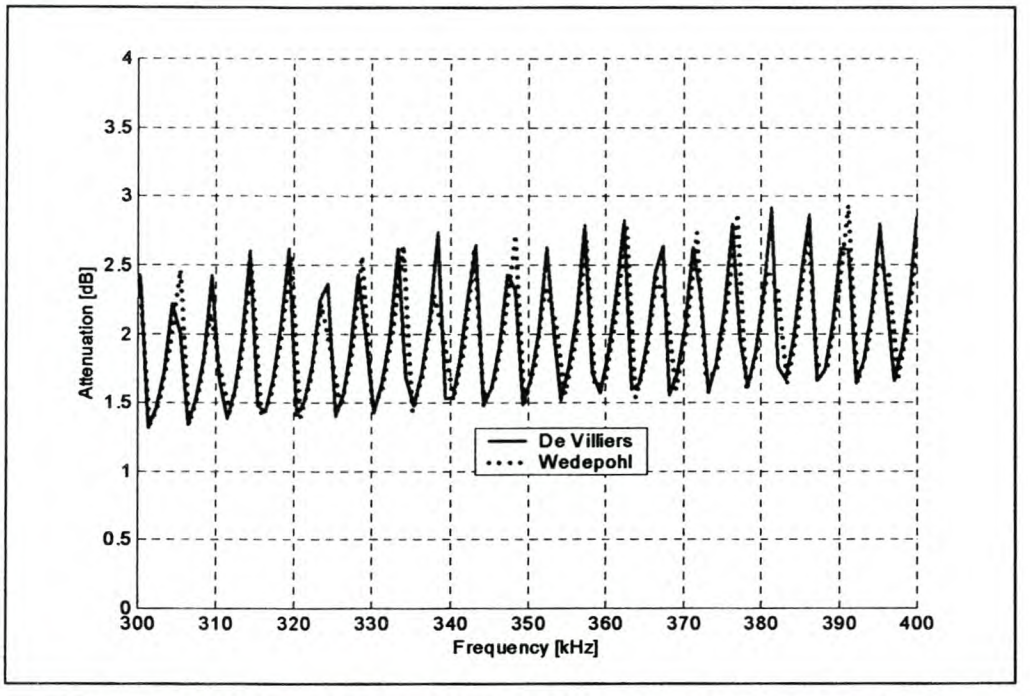

Figure 4.1 PLC signal attenuation(300kHz – 400kHz) introduced by the transmission line for standard coupling configuration (1,-1,0) signifying the standing wave effect

4.3 Comparison between programs, excluding the coupling equipment and the standing wave.

In order to clearly present the results of the signal attenuation simulations effectively the standing-wave effect will be filtered out for all the attenuation graphs in this thesis. A zero-phase forward and reverse digital filter is used to filter the data. The Matlab function used to realize such a filter operation is called "filtfilt". The filter introduces zero phase distortion and is suitable for data processing.

The attenuation of the transmission line alone is demonstrated in Figure 4.2 for both the standard (1,-1,0) and the single outer phase (1,0,0) coupling configurations. It can be seen that the two simulation programs produce very similar results. See Figure 4.2 for the whole PLC spectrum.

For the results shown in Figure 4.2 the soil resistivity is chosen as 300 ohm-meter and the average height of the ground conductor is taken as the attachment height.

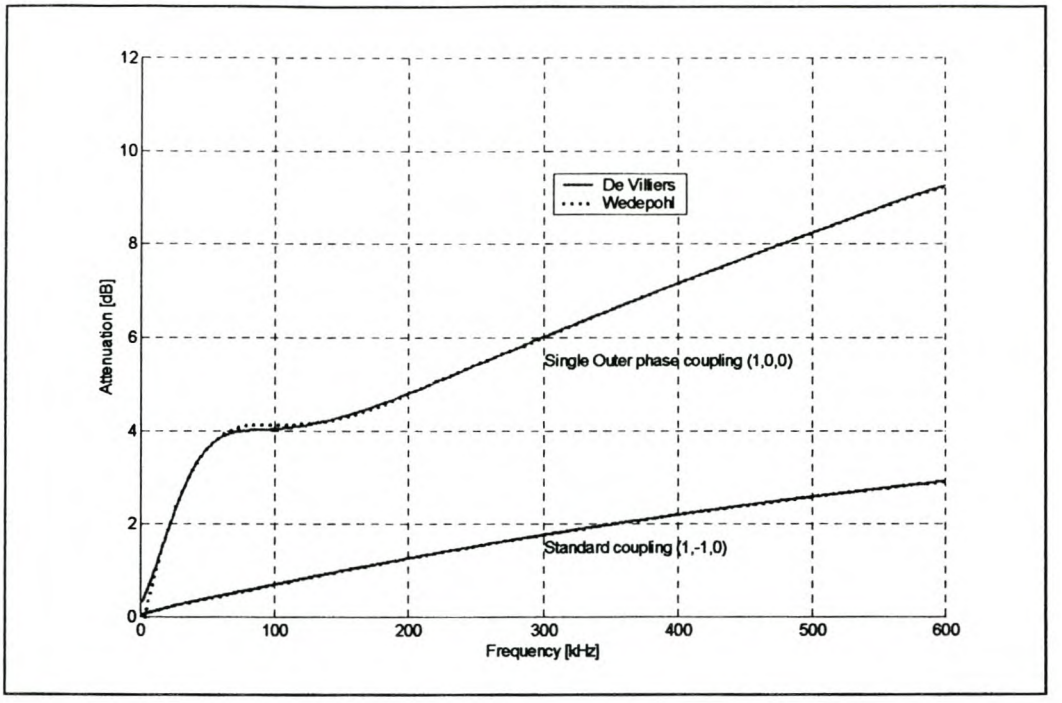

Figure 4.2 Comparison between Prof Wedepohl's simulation program and De Villiers program for the line attenuation only.

4.4 The insertion loss introduced by the Coupling Capacitor (CC) and the Line Trap (LT).

The following two graphs (Figure 4.3), produced respectively by De Villiers' and Professor Wedepohl's programs, demonstrate the insertion loss introduced by the CC and the LT. Again close agreement between the two simulation programs can be observed.

At the mid frequency, 224 kHz (Figure 4.3), it is clearly evident that the additional loss introduced by the coupling capacitor is approximately zero (a minimum) and on the other hand that the insertion loss of the line trap is a maximum for the PLC band, 50 – 500 kHz. The sum of the insertion losses of the CC and the LT results in a relatively flat frequency response over the frequency band.

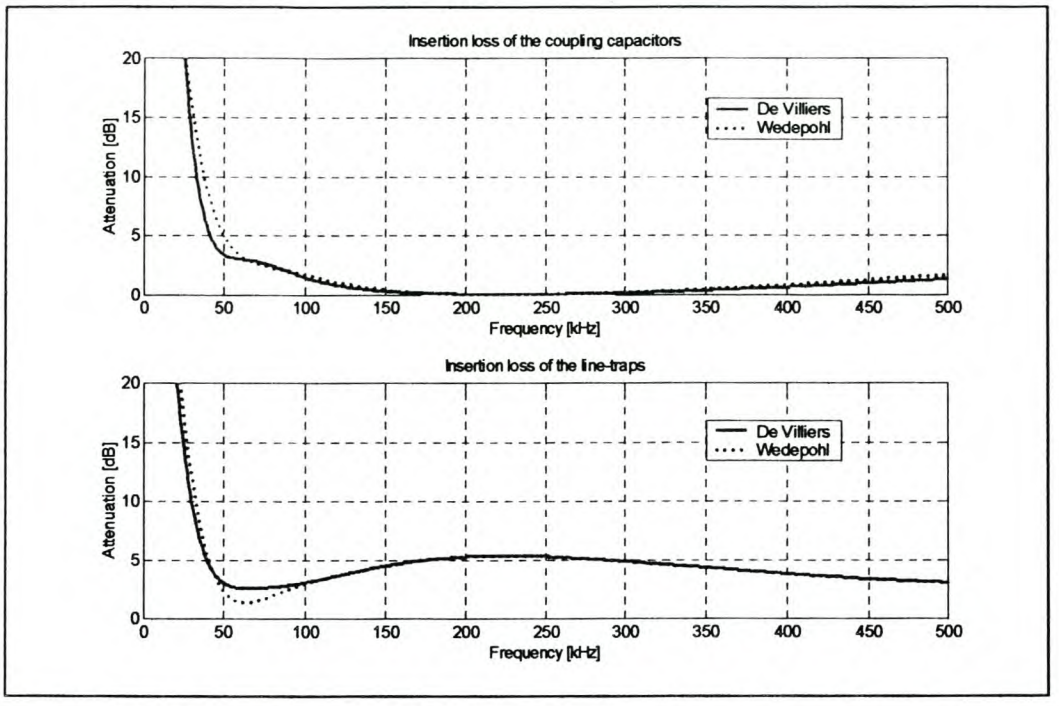

Figure 4.3 The insertion loss introduced by the coupling capacitor and the line trap.

4.5 Total attenuation for the PLC band including the coupling equipment

Figure 4.4 shows the total attenuation of the two coupling configurations.

With this result the testing process against Professor Wedepohls' program is concluded. The newly developed De Villiers simulation program proved itself and produces trustworthy results when compared to Professor L.M. Wedepohl's simulation program. In Chapter 7 the program is tested in a practical field environment and the results again indicated close agreement.

From the graphs in Figure 4.4 it can be concluded that the attenuation of single phase coupling on the outer phase (1,0,0) and the attenuation of the standard coupling configuration (1,-1,0) do not differ as much as expected. In the simulations done (Figure 4.1 to 4.4) the average height of the phase conductors is equal to the attachment height as previously mentioned. The expectation of the higher attenuation (for single outer phase coupling) is validated in Figures 4.6 to 4.8 (in the following section) showing the changes as the average height of the phase conductors are varied.

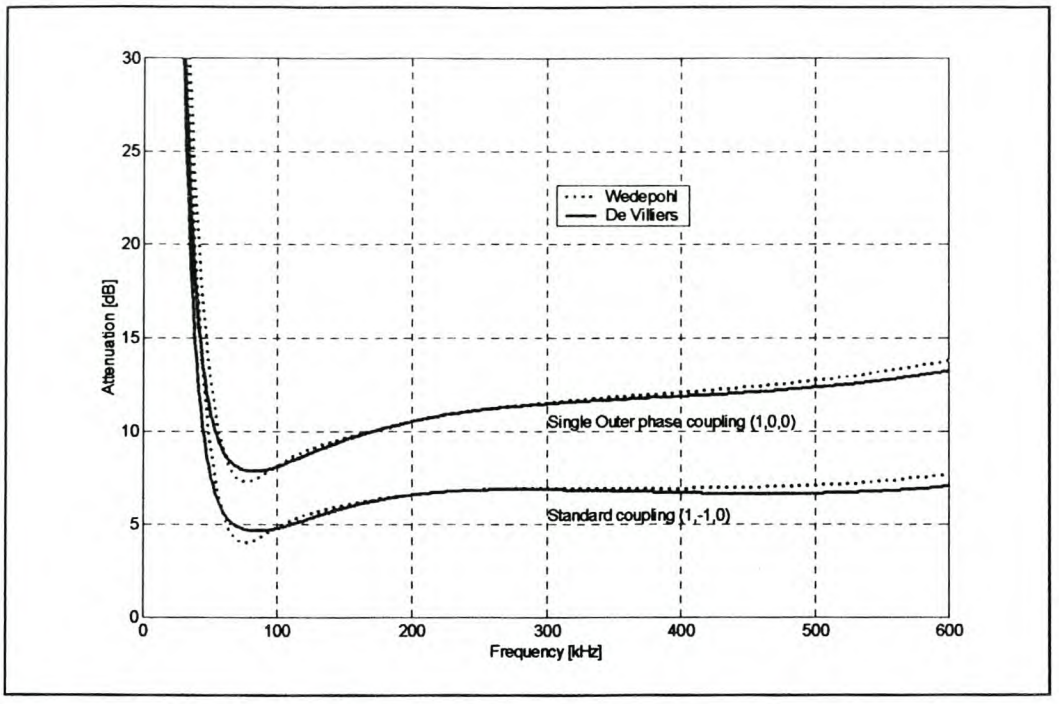

Figure 4.4 Total attenuation, including the coupling equipment, for the two different coupling configurations.

4.6 Simulation of the Koeberg-Acacia 400 kV PLC signal attenuation (varying average conductor height and soil resistivities).

This section deals with the simulation of the PLC signal attenuation for the standard and single phase coupling schemes with variation in average conductor height and soil resistivities.

The average height of the phase conductors is varied from 9m to 14m above the ground plane. The ground conductors are varied in tandem with the phase conductors (5.5m distance between ground- and phase conductors). This assumption is tested in Figure 4.5 and will be discussed in the following paragraph.

The phase conductor will not always sag with the same amount as the ground conductor (therefore the distance between the ground conductor and the phase conductor will not be constant), due to different coefficients of linear expansion and the current in the phase conductors that produces extra heat. In the simulation showed in Figure 4.5 to test this assumption the average height of the phase conductor is taken as 12m. The distance between the ground conductor and the phase conductor is varied between 3 and 6 meters (Figure 4.5) in one-meter steps. The simulation indicates that the vertical distance between the phase conductors and the ground conductor does not affect the PLC attenuation much for the standard coupling (1,-1,0) configuration. Special care must be taken when considering detailed simulations of the nonstandard coupling configuration but in this thesis the distance between the ground- and phase conductor will be taken as a constant (5.5m).

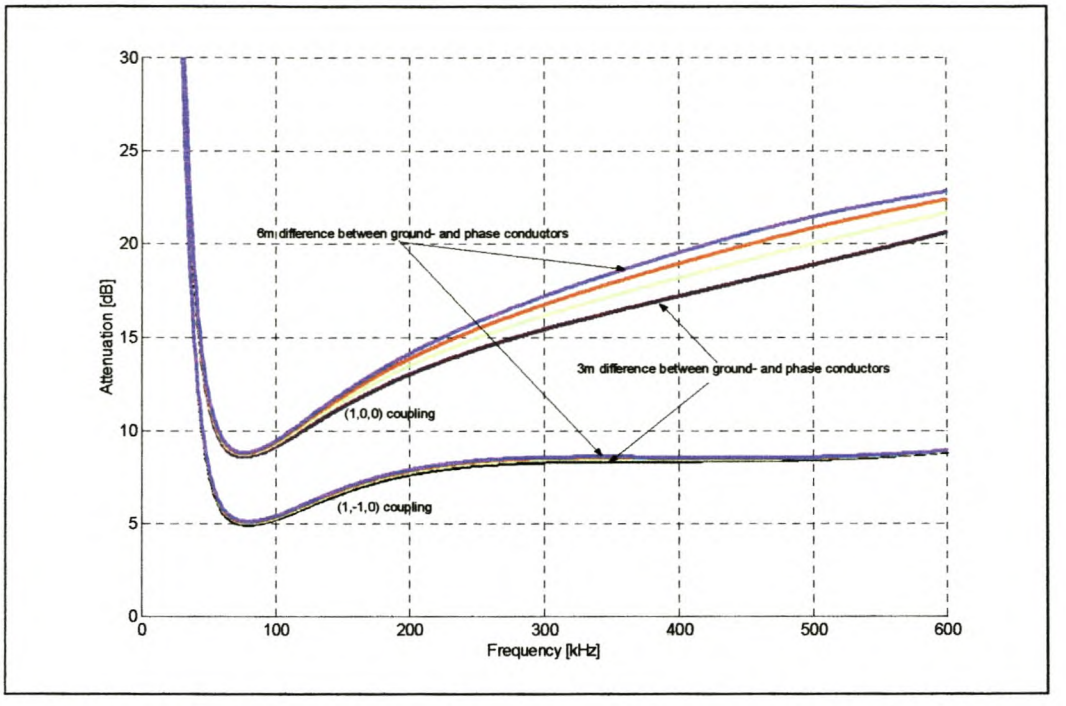

Figure 4.5 PLC signal attenuation where the distance between the phase conductor and ground conductor is varied

Figures 4.6, 4.7 and 4.8 shows the PLC signal attenuation for different phase conductor heights and for soil resistivities of 100, 300 and 500 ohm- meter respectively.

In all these Figures it can clearly be noted that the single phase coupling on the outer phase (1,0,0) signal attenuation is much more sensitive to variation in the average phase conductor height than for the standard coupling scheme.

The soil resistivity influences the attenuation as shown in the Figures. In Chapter 5 the role that different types of ground conductors play in the PLC system will be studied in depth to fully understand how changes in soil resistivity influence the PLC signal attenuation.

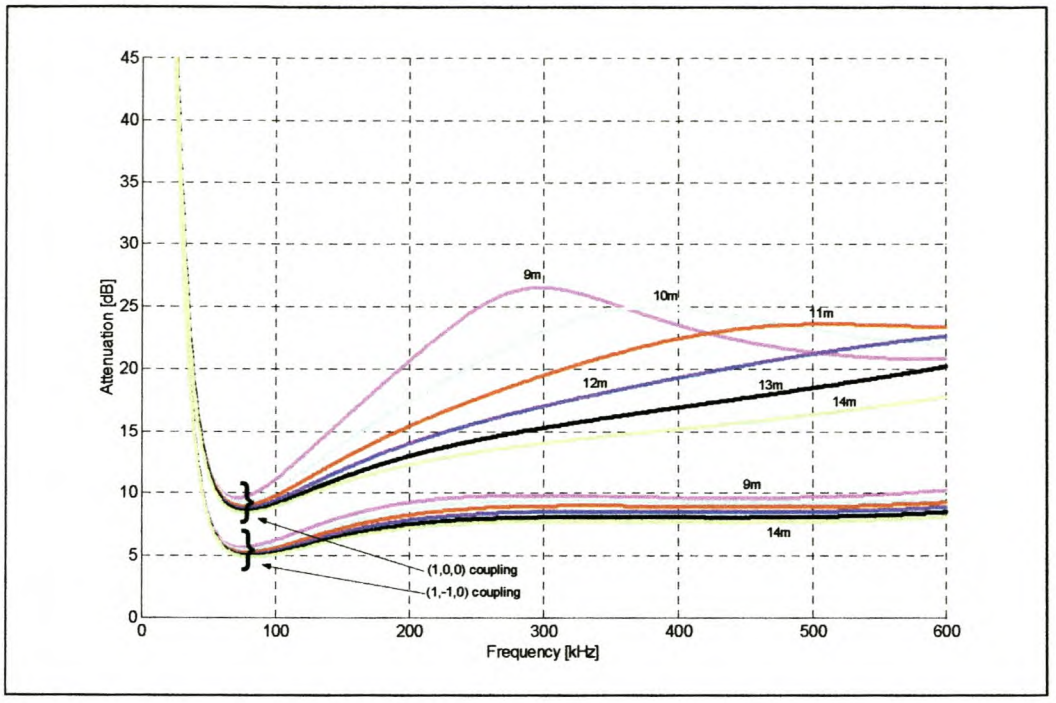

Figure 4.6 PLC signal attenuation with different average phase conductor heights for 100 ohm – meter soil resistivity

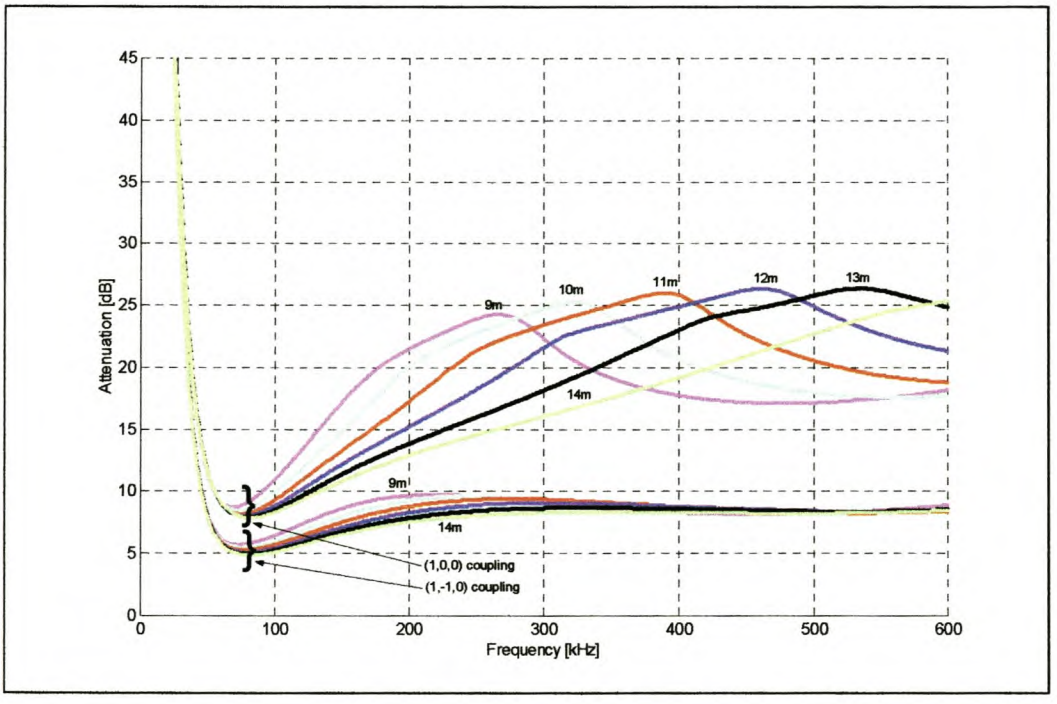

Figure 4.7 PLC signal attenuation with different average phase conductor heights for 300 ohm – meter soil resistivity.

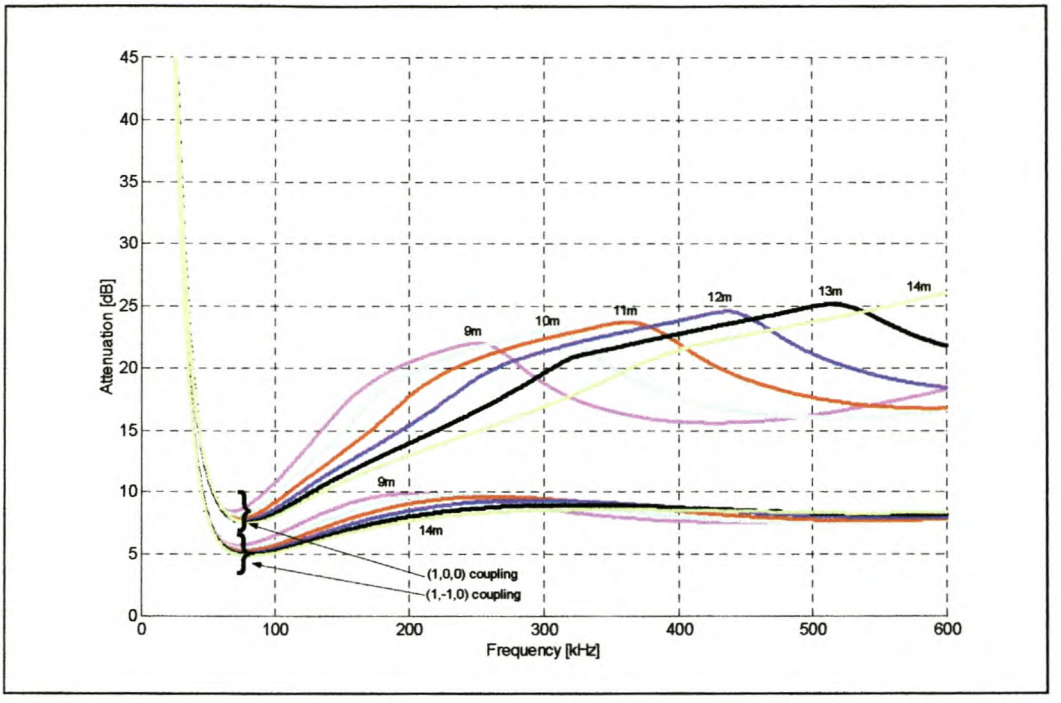

Figure 4.8 PLC signal attenuation with different average phase conductor heights for 500 ohm – meter soil resistivity.

4.7 Conclusion

The De Villiers' simulation program gave trustworthy results when compared to Prof Wedepohl's simulation program. This comparison was very time consuming but extremely important because there are so many variables in the field (and by implication so many potential errors) that the user must have confidence in the simulation program.

PLC signal attenuation for the standard coupling configuration (1,-1,0) proved to be less sensitive for variation in the average conductor height than the single phase coupling on the outer phase (1,0,0).

Following this result an experiment was designed to incorporate single phase coupling on the outer phase in order to measure the effect demonstrated in the above Figures. The experiment is discussed in Chapter 6 and the measured results are shown in Chapter 7.

Chapter 5

The influence of ground conductors on PLC systems

5.1 Introduction

The ground conductor influences the PLC signal propagation in mainly two ways.

Firstly, the most common effect associated with the ground conductor is the resonance occurring at the frequency where the spacing between the towers is equal to a half wavelength. In order to investigate this effect a sub-program in Matlab was developed. The theory used in the program is based on [1]. In Section 5.2 this theory will be shown and discussed. The results generated by this sub-program (Section 5.3) are similar to the results shown in [1] and thereby give some indication of the correct implementation of the theory. The results could not be tested against Prof L.M. Wedepohl's program due to the unavailability of this module in his program.

Secondly, the ground conductor parallel with the ground plane acts as a return path for the currents (at low as well as high frequencies). The properties of both return paths play a role in the PLC signal attenuation and must be analysed simultaneously. In Section 5.4 interesting Figures demonstrates the unexpected impact that the type of ground conductor has on modal propagation. More detailed simulations (Section 5.5) are shown in order to explain this phenomenon.

The soil resistance is a difficult parameter to determine accurately in PLC signal attenuation simulations due to its geological in homogeneity and seasonal and climatic variability. This Chapter gives the reader insight into the PLC signal attenuation variation due to the changes in soil resistivity.

5.2 Resonance effects due to discretely bonded ground conductors.

The theory is described in [1] and is implemented in the simulation program. The important formulas are shown to give background on this effect and to demonstrate how the effect is simulated.

5.2.1 Theory of the resonance effect

Figure 5.1 shows a line diagram of the model of a transmission line between two towers.

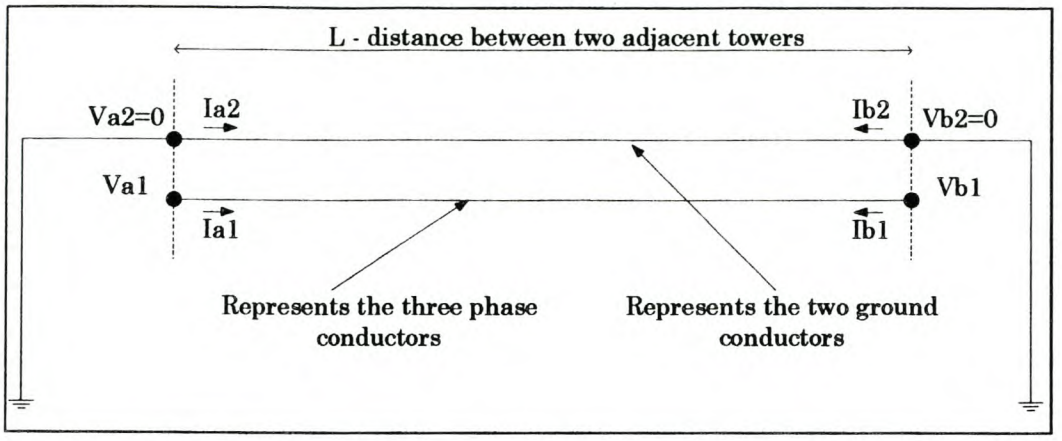

Figure 5.1 Model between two towers for the resonance effect

Eqn. 5.1 is similar to eqn. 3.22 except that the matrices are not reduced and therefore are of size 5×5.

$$\begin{bmatrix} I_a \\ I_b \end{bmatrix} = \begin{bmatrix} A & -B \\ -B & A \end{bmatrix} \begin{bmatrix} V_a \\ V_b \end{bmatrix} \tag{5.1}$$

where A and B were described in Section 3.3

Eqn. 5.1 can be partitioned into phase-conductor and earth-conductor groups (eqn. 5.2) before the appropriate boundary conditions, shown in Figure 5.1, are inserted.

$$\begin{bmatrix} I_{a1} \\ I_{a2} \\ I_{b1} \\ I_{b2} \end{bmatrix} = \begin{bmatrix} A_{11} & A_{21} & -B_{11} & -B_{12} \\ A_{21} & A_{22} & -B_{21} & -B_{22} \\ -B_{11} & -B_{12} & A_{11} & A_{12} \\ -B_{21} & -B_{22} & A_{21} & A_{22} \end{bmatrix} \begin{bmatrix} V_{a1} \\ V_{a2} \\ V_{b1} \\ V_{b2} \end{bmatrix} \tag{5.2}$$

Since V_{a2} and V_{b2} equal zero (Figure 5.1) and there is no need to calculate the earth wire currents eqn. 5.2 can be reduced to eqn 5.3:

$$\begin{bmatrix} I_{a1} \\ I_{b1} \end{bmatrix} = \begin{bmatrix} A_{11} & -B_{11} \\ -B_{11} & A_{11} \end{bmatrix} \begin{bmatrix} V_{a1} \\ V_{b1} \end{bmatrix} \tag{5.3}$$

Eqn. 5.3 is a complete description of the transmission line section but is not in a practical form because it has to be cascaded by a very large number of sections. Introducing the concept of equivalent natural modes solves the problem.

A_{11} and B_{11} are set to

$$\begin{aligned} A_{11} &= Y_{01}\coth(\tau_l) \\ B_{11} &= Y_{01}\operatorname{cosech}(\tau_l) \end{aligned} \tag{5.4}$$

where τ_l is the propagation coefficient matrix per tower section.

The transmission line eqn. 5.3 for ***r*** tower sections (assumed identical) in cascade can be reformulated to form eqn. 5.5. The proof for this step is given in [1].

$$\begin{bmatrix} I_{a1} \\ I_{b1} \end{bmatrix} = \begin{bmatrix} Y_{01}\coth(r\tau_l) & -Y_{01}\operatorname{cosech}(r\tau_l) \\ -Y_{01}\operatorname{cosech}(r\tau_l) & Y_{01}\coth(r\tau_l) \end{bmatrix} \begin{bmatrix} V_{a1} \\ V_{b1} \end{bmatrix} \tag{5.5}$$

In Eqns. 5.4 and 5.5 Y_{01} and τ_l must be determined, whereas in Chapter 3 the eigenvalues and eigenvectors of the propagation coefficient matrix (per unit length) were used to calculate the ***A*** and ***B*** matrices. The process is turned around and the known matrices A_{11} and B_{11} are used to calculate the eigenvalues and eigenvectors which then describe the effective propagation.

The admittance matrix can be eliminated by formulating the product of the inverse of B_{11} and A_{11} in eqn. 5.6.

$$B_{11}^{-1}A_{11} = \sinh(\tau_l)Y_{01}^{-1}Y_{01}\coth(\tau_l) = \cosh(\tau_l) \tag{5.6}$$

The $\cosh(\lambda_l)$ matrix can be expressed by its eigenvalues (λ_l) and eigenvectors (S_l) in eqn. 5.7.

$$\cosh(\tau_l) = S_l\cosh(\lambda_l)S_l^{-1} \tag{5.7}$$

Finally, the effective propagation matrix can be written as

$$\psi_{effective} = S_l\left(\frac{\lambda_l}{l_{tower}}\right)S_l^{-1} \tag{5.8}$$

where l_{tower} is the average distance between the towers. and eqn. 5.5 becomes

$$\begin{bmatrix} I_{a1} \\ I_{b1} \end{bmatrix} = \begin{bmatrix} Y_{01}\coth(\psi_{effective}l_{total}) & -Y_{01}\operatorname{cosech}(\psi_{effective}l_{total}) \\ -Y_{01}\operatorname{cosech}(\psi_{effective}l_{total}) & Y_{01}\coth(\psi_{effective}l_{total}) \end{bmatrix} \begin{bmatrix} V_{a1} \\ V_{b1} \end{bmatrix} \tag{5.9}$$

5.2.2 Implementation in Matlab

This theory was implemented in the sub-program to investigate the resonance phenomenon. The simulation is shown in Section 5.3.

One of the most frequently used techniques in the implementation of the theory will be described in this discussion.

The Matlab command ***cosech(A)*** where ***A*** is a 5 by 5 matrix with complex arguments does not work correctly. The theory of idempotents [2] is a powerful tool in linear algebra and was used to overcome this problem.

Any matrix can be written in terms of its eigenvalue matrix (λ) and it eigenvector matrix (M).

$$A = [M][\lambda][M]^{-1} \tag{5.10}$$

The right hand side of eqn. 5.2 can be rewritten as

$$[M][\lambda][M^{-1}] = \sum_{i}^{n}[M_i][M_i^{-1}]\lambda_i \tag{5.11}$$

where n is the size of the matrix.

The product of $[M_i][M_i^{-1}]$ is called an idempotent. If sum of all the idempotents of a matrix are summated equals the unit matrix. The eigenvalue matrix $[\lambda]$ is a diagonal matrix and therefore λ_i is a scalar where $[M_i]$ and $[M_i^{-1}]$ are column and row matrices respectively.

With the use of equation 5.10 and 5.11, the function ***cosech(A)*** can be incorporated into the Matlab code as eqn. 5.12 demonstrates.

$$\text{cosech}(A) = [M]\text{cosech}([\lambda])[M]^{-1} = \sum_{i}^{n}[M_i][M_i^{-1}]\text{cosech}(\lambda_i) \tag{5.12}$$

From eqn. 5.12 it can be seen that the function ***cosech( )*** operates on scalar numbers and is therefore compatible with the Matlab environment.

5.3 Simulation results: resonance effects due to discretely bonded ground conductors.

Figure 5.2 shows the resonance effect. The transmission line information given in Chapter 2 is used (336.7m average tower spacing) for this simulation. The x-axis in Figure 5.2 is plotted in terms of the normalized section length. From the Figure it can clearly be seen that the effect is occurring where the normalized section length is equal to 0.5. Thus for the Koeberg-Acacia transmission line the resonance effect occurs at 445.5 kHz (eqn. 5.13).

$$\begin{aligned} 0.5 &\simeq \frac{fl}{c_0} \\ f &\simeq \frac{0.5\times 3\times 10^8}{336.7} = 445.5 \text{ kHz} \end{aligned} \tag{5.13}$$

The most attenuated mode, mode 3, is influenced by this effect at the frequency where the spacing between the towers is equal to a half wavelength. It is should be noted that the smooth-line theory (Simulation program described in Chapter 3, and also plotted in Figure 5.2) and the resonance theory (Section 5.1) give similar results outside the critical region. It can also be observed that mode 2 attenuation only indicates a little deflection due to the resonance effect and mode 1 shows zero deflection.

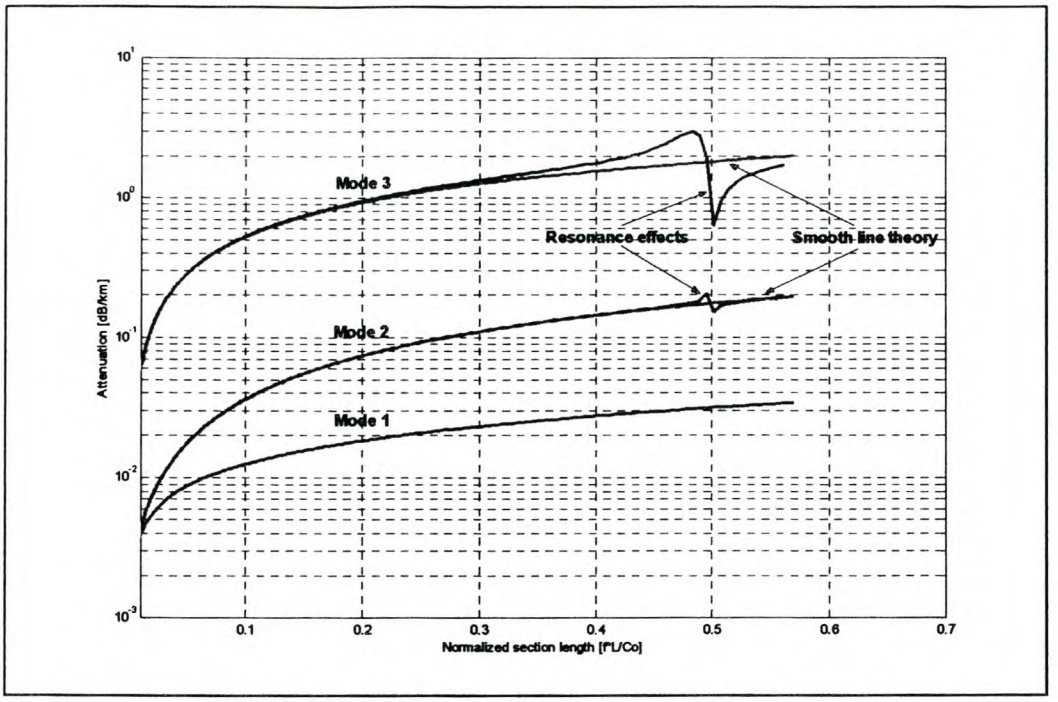

Figure 5.2 Resonance effects on the natural modes due to discretely bonded ground conductors

5.4 Influence on PLC signal attenuation due to the type of ground conductor and soil resistivity

5.4.1 The attenuation of the natural modes for steel and aluminium ground conductors compared with a no ground conductor case

Figure 5.3 indicates the modal attenuation of the three modes for a steel ground conductor, ACSR ground conductor and a transmission line with no ground conductor, respectively. The properties of the two conductors are summarized in Table 5.1. The attenuations of the modes are calculated for a frequency interval from 50 to 500 kHz and the soil resistance is set to 300 ohm - meter.

Table 5.1 Characteristics of the ACSR and Steel ground conductor

Type of ground conductor	Steel	ACSR, aluminium
Overall radius [mm]	6.6	8.26
Radius of strands [mm]	1.3	1.18(outer Al strands)
Number of strands	6 (outer) and 7 (total)	18 (outer) and 30 (total)
Conductor resistivity	2e-7	3.2e-8
Relative Permeability	1000	1

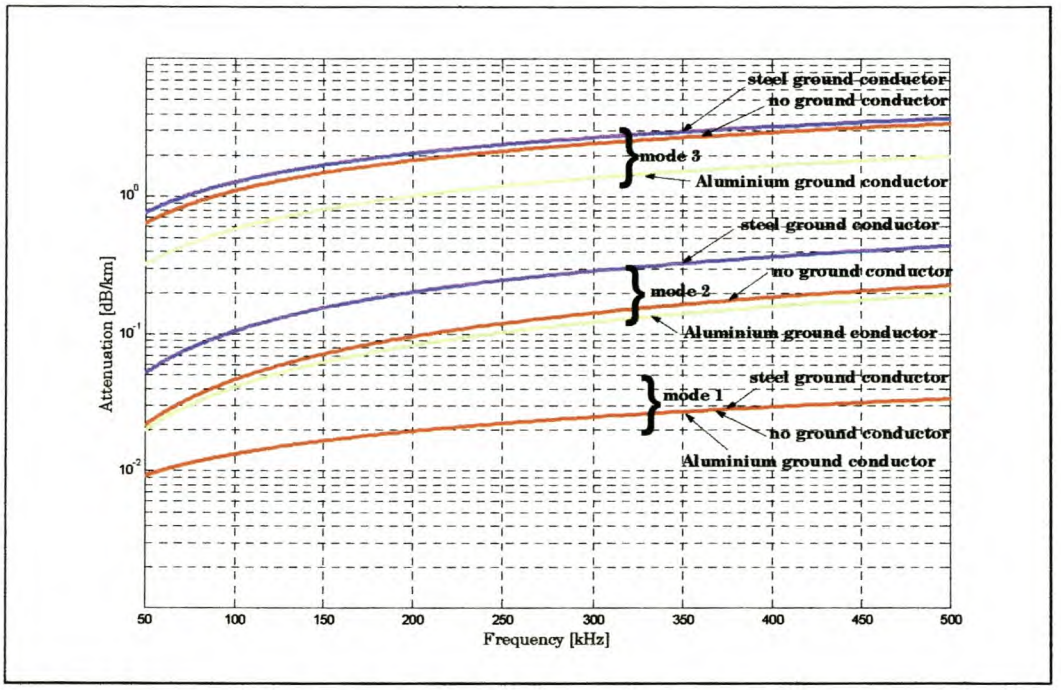

Figure 5.3 Propagation of the main modes on a PLC system with no / steel / aluminium ground conductors.

It should be noted that the type of ground conductor does not influence mode 1 attenuation. Mode 2 attenuation is largely influenced by the presence of the steel conductor. Mode 3, on the other hand, is mainly influenced by the presence of the aluminium conductor. This is a very interesting phenomenon. From Figure 5.3 it can be concluded that the properties of the ground conductor have a prominent role in the PLC signal propagation.

The only parameters that distinguish the two ground conductors are conductivity, permeability and size. The size difference of the ground conductor in proportion to the dimensions of the whole system is very small. Simulations (not shown in the thesis) prove that the size difference is not responsible for the effects shown in Figure 5.3. The explanation of this effect will start with an introductory discussion of a single ground and phase conductor above a ground plane.

5.4.2 Model of a single phase conductor with one ground conductor

Figure 5.4 demonstrates this simplified model. Consider the case where the impedance of the ground conductor, ***Zgc***, approaches infinity with both ends of the ground conductor connected to ground. No current will flow in the ground conductor and the loss due to the ground conductor will thus be zero. The other extreme is to have the impedance of the ground conductor, ***Zgc***, tending to zero. There will then be a current flow in the ground conductor mainly due to the magnetic flux coupling, but the loss will be zero because the resistance of the ground conductor is zero.

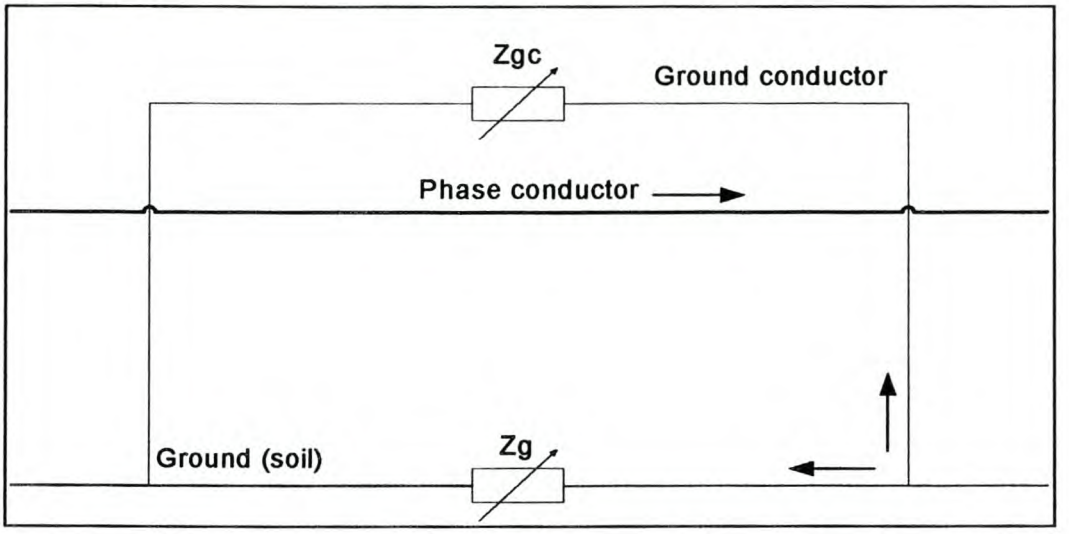

Figure 5.4 Single conductor with one ground conductor above the ground plane.

From the explanations in the previous paragraph it can be concluded that for either low or high values the supplementary loss due to the ground conductor impedance tends to zero. There must therefore be a maximum value for the loss in between the two extreme cases. The same argument can be used for the loss introduced by the soil resistivity. Thus, there also exists a maximum loss in between the two extreme cases of soil resistivity.

For Figures 5.5 to 5.7:
In these Figures the mesh grid represents the attenuation of the transmission line with a ground conductor and the surface plot represents the attenuation of a transmission line without a ground conductor. *The surface plot, transmission line with no ground conductor, can be used as a reference plane.*

5.4.3 Mode 2 attenuation for the variation in the soil resistivity and ground conductor conductivity

Studying Figure 5.5 it will be noted that for all the extreme cases (extreme values of conductivity and soil resistivity) mode-2 attenuation is close to the no-ground conductor reference plane. For the high ground conductor conductivity and low ground resistance the current will flow in both mediums with low losses. The loss is defined as $Loss = I^2R$ and for the previously case R is insignificant in both mediums (ground conductor and soil) and therefore the loss is negligibly small. This part of Figure 5.5 is identified with a number '1' printed on the graph, for future references the notation ('1' as in Figure 5.5) will be used. If the resistance of the soil is very large and the conductivity of the ground conductor is very low most of the current will flow in the ground conductor. But the loss will still be very small because of the high conductivity of the ground conductor ('2' in

Figure 5.5). The same explanation follows for the low attenuation at point '3' in Figure 5.5.

For the single-conductor case described in Subsection 5.4.2 (Figure 5.4) the loss in the system will be high for low values of the ground conductor conductivity (high resistivity) and for high soil resistivities because the return current must return via one of the two mediums.

For the multi-conductor case the situation is different. For the low values of ground conductor conductivity and high soil resistance the current can still return via the other phase conductor for the differential mode (mode 2). Thus the upper right hand square in Figure 5.5 (which cannot be seen due to the angle of the plot) is also close to the reference plane (transmission line with no-ground conductor).

The maximum attenuation in the ground conductor conductivity, occurs at σ = 7196,85 S/m ('4' in Figure 5.5) and in ground resistivity, at ρ = 268 Ω- m ('5' in Figure 5.5). Both steel and aluminium conductors have conductivities much higher than 7196,85 (typically for steel σ = 5e6 (ρ = 2e-7) and for aluminium σ = 35e6 (ρ = 2.85e-8)). The maximum attenuation peak occurring in the x-axis (due to the soil resistivity) is a physically realistic value where the peak in the y-axis due to the conductivity is not. The ground resistivity is one of the parameters in the PLC system that is difficult to determine due to the fact that it can vary. Figure 5.5 shows that the attenuation in mode 2 can vary by approximately 3 dB for soil resistivity variation. It will also be observed that the crest of maximum attenuation is not as sharp as on the y-axis. Small variations in the ground resistivity will thus not influence attenuation in mode 2 dramatically.

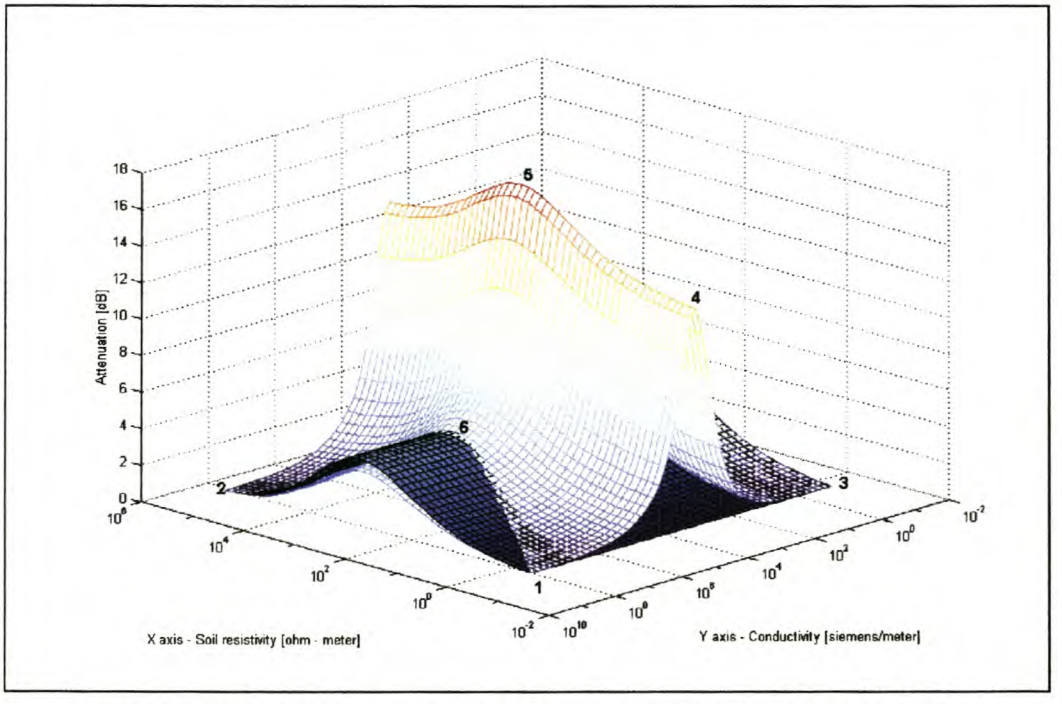

Figure 5.5 Attenuation of mode 2 if the soil resistivity and the ground conductivity are varied. (Permeability = 1)

It should be noted that the reference plane cuts the mesh grid at high conductivity values for the ground conductor with intermediate values of the soil resistivities ('6' in Figure 5.5). This means that the attenuation for a ground conductor with good conductivity properties and no magnetic properties (permeability = 1) is less than the no-ground

conductor case. This explains why mode 2 attenuation for the aluminium conductor is just less than the no-conductor case in Figure 5.3.

5.4.4 Mode 3 attenuation for the variation in the soil resistivity and ground conductor conductivity

The attenuation for mode 3 is very high and this is why it is called the "high loss mode". The scale difference in the z-axis (attenuation) is clearly evident from Figures 5.5 and 5.6. Points '7' in Figure 5.6 and '9' in Figure 5.6 can be explained in the same way as point '1' in Figure 5.5 and '3' in Figure 5.5. The maximum attenuation in the x-axis, occurs at 6000 Ω-m ('11' in Figure 5.6). The soil resistivity is varied with the same amount, 1 to 10e4, in Figure 5.5 and Figure 5.6. It can be seen that the attenuation dropped at point '8' in Figure 5.6 and will eventually meet the zero attenuation for higher values. Therefore the same argument used to explain point 2 in Figure 5.5 is still valid.

For high soil resistivity and low ground conductor conductivity the attenuation will be high and above the reference plane. For mode 3 propagation (1,1,1) the current must return via the ground conductor or the soil, the same as the simplified model in Figure 5.4. Thus if both paths contain high resistance then the loss of mode 3 must also be high, ('10' in Figure 5.6).

At point '11' in Figure 5.6 the reference plane cuts through the mesh grid. This indicates that mode 3 attenuates (with a ground conductor with good conductivity properties and no magnetic properties) less than the no ground conductor case. This phenomenon is understandable as it indicates that the return current (initiated by mode 3) flowing through a good ground conductor (high conductivity properties) experiences less loss than flowing through soil ('11' in Figure 5.6). This also explains the lower attenuation in mode 3 for the aluminium ground conductor shown in Figure 5.3.

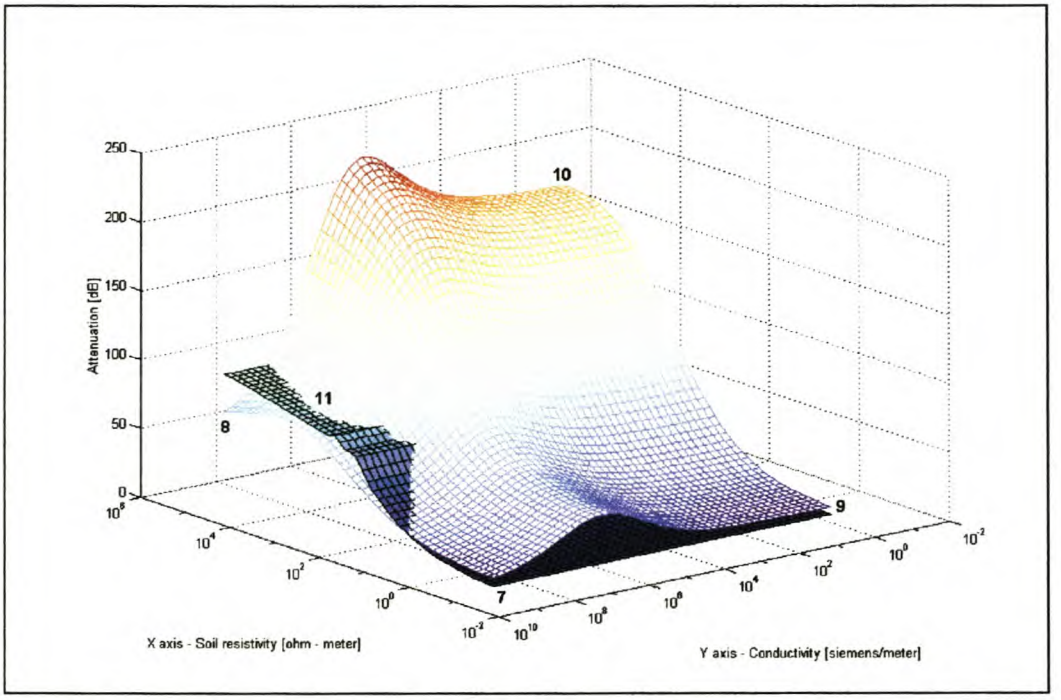

Figure 5.6 Attenuation of mode 3 if the soil resistivity and the ground conductivity are varied. (Permeability = 1)

5.4.5 Mode 2 attenuation for the variation in the soil resistivity and ground conductor permeability

Figure 5.7 demonstrates mode 2 attenuation of a ground conductor with a fixed resistivity of 2e-7. This is an approximated value of the resistivity for a steel conductor. The conductor impedance is directly proportional to the permeability. Therefore an increase in permeability will result in an increase in impedance and the same explanations as previously discussed can describe the shape.

The maximum attenuation in the x-axis, ground resistivity ('12' in Figure 6), occurs at σ = 268 (the same as in Figure 5.5). For the y-axis the maximum permeability value occurs at μ=3,9e3 ('13' in Figure 5.7). For a permeability of 1000 (typical for a steel ground conductor) the attenuation is much higher than the reference plane. In Figure 5.3 it can be seen that mode 2 attenuation for a steel conductor is a great deal more than the no conductor case.

The maximum crest for both parameters is not very sharp (round ball shape at '14' in Figure 5.7). For a permeability of 1000 the maximum attenuation is 9.04 dB. 99% of the maximum attenuation value is 8.95 dB and occurs at soil resistivities of 240 and 660 ohm meter. Therefore it can be concluded that mode 2 attenuation is not very sensitive to change in the soil resistivity.

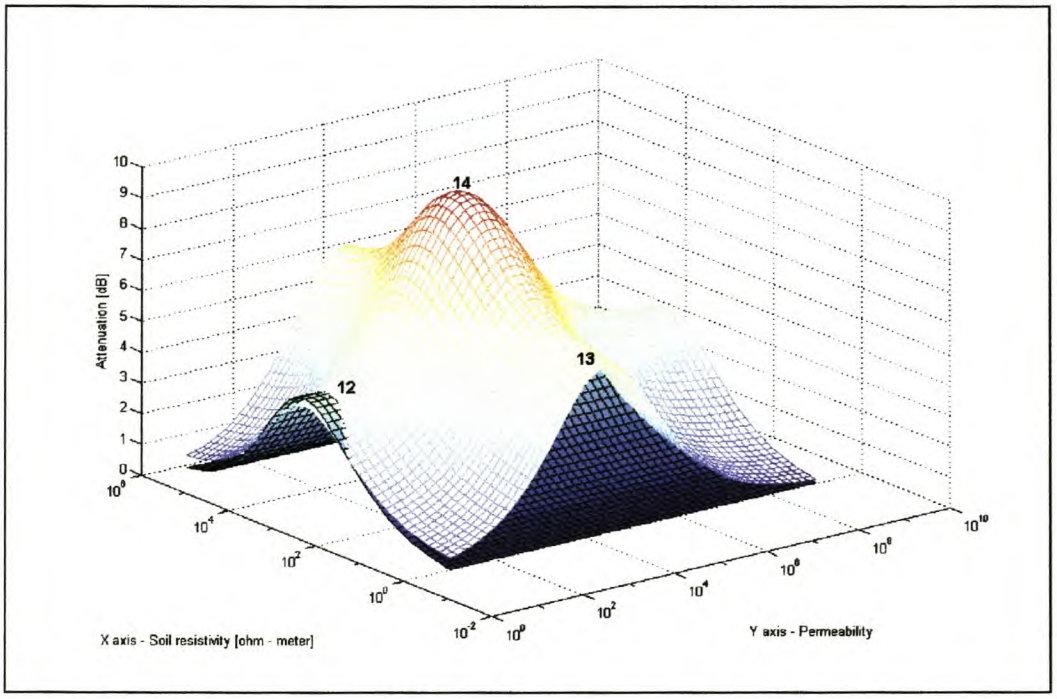

Figure 5.7 Attenuation of mode 2 if the soil resistivity and the permeability are varied (conductivity = 2e7).

5.4.6 Current division between the ground conductor and soil

A different viewpoint will be described to explain the effects introduced by the ground conductor and soil resistivities in general.

A way to think about the effects due to the difference in ground conductor and soil resitivity properties is to formulate the loss introduced in the system by the two paths independently. Consider the simplified system as demonstrated in Figure 5.4 again.

The total current at any point of the transmission line, Figure 5.4, must be zero therefore eqn. 5.14 can be formulated as

$$0 = I_p + I_{gc} + I_g \tag{5.14}$$

where

I_p = current in the phase conductor

I_{gc} = current in the ground conductor

I_g = current in the ground(soil)

The loss introduced to the PLC system through the ground conductor and soil can be stated as

$$Loss = |I_g|^2 R_g + |I_{gc}|^2 R_{gc} \tag{5.15}$$

From equation 5.15 it shall be observed that the presence of the ground conductor can either reduce or increase the loss. It all depends on the current splitting (the relative relationship between $|I_g|$ and $|I_{gc}|$) and the values of the resistance of the two media.

5.5 Conclusion

A subprogram was developed to investigate the resonance effects due to discretely bonded ground conductors. The theory used in the simulation is briefly discussed [1]. The graph in Figure 5.2 indicates that the resonance effect for the Koeberg -Acacia PLC system occurs at approximately 445.5 kHz and is mainly influenced by the "high loss mode", mode 3.

The phenomena of different attenuations of the modes are demonstrated and are due to changes in the ground conductor and soil parameters. Mode 1 attenuation is not influenced by the changes because the two ground conductors are very close to the magnetic equipotentials of the Faraday induction currents in the phase conductors therefore low magnetic flux coupling occurs.

Modes 2 and 3 indicated noticeable changes and were studied for various combinations of parameters. It is interesting to note that a region exists where the attenuation of the no - ground conductor case is more than a transmission line with a ground conductor. This can be understood by noting that return current is taken "away" from the soil via a ground conductor and it results in less total attenuation. The effect is more prominent when aluminium ground conductors are installed due to the fact that aluminium's impedance is less than steel.

5.6 Reference

[1] **L.M. Wedepohl**, "Wave propagation in polyphase transmission systems – Resonance effect due to discretely bonded earth wires", IEE proceedings, Volume 112, No. 11, December 1965, pp. 2113-2119.
[2] **L.M. Wedepohl**, The Theory of Natural Modes in Multi-Conductor Transmission Systems, unpublished lecture notes, Westbank, British Columbia, Canada, 10 January 1999.

Chapter 6

Design of the Acacia-Koeberg experiment

6. 1 Introduction

The experiment is aimed at monitoring the PLC signal attenuation variation and effects like modal cancellation that may occur, over a long period of time.

The design of the experiment can be divided in two parts. The first part will focus on how an additional signal is introduced into the system and the influence it will have. The second part describes the signal generation and monitoring (logging).

Part 1 (sections 6.2 and 6.3)

The first step of the experiment was to propose an experimental layout (Section 6.2). Mr Dave Smith from Eskom proposed this basic experimentation layout and De Villiers had to do the calculations to determine how it would influence the operational system (Section 6.3). These calculations were the main test for the feasibility of the experimental layout. The results from the simulations and the calculations (Section 6.3) showed that the experiment would not influence the system noticeably.

Part 2 (section 6.4)

The design of the signal generator and the logging of the attenuation will be described. This section is divided into subsection 6.4.1 (describing the transmitter) and subsection 6.4.2 (describing the receiver).

6.2 Experimental layout

6.2.1 Standard coupling scheme.

The standard coupling scheme [1] that Eskom uses on the Koeberg-Acacia PLC-link system is demonstrated in Figure 6.1. The symmetrical hybrid, A1AC manufactured by BBC, in Figure 6.1 is generally referred to as a "phase combiner". The name is quite descriptive as the symmetrical hybrid combines the signals from the two phases. In this thesis the symmetrical hybrid in Figure 6.1 will be referred to as the "phase combiner".

The phase combiner splits the power received at port 1('p1' in Figure 6.1) equally to ports 2 and 3. Thus the loss of signal power from port 1 to port 2 and port 1 to port 3 is approximately 3 dB. The loss between ports 2 and 3 is called the trans-hybrid loss and is approximately 23 dB. The phase combiner is wired in such a way that it introduces a 180° phase shift to port 2 relative to the signal phase of port 1. The phasing of the signal at port 3 is the same as at port 1.

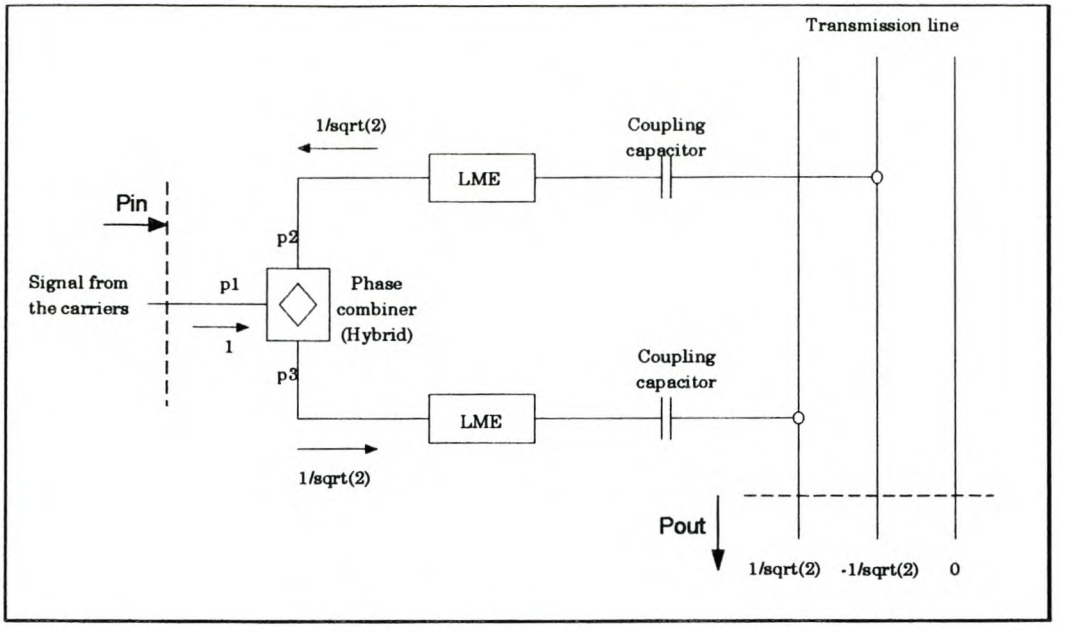

Figure 6.1 Standard coupling scheme

In Figure 6.1 the power inserted into the system is called *Pin* and the power delivered to the transmission line is called *Pout*. It is assumed that the line matching unit, coupling capacitor and coaxial cables are ideal. Therefore it can be shown that *Pin* equals *Pout*.

$$Att = 10\log\left[\frac{Pin}{Pout}\right] \text{ dB} \tag{6.1}$$

and by substituting the voltage ratios as indicated in Figure 6.1 in eqn. 6.1 the loss can be formulated as:

$$Att = 10\log\left[\frac{1}{\left(\frac{1}{\sqrt{2}}\right)^2 + \left(-\frac{1}{\sqrt{2}}\right)^2 + 0}\right] = 0 \text{ dB} \tag{6.2}$$

There will be modest losses in an operational system but the phase combiner in Figure 6.1 is idealized. The phase combiner operates in the same way as a 3 dB power splitter.

6.2.2 Important coupling condition for the new coupling scheme

From natural modal theory, as described in Chapter 3, it is known that any signal that is coupled to the HV transmission line will couple to its natural modes. This concept will be used to calculate the distribution of a coupled signal in its natural modes.

Studying Figure 6.1 the coupling vector can be derived as:

$$C_c = \begin{bmatrix} 1 \\ -1 \\ 0 \end{bmatrix} \tag{6.3}$$

The $\frac{1}{\sqrt{2}}$ quantity shown at the transmission line in Figure 6.1 is normalized to 1 as in eqn. 6.3. The coupled vector will distribute according to its natural modes, ***M***, (Section 3.3) on the transmission line.

The vector A in the equation 3 contains the modal distributions,

$$C_c = [M][A] \tag{6.4}$$

where A is a column vector. For the standard coupling configuration as shown in Figure 6.1 ***A*** can be calculated as

$$A = \begin{bmatrix} 0.5 \\ 1 \\ 0 \end{bmatrix}$$

The power distribution of the different modes can be calculated as:

$$Mode1 = \frac{\sum_{i=1}^{3} A(1,1)M(i,1)C_c(i,1)}{\sum_{i=1}^{3} A(i,1)^2} 100 = 75\% \tag{6.5}$$

$$Mode2 = \frac{\sum_{i=1}^{3} A(2,1)M(i,2)C_c(i,1)}{\sum_{i=1}^{3} A(i,1)^2} 100 = 25\% \tag{6.6}$$

$$Mode3 = \frac{\sum_{i=1}^{3} A(3,1)M(i,3)C_c(i,1)}{\sum_{i=1}^{3} A(i,1)^2} 100 = 0\% \tag{6.7}$$

It can be observed that three quarters of the power is contained in mode 1. Mode 1 is the lowest attenuated mode. It makes sense to couple in such way that mode 1 contains a major part of the signal. It is also a safe way to couple in order to prevent effects like modal cancellation. Modal cancellation is more likely to occur when mode 2 is exited with a larger amplitude mode 1 [2]. Modal cancellation will typically occur between those modes.

For the experiment a signal must be coupled in such a way that the power in mode 2 is more than in mode 1 and therefore increases the possibility for effects like modal cancellation to occur.

For a single phase coupling on the outer phase C_c in eqn. 6.3 will change to

$$C_c = \begin{bmatrix} 1 \\ 0 \\ 0 \end{bmatrix} \tag{6.8}$$

By using Eqns. 6.5 and 6.7 the power distribution in the modes are calculated as: mode 1 = 16.6%, mode 2 = 50% and mode 3 = 33.33%. Modal distribution for the centre phase coupling is calculated in the same way. It is: mode 1 = 66.6%, mode 2 = 0% and mode 3 = 33.3%.

From these calculations it is concluded that the only coupling that will contain a possibility for modal cancellation is the single phase coupling to the outer phase.

6.2.3 Coupling configuration proposed by Mr Dave Smith

With this coupling arrangement in mind Mr Dave Smith from Eskom proposed the following scheme. As shown in Figure 6.2 he suggested the incorporation of an additional hybrid into the operational PLC system.

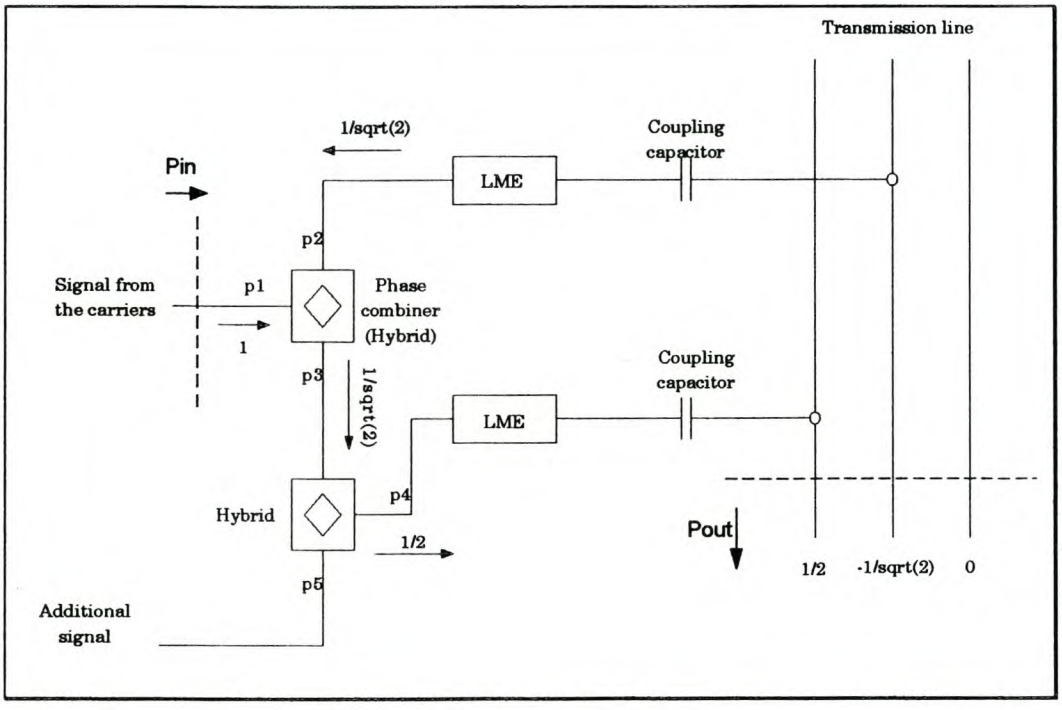

Figure 6.2 Experimental layout to include the additional signal

An additional symmetrical hybrid is inserted between port 3 ('p3' in Figure 6.2) of the phase combiner and the LME of the outer phase. The newly inserted symmetrical hybrid is exactly the same as the phase combiner. Port 5 of the hybrid gives access to an additional signal to be coupled to the outer phase of the transmission line.

The trans-hybrid loss between ports 3 and 5 provides isolation between the operational carriers that are connected to port 1 and the additional signal that is connected to port 5.

The hybrid will introduce an extra 3 dB loss for the signal power transmitted to the outer phase. This then introduces a non-standard and unbalanced coupling vector to the transmission line.

Before the proposed coupling layout could be installed on Eskom's system the effect(s) had to be quantified to ensure that Eskom would take no risks with the installation. In the following section the influence of the hybrid will be discussed and quantified.

6.3 Calculation of the additional insertion loss introduced by the experiment.

The insertion loss due to the experiment (see Figure 6.2) can be divided into two parts. The first part is the power loss introduced in the outer phase and the second part of the insertion loss is due to the unbalanced coupling configuration.

6.3.1 Power loss in the outer phase:

From Figure 6.2 it shall be seen that the coupling vector is

$$C_c = \begin{bmatrix} \frac{1}{2} \\ -\frac{1}{\sqrt{2}} \\ 0 \end{bmatrix}$$

Using eqn. 6.1 under the aforementioned conditions the attenuation of *Pin* to *Pout* in Figure 6.2 can be calculated as:

$$Att = 10\log\left[\frac{1}{\left(\frac{1}{2}\right)^2 + \left(-\frac{1}{\sqrt{2}}\right)^2 + 0}\right] = 1.25 \text{ dB}$$

Because the power loss between *Pin* and *Pout* was 0 dB for the standard coupling configuration (eqn. 6.2) the introduced power loss is 1.25 dB for the new configuration.

6.3.2 Additional attenuation due to the unbalanced coupling vector

Because the transmission line is so short it can be expected that the extra loss due to the transmission line should be very small, but it had to be confirmed.

In the simulations the following parameters were used. The average phase-conductor height above the ground plane is 11 m. The earth's resistivity is taken as 100 ohm meters. The rest of the line data used in the simulation program were described in Chapter 2.

In order to compare the line attenuation of the PLC signals, unity power is coupled to the line in both cases (standard and experimental coupling configurations). Both the coupling vectors must represent the voltage distribution and must satisfy the condition in eqn. 6.9 for unity power.

$$1 = \sqrt{(V_1)^2 + (V_2)^2 + (V_3)^2} \tag{6.9}$$

V stands for the voltage vector. The subscripts indicate the different phases of the transmission line.

For the non-standard coupling configuration V_2 must be double the power of V_1. By using eqn. 6.9, eqn. 6.10 can be reformulated as

$$1 = \sqrt{(x)^2 + (2x)^2 + (0)^2} \tag{6.10}$$

where x can be calculated as 0.447. Finally the coupling vector for the non-standard configuration can be given as

$$C_{\text{non-standard}} = \begin{bmatrix} 0.45 \\ -0.89 \\ 0 \end{bmatrix}$$

The coupling vector ($C_{\text{non-standard}}$) is used in the simulation program.

Figure 6.3 shows the line attenuation for the standard and non-standard coupling configurations. The simulation is done for an average conductor height of 11m and 100 ohm-meter soil resistivity. In Chapter 7 it will be shown that measurements indicated that the above-mentioned parameters are those most likely describing the current conditions of the Koeberg-Acacia PLC system.

It was noted that the simulations indicated less attenuation for the non-standard coupling configuration (1,0,0) than the standard coupling configuration (1,-1,0).

What this result practically means is that the standard coupling configuration is not the optimum-coupling configuration. In [3] it is proven that with the use of "Lagrange multipliers" the optimum coupling for a two phase installed PLC system is equal to the non-standard coupling configuration. The reason why Eskom is using the (1,-1,0) coupling scheme is because there is better communications reliability under fault scenarios.

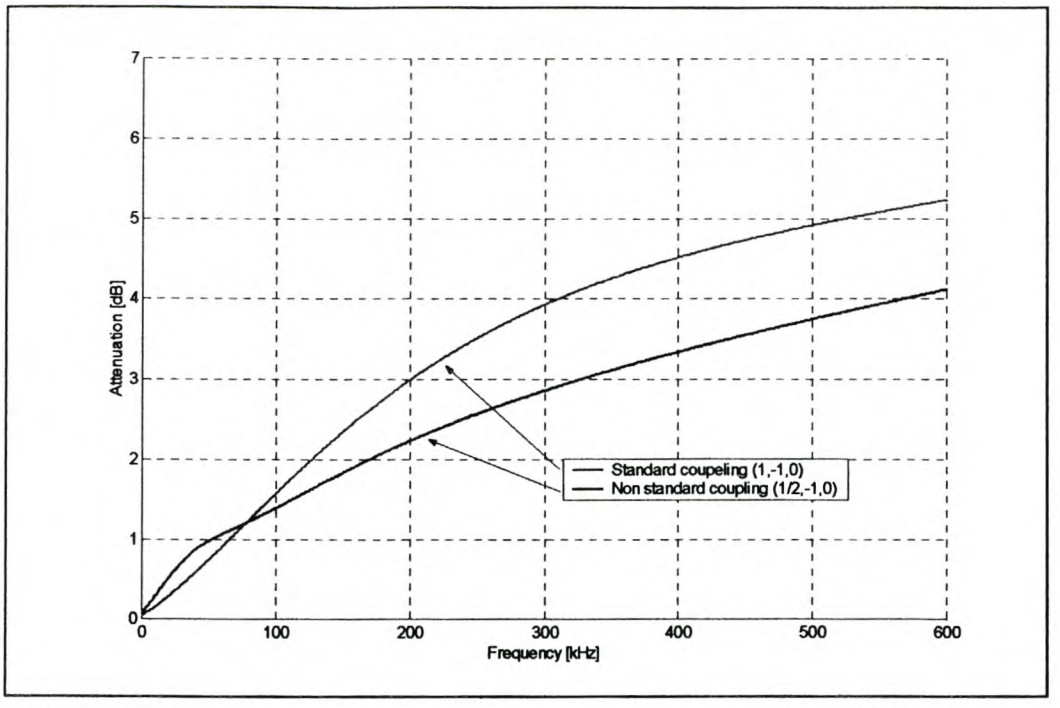

Figure 6.3 Simulation of the standard coupling configuration (1,-1,0) and the non standard configuration(1/2,-1,0) due to the experiment.

6.3.3 Total additional insertion loss introduced by the experiment

The total additional insertion loss can now be calculated. Figure 6.4 is a diagrammatic representation of the losses that the operational PLC signals will experience due to the presence of the experiment (Figure 6.2).

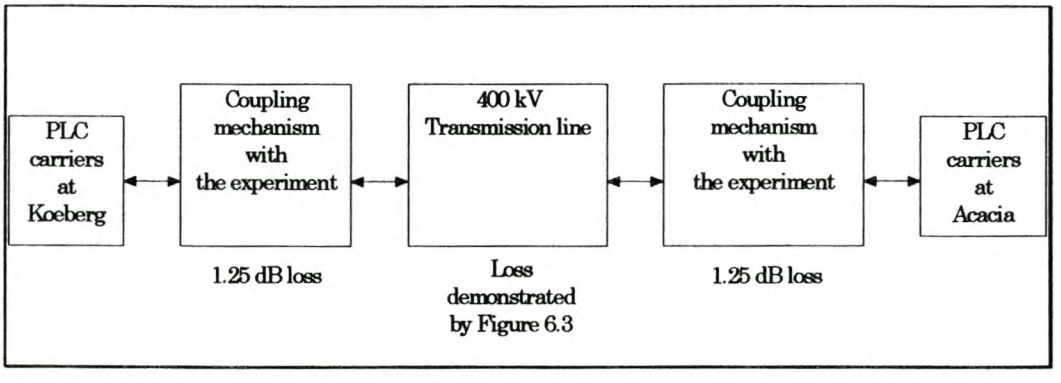

Figure 6.4 Representation of the losses introduced by the experiment

The summation of the total losses is shown in Figure 6.4. The following section will discuss the design of the monitoring system.

6.4 Design of the monitoring system

In part 1 it was shown that that the two additional hybrids (Figure 6.2), one at each side, give access to a single phase coupling on the outer phase.

This section will describe the design of the experimental transceiver system. Figure 6.5 describes the overall experimental layout. The experimental layout can be subdivided between the transmitter and the receiver. The transmitter and the receiver will be described, respectively, in sections 6.4.2 and 6.4.3.

6.4.1 Specifications of the monitoring system

The transmitter at Koeberg power station must have the following characteristics

- An output resistance of 75 ohms. The characteristics of the hybrid described in section 6.2.3 are only valid if the terminals of all three ports (of the hybrid) are terminated in 75 ohms.
- The ability to sweep through a frequency spectrum slowly. The goal of the experiment is to monitor a specified spectrum of the frequency band in order to establish the variation in attenuation. For example, the spectrum of 400 kHz to 500 kHz must be swept in a time period of 15 min.

The receiver at Acacia sub-station must have the following characteristics

- 75 ohm input impedance.
- The ability to measure the signal strength and its location in the frequency spectrum of the received signal (from the transmitter).
- The ability to log the above stated measurement (in dBm) and the location in the spectrum (in Hz) and the time that it logged the data.

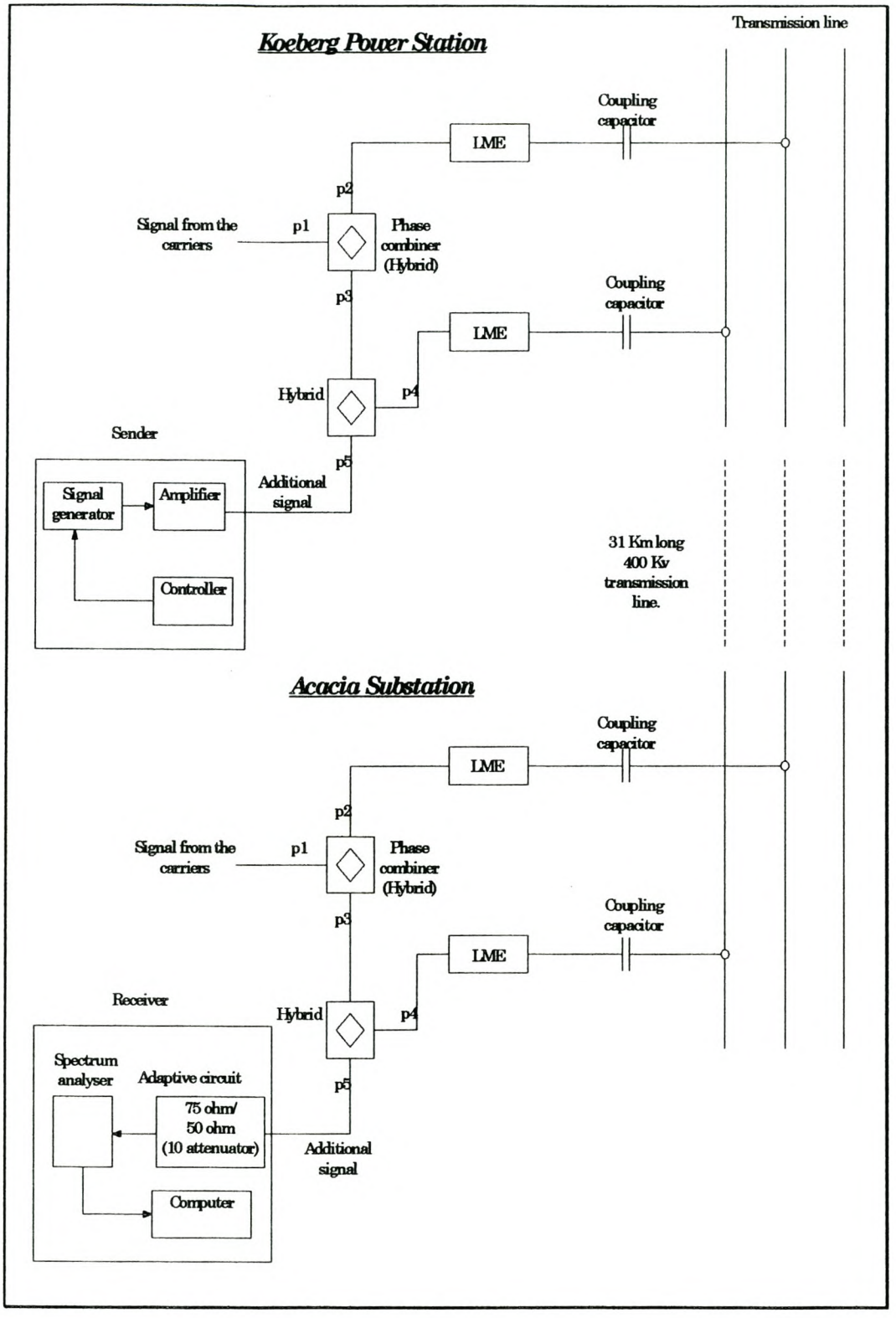

Figure 6.5 Experimental layout

6.4.2 Transmitter

The transmitter comprises a controller, signal generator and amplifier (Figure 6.5). The transmitter is located at Koeberg power station. The reason for locating the transmitter at Koeberg is due to the difficulty to gain frequent access (tight security). Once the experiment is running the results should be downloaded on a frequent basis. Acacia sub-station is more convenient for frequent access. It is thus practical to locate the transmitter at Koeberg power station and the receiver at Acacia sub-station.

The first problem was to get a signal generated that has the ability to satisfy the design specifications. Most of the systems in use at US are based on 50-ohm characteristic impedance. Eskom on the other hand had some equipment and measurement devices that are based on 75-ohm characteristics. During a visit to Eskom by W de Villiers one of the older signal generators in the store was investigated. It has an output impedance of 75 ohm and an external frequency control input for the matching transmitter. This signal generator PS-3, manufactured by Wandel u. Goltermann was ideal for the purpose of the experiment and its functionality could be exploited.

The idea is to generate (with a function generator) the external frequency control input signal for the signal generator that is usually generated via the matching unit (SPM-3 selective level meter). Frequency location control will thereby be gained via the function generator. The following discussion describes how the signal generator (PS-3) functions and how it is used in the experimental setup.

Beat-frequency generator (PS-3) [4]

The beat-frequency generator (PS-3) generates its operating frequency (f_s) 0.3 to 612 kHz from the difference between two oscillator frequencies (eqn. 6.11), both oscillating above the operating frequency.

$$f_s = f_\Omega - f_\omega \tag{6.11}$$

The signal oscillator (f_ω) is approximately fixed at 650 kHz and can be varied by +/- 4 kHz via a control knob located on the front panel. The other frequency, carrier oscillator (f_Ω), is tuneable between 650.3 and 1262 kHz. The desired operating frequency of the generator is adjusted by changing the carrier frequency. If the signal generator PS-3 is used in conjunction with the selective level meter SPM-3, then the variable carrier oscillator in the PS-3 can be replaced by the carrier oscillator in the selective level meter via an additional external-control wires between the two units.

This mechanism creates an opportunity to control the frequency of the generator. Instead of substituting the carrier oscillator in the generator with the carrier oscillator in the SPM-3, the carrier oscillator signal is generated with two signal generators. The discussion to follow will explain the details of the control circuit.

Control circuit

The control system must produce an output signal between the operational regions 650.3 and 1262 kHz of the generator. This control signal will substitute the internal signal f_Ω (eqn 6.11). The frequency of the control signal can then be varied between two specified boundaries. Using eqn. 6.11 the boundaries for the control signal can be specified.

A voltage-controlled oscillator (VCO) is used to generate the required control signal.

Mathematically, a VCO can be described by eqn 6.12 [5].

$$K_V e_v(t) = 2\pi f = \omega \tag{6.12}$$

The output frequency, ω, is proportional to the input signal, $e_v(t)$. The parameter, K_v, is known as the VCO constant. The unit of K_v is radians per second per unit of input.

A voltage-controlled frequency (VCF) generator (Model 123) is used and is manufactured by "Exact Electronics". The only difference between the VCF generator and the VCO described in eqn. 6.12 is that an offset frequency can be set with K_{pre}. Eqn. 6.13 demonstrates this:

$$\omega = K_v e_v(t) + K_{pre} \tag{6.13}$$

For the VCF generator K_{pre} can be adjusted and K_v is constant. K_v can easily be determined by means of measurements. The maximum and minimum value of signal $e_v(t)$ can accordingly be determined to the specification of the required signal.

An example

The experimental transmitter settings are not fixed and are subjected to change according to the transmission line configuration. In order illustrate this explanation an example will be discussed showing the settings of the different units used in the transmitter configuration.

For example: Generate a signal that sweeps between frequencies 400 and 500 kHz in a 15 second period.

With the use of eqn. 6.11 the control signal's frequency (for the PS-3 generator) can be calculated as 1050 and 1150 kHz. The preset frequency of the VCF generator can be set to 1028 kHz and the unknown parameter constant, K_v (in eqn. 6.13), can then be empirically determined as 183. From eqn. 6.13 the maximum and minimum values of e_v can be calculated as 0.12 and 0.67V respectively. The specific sweep function (model 121 manufactured by "Exact Electronics") can be set to generate the sinusoidal signal variation (0.12 to 0.67V) in a period of 15 seconds. Figure 6.6 shows the interaction between the different components in the transmitter layout described.

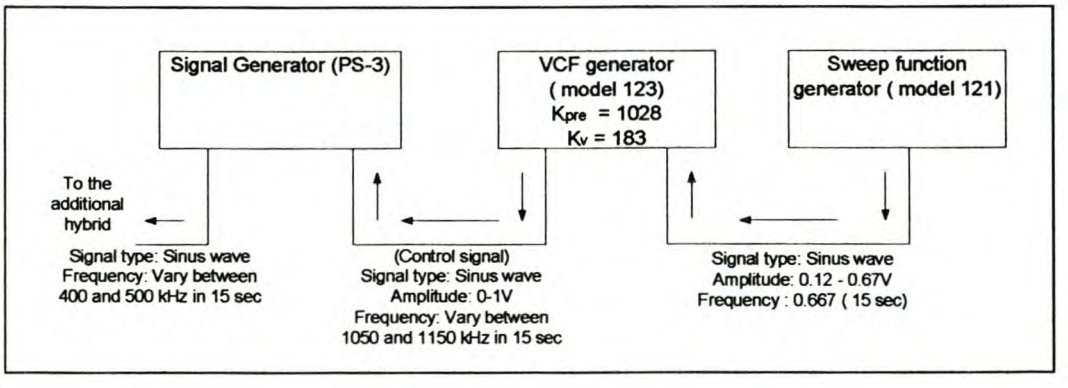

Figure 6.6 An example of the transmitter configuration.

6.4.3 Receiver

The receiver consists of an impedance matching circuit, spectrum analyser and a computer. The two issues that must be taken into account before connecting the spectrum analyser to the PLC system are:

Firstly, the input power of the spectrum analyser is limited to 1W (30 dBm). Next to this sensitive piece of equipment is a carrier that delivers 20W power into the PLC system. Thus the power levels of the different sources must be calculated carefully.

Secondly, the characteristic impedance of the spectrum analyser is 50 ohms. If the spectrum analyser is connected directly to the system with 75-ohm characteristic impedance, the hybrids will be unbalanced. Consequently, it will influence Eskom's operational PLC system. This must be used as design specification for an impedance matching circuit that will match the spectrum analyser to the PLC system.

A short description of the contents that follows in this section is as follows: The power levels will be calculated. According to the results of the power calculations and above mentioned design criteria an impedance matching circuit will be designed. Lastly, the program (in HPVEE) designed to log the data from the spectrum analyser to the computer will be discussed.

Power levels in the system.

The local (Acacia) and the remote (Koeberg) carrier delivering 20 watt each are the main sources responsible for high power levels in the PLC – system and must therefore be considered in order to protect the spectrum analyser. The spectrum analyser is limited to 1W (30 dBm) power input to its port. The induced signals on the specific line due to neighbouring carriers are small in comparison with the operational carriers on the transmission line. The two carriers operate at different frequencies and for this reason the power calculation can be done independently of each other. At Acacia sub-station the transmission band is specified as 344-348 kHz and the receiving band as 348-352 kHz.

The attenuation of the impedance matching circuit can be designed for acceptable power levels. Figure 6.7 shows the power levels in the circuit layout introduced by the local carrier at Acacia sub-station.

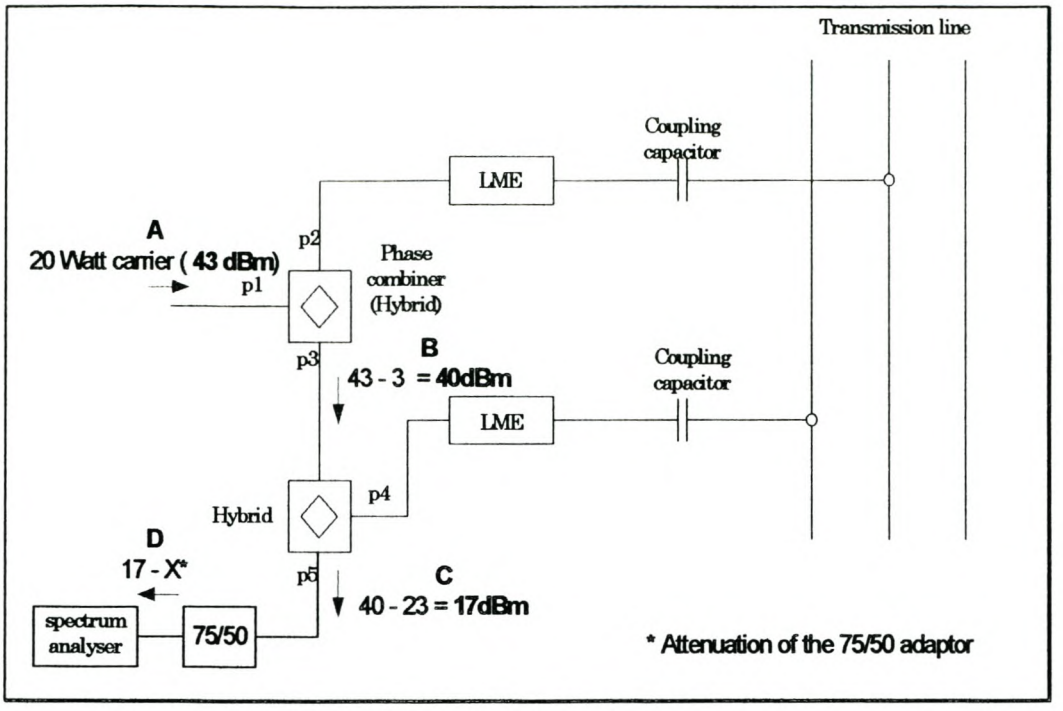

Figure 6.7 Power levels at Acacia sub-station

The operational carrier transmits 20-watt power ('A' in Figure 6.7). The phase combiner introduces an attenuation of 3 dB ('B' in Figure 6.7) and the additional hybrid adds a 23 dB trans-hybrid loss ('C' in Figure 6.7). The power level at point C in Figure 6.7 is far below 30dBm and is therefore not problematic. Figure 6.8 illustrates the power levels introduced by the remote carrier located at Koeberg power station. This calculation is a bit more involved because the attenuation of the transmission line must be considered.

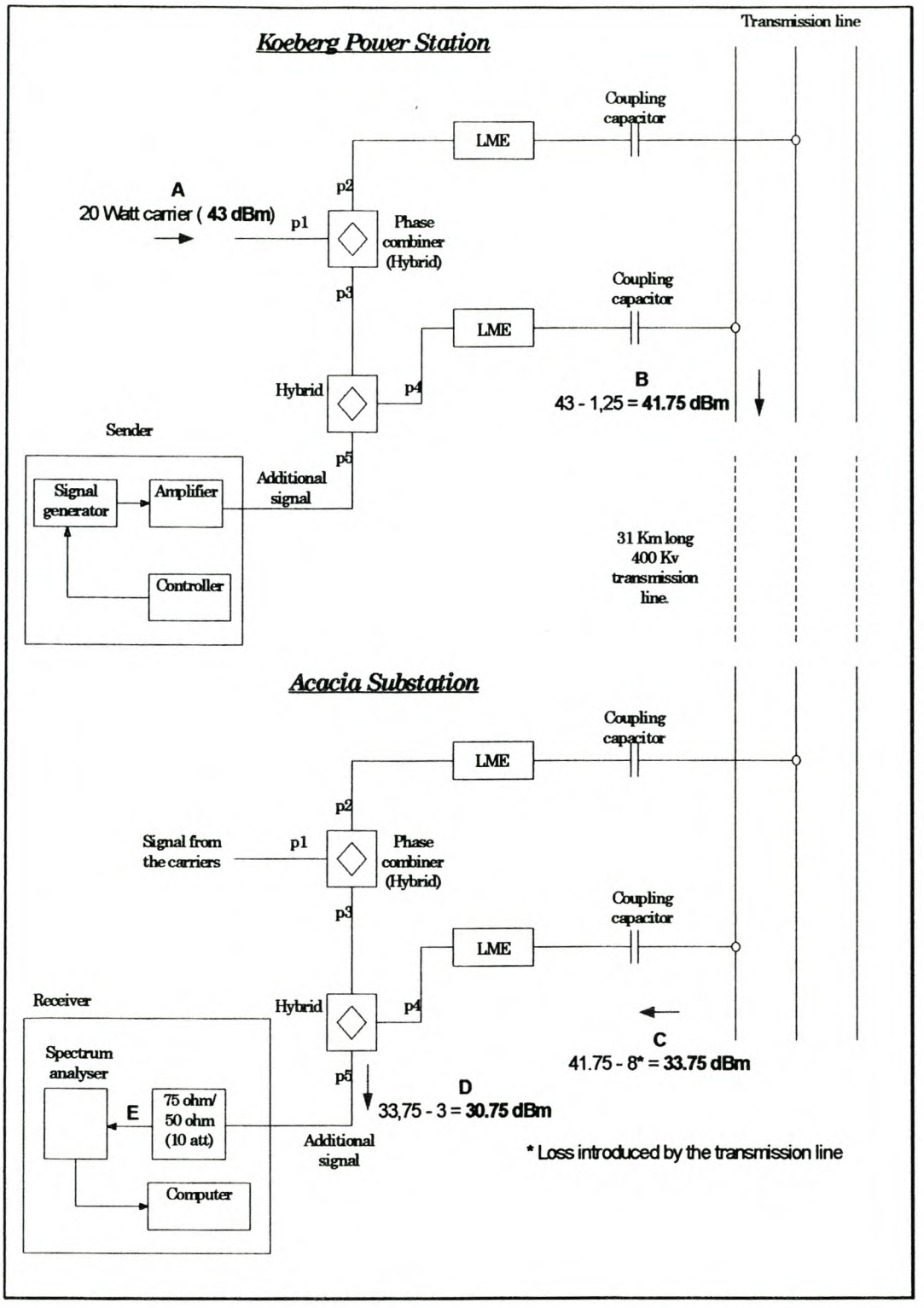

Figure 6.8 Power level due to the remote carrier at Koeberg power station.

The total power coupled to the transmission line is 1.25 dB less than the transmitting power from the carrier ('B' in Figure 6.8) due to the additional hybrid in the lower branch of the coupling path at Koeberg. The line attenuation for the following coupling scheme

must be calculated, at Koeberg power station $\left[\frac{1}{\sqrt{2}} \quad -1 \quad 0\right]$ and $\left[1 \quad 0 \quad 0\right]$ at Acacia sub-station. The reason for considering the power only from the outer conductor is because the power from the centre conductor (to the spectrum analyser) is attenuated by two trans-hybrid losses, approximately 46 dB together.

The simulation program is used to calculate the attenuation for 100 ohm meter soil resistivity and an average conductor height of 16m. 16m is a conservative average height and for lower values the attenuation will increase. The insertion losses introduced by the coupling equipment and line traps are included.

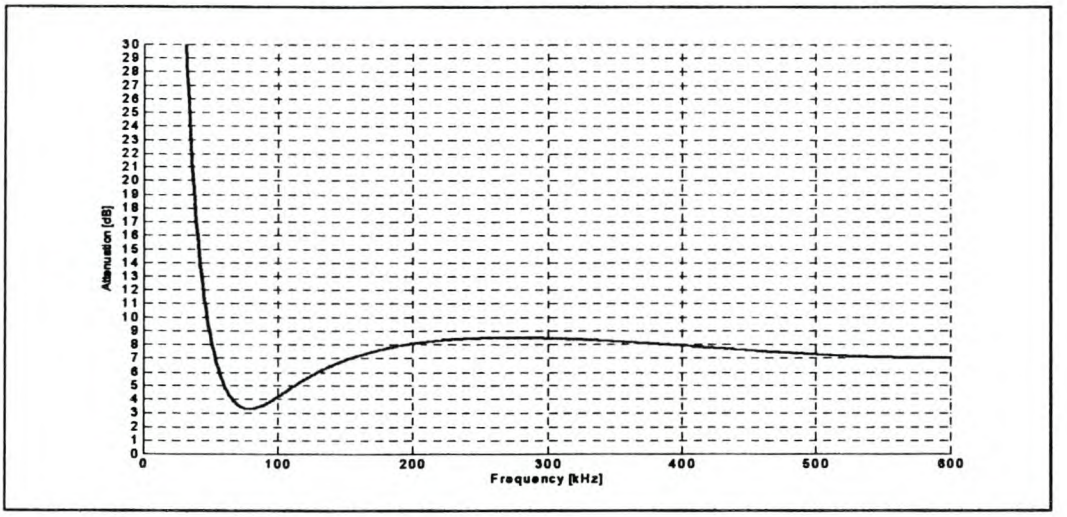

Figure 6.9 Attenuation for (1/sqrt(2),-1,0) coupling at Koeberg and (1,0,0) at Acacia sub-station.

From Figure 6.9 the attenuation can be identified as 8 dB at 350 kHz. The level at point D in Figure 6.8 is 30.1 dBm as the additional hybrid introduces another attenuation of 3 dB. Usually the transmission line introduces higher attenuation, but due to the short distance of the Koeberg-Acacia transmission line (31 km) the losses are not so large. It was decided to build a 10 dB attenuation into the impedance matching circuit (75/50) as it would provide a 9.9 dB (30 – (30.1-10)) safety factor. The design of an impedance matching circuit will be discussed next.

Impedance matching network

The specifications for the design are the following:

a) Input impedance of port 1 must be 50 ohm (to match the spectrum analyser with the system)
b) Input impedance of port 2 must be 75 ohm (to terminate the additional symmetrical hybrid correctly)
c) 10 dB attenuation.

Figure 6.10 demonstrates these design criteria.

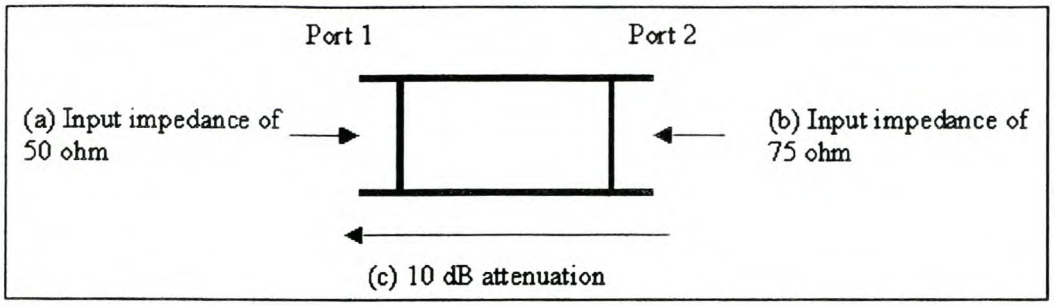

Figure 6.10 Impedance matching network (and 10 dB attenuator) illustrating the design criteria.

Figure 6.11 shows the proposed circuit layout with x, y and z as the unknown resistors.

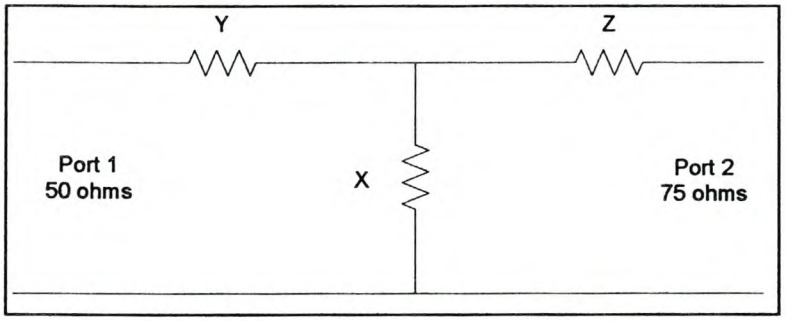

Figure 6.11 Circuit layout of the impedance matching circuit.

From the first two-design criteria the following equation can be derived.

$$50 = \left[\frac{(75+z)x}{75+z+x}\right] + y \tag{6.14}$$

$$75 = \left[\frac{(50+y)x}{50+y+x}\right] + z \tag{6.15}$$

Assuming port 2 is connected to an ideal voltage supply of 1V. The power delivered by the 1 V supply at port 2 is

$$P_{port2} = \frac{V_2^2}{75} = 0.0133 \tag{6.16}$$

Design criterion *c* specifies a 10 dB attenuation. Therefore the power at port 1 must be 10 dB less than port 1. Eqn. 6.17 incorporates this design criterion

$$10dB = 10\log\left(\frac{P_{port2}}{P_{port1}}\right) \tag{6.17}$$

and substituting eqn. 6.16 in 6.17, P_{port1} can be calculated as 0.01333 and consequentially V_1 as 0.25819. The final design equation can be formulated as the ratio of $\frac{V_1}{V_2}$. Solving the equations simultaneously produced the following results: $x = 43.3$, $y = 18.1$ and

$z = 48.6$. High wattage resistors (± 25 Watt) are used with the following combinations: $x = 33 + 10$, $y = 18$ and $z = 39 + 10$.

The matching circuit was tested after it was built. If port 1 is terminated into 50 ohms then the input resistance of port 2 is 75.5 ohms. On the other hand, terminating port 2 provides an input resistance of 50.1 ohms at port 1. The attenuation of the circuit is measured to be 9.7 dB.

Hpvee program to log the data from the spectrum analyser

HPVEE is a program that acts as an interface between the HP instrumentation and the computer [6]. This computer program contains various functions and applications in order to remotely control the instrument via the computer.

An HPVEE program was designed to log the data from the network analyser to the computer. Figure 6.12 contains the block diagram of the program. Studying the block diagram a delay block of 1 second shall be noted. This means that each second data will be logged. This delay can be adjusted. Each time the program logs data three parameters are saved on different files. The first parameter is the maximum amplitude in the specified frequency band (sweep band of the PS-3 generator). The second parameter is the location (frequency) of the maximum amplitude. Lastly, the third parameter, the time ("Now" in Figure 6.13) of each event is saved.

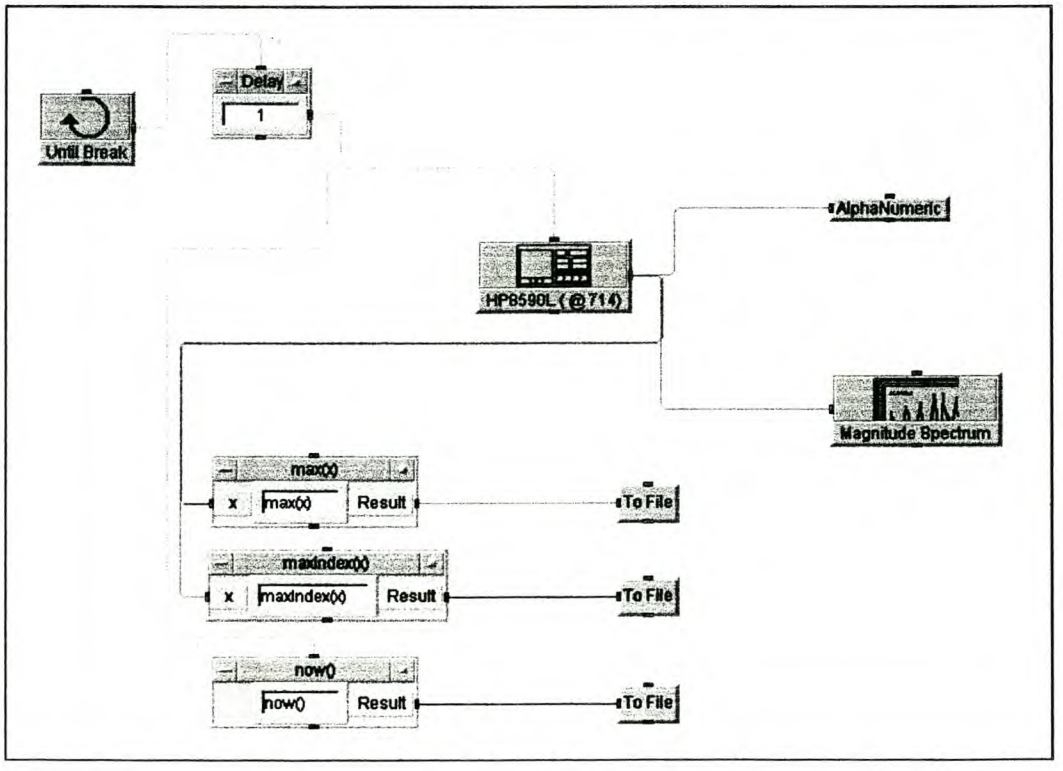

Figure 6.12 Block diagram of the HPVEE program

Saving the data in this way it ensures that the signal amplitude from the SP-3 generator is well above the noise level and also above other signals in the sweep band. The data of the complete frequency band can be saved but that makes the data analysing process very complicated and produces huge data files.

Photograph 6.1 illustrates the test setup of the HPVEE logging program. The program and the relevant functions were thoroughly tested and confirmed to be practically viable and safe before the experiment was installed in the field.

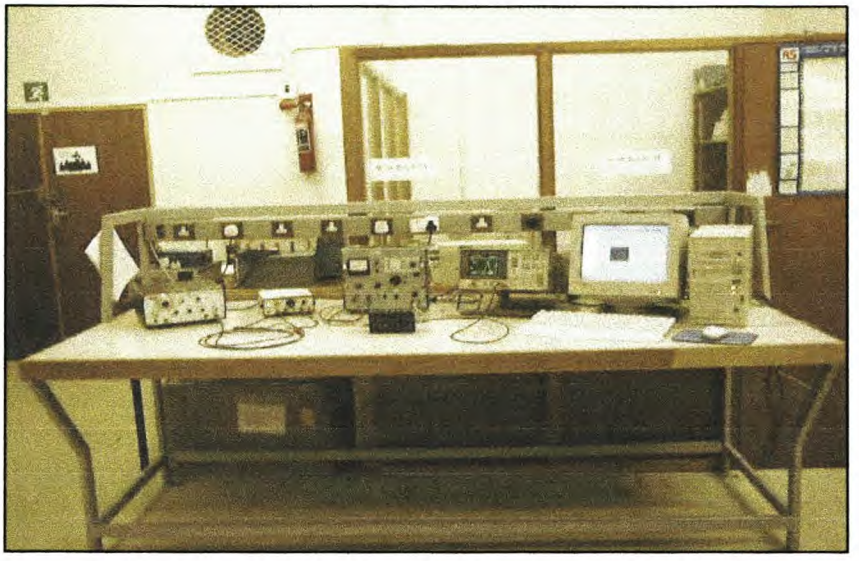

Photograph 6.1 Test setup of the logging program

6.5 Conclusion

A coupling scheme for the experiment is chosen in order to inject a signal on the existing PLC system. The coupling configuration for the injection is: single phase coupling on the outer phase (1,0,0). Simulations and calculations indicated that the operational system would not be influenced in a significant way by the presence of the experiment.

The design of a transmitting and monitoring system is discussed. An SP-3 generator's frequency is controlled (via a VCF generator and function generators). The spectrum analyser operates as a logging device and is controlled via the HPVEE program.

This experiment is designed to monitor PLC signal attenuation variation and effects such as modal cancellation that occurs on transmission lines.

6.6 Reference

[1] **Brown Boveri** (BBC) application sheet for **A9BM**, Carrier combiner Unit used for Phase to Phase Coupling, BBC stock no. henf 105 169 R1, edition 1981.
[2] **W de Villiers**, An investigation into overhead feeder ampacity control, Final year project at University of Stellenbosch, 5 November 1999.
[3] Private E-mail with Professor Martin Wedepohl, 12 December 2000.
[4]Description and operating manual of: **Signal generator 0.3 to 612 kHz**, model PS-3, manufactured by Wandel u. Goltermann, 1966/07/1.
[5] **R.E. Ziemer** and **W.H. Tranter**, *Principles of Communications*, Fourth Edition, John Wiley & Sons, 1988.
[6]Operating manual of HP-VEE program language, **HP-VEE Advanced Programming Techniques**, by Hewlett Packard Company (HP), Edition 4, May 1998.

Chapter 7

Field measurements of the Acacia-Koeberg PLC system

7.1 Introduction

Measurements indicated that the simulation program delivered trustworthy results. In this Chapter the last measurements will be shown and discussed (the other measurements made in the field are shown in appendix B).

In section 7.2 the different measurement events will be discussed. Section 7.3 shows the results of the PLC signal attenuation for single outer-phase to outer-phase coupling (1,0,0). This is an important result as it proves that the simulation program (Chapter 3 and 4) produces trustworthy results. The additional loss due to the experiment is negligible (Chapter 6) as confirmed by the measurement in Section 7.4. The tower effect, discussed in Chapter 5, is also observable in the measurements (Section 7.4).

The experiment discussed in Chapter 6 was partly activated for two weeks. The receiver logged the incoming operational signal (generated via the carrier) and not by the signal generator. Attenuation variation is evident in logged data. This is an important result as it gives strong indication that there is correlation between sag and the attenuation for the PLC signals.

After the line traps were fixed, 28 days were monitored using the experimental configuration. Another simulation program was written in Matlab to estimate the conductor temperature from measured transmission line conditions. Extremely good correlation between conductor temperature and PLC signal attenuation is observed.

7.2 Log book of the different field measurement events

In order to conduct measurements of this nature there are numerous people involved to plan contingency measures for ensuring uninterrupted supply to Eskom's clients. Eskom did all the planning of that nature and provided the skilled staff to assist De Villiers in the measurements.

Reports were written on the different events including the technical details, observations and proposals. This section gives a summary of the recorded notes.

7.2.1 Installation of the additional symmetrical hybrid on 18 February 2001

- System condition: the 400 kV transmission line was isolated.
- Primary goal: To install the additional hybrids
- Secondary goal: To measure the PLC-signal attenuation for various coupling configurations
- Observations:
  - Two damaged surge arresters located in the LMEs at Acacia sub-station.
  - Bad overall correlation between theory and measurement.
  - An attenuation peak located at 200 kHz that was unexplained.
  - Bad return loss measurements (it was suspected that the old phase combiners might be contributing to the problem)
- Proposals and planned actions (due to the measured results):

- Replace the blown surge arresters
- Replace the old phase combiners (symmetrical hybrids)
- Plan a date to install the monitoring part of the experiment and to do limited measurements under live conditions.

7.2.2 Measurements while the system was operational (installation of the logging device) on 19 March 2001

- Changes to the system:
- New surge arresters installed at Acacia sub-station.
- Outer phase LME changed at Acacia sub-station (Installed on the day of measuring).
- New phase combiners installed at Acacia sub-station and Koeberg power station.
- System condition: The 400 kV transmission line and the PLC system were operative during the experiment. We did measurements on the one phase while the PLC was operating through the other phase and other way around. A "risk of trip" status was organized at National Control in Simmerpan for the experiments.
- Primary goal: To install the second phase of the experiment (The transmitting and logging devices)
- Secondary goal: To measure the PLC signal attenuation.
- Observations
- While installing the LME on the outer phase at Acacia sub-station a bad connection was found on the PLC system (and temporarily fixed).
- Bad overall correlation between theory and measurement.
- The peak at 200 kHz was still present.
- The noise level was too high to observe transmitted signal with the spectrum analyzer and the logging system was not activated.
- Proposals and planned future actions:
- That the line traps could be faulty.
- Have to get an appropriate amplifier for the signal transmitter at Koeberg power station.

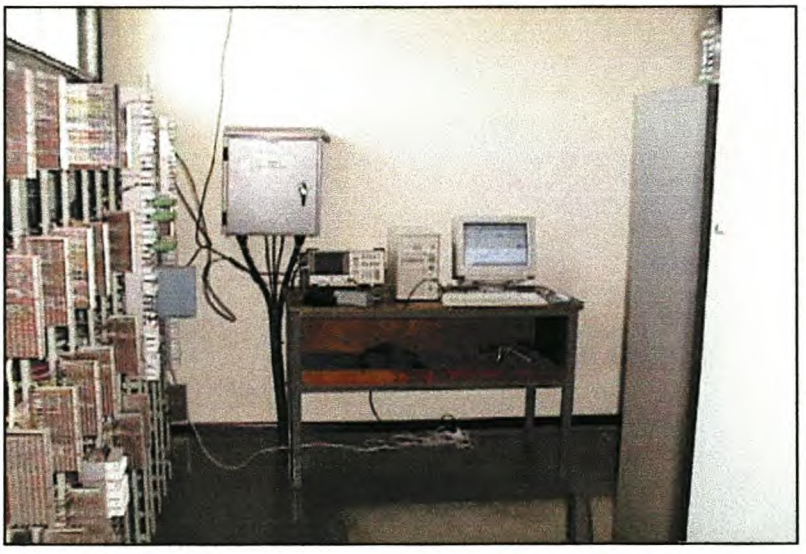

Photograph 7.1 Monitoring system (mainly computer and spectrum analyser) at Acacia sub-station

7.2.3 Logging of the signal generated by the operational carrier started on 11 May 2001

- No changes on the PLC system.

- Primary goal: To start logging the attenuation of the Koeberg carrier that transmits to Acacia
- Observations:
  - That the line traps may be faulty because adjacent carrier signals were observed.
  - From the logged data (two weeks later) signal "jumps" and variations were noted (this is shown in Figure 7.3 and explained)
- Proposals and planned future actions:
  - Check the tuning unit in the line traps (the transmission line must be isolated and earthed for this operation)

7.2.4 Measurement and installation of the tuning units (part of the line trap) on 23 June 2001

- Primary goal: To measure and install the tuning units.
- Secondary goal: To measure the attenuation for various coupling configurations.
- Observations:
  - Three of the four tuning units were faulty.
  - Theory and measurements correlate well for the outer phase (1,0,0) coupling scheme. (No peak at 200 kHz observed)
  - A peak present for the standard coupling configuration. The theory and the measurements do not correlate (the peak at 200 kHz is still present).
- Proposals and planned actions due to measurements:
  - Far less attenuation is predicted for the standard coupling configuration. Due to the fact that the outer phase attenuation does not contain the unwanted peak (200 kHz) and that the theory correlates well with the measurements indicates that the center phase may still have a fault.
  - In the future the center phase coupling component must be inspected.

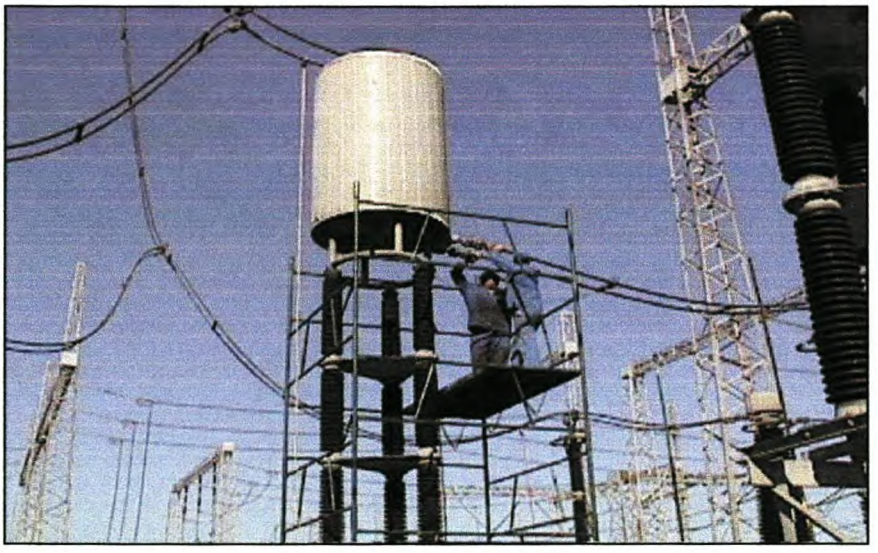

Photograph 7.2 Eskom team working on the line trap in order to do the tests on the tuning unit (The tuning unit of this particular line trap was faulty)

7.3 Outer phase coupling (1,0,0)

After the Koeberg-Acacia PLC-system was changed according to Section 7.2 the PLC signal attenuation of a single outer phase (1,0,0) coupling scheme is shown in Figure 7.1. This result proves that the developed simulation program developed delivers trustworthy results. In the coupling band, 100 - 500 kHz, close correlations between theory and the measurement is evident. Some deviation can be seen, above 500 kHz, due to the stray capacitance of the Line Trap that is not included in the model (suggested by Mr Dave Smith from Eskom).

The simulation was done for an average phase conductor height of 11m above the ground plane and 100 ohm-meter soil resistivity. The rest of the transmission line and PLC-system parameters are used as defined and explained in Chapter 2.

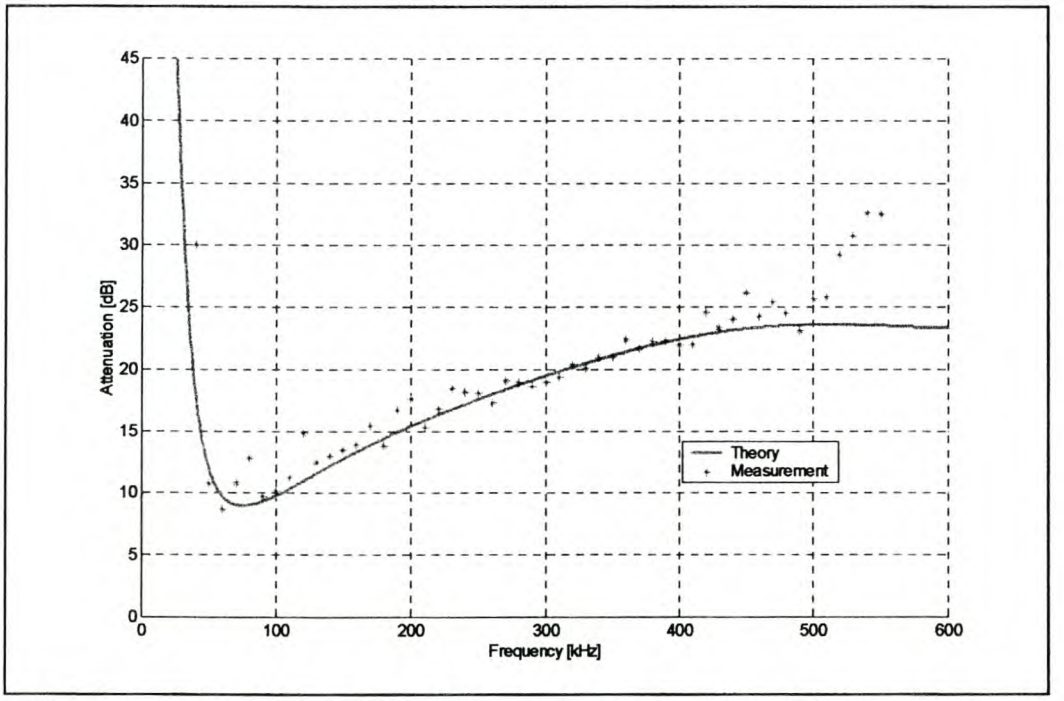

Figure 7.1 Measurement and theory for single phase coupling on the outer phase attenuation(1,0,0).

Before the line traps were replaced both the standard (1,-1,0) and experimental coupling (1,0,0) configuration contained an undefined attenuation peak at 200 kHz. In Appendix B, the attenuation peak can be seen in numerous measurements. Figure 7.1 does not show such a prominent peak and the theory correlates well with the measurements. The standard coupling configuration (1,-1,0) measurements still shows (Appendix B, Figure A.10) an attenuation peak at 200 kHz that is undefined after the installation of the new tuning units (part of the line traps). This measurement does not correlate with the theory (Chapter 4) but the presence of the attenuation peak indicates that there is probably still a faulty component in the center phase coupling mechanism. Due to lack of time there will not be an immediate investigation into this hypothesis of potential faulty equipment on the center phase. The experimental coupling (1,0,0) prediction correlates with the measurements, the goal of this research.

7.4 Additional loss

The additional losses introduced by the experiment are calculated in Chapter 6. The theory and measurements are shown in Figure 7.2. The measurement graph in Figure 7.2 is the difference between the graphs in Figure A.10 and A.11 (Appendix B).

From Figure 7.2 it is observed that the theory predicted less attenuation compared to the field measurements. This suggests that each symmetrical hybrid is introducing more than 1.25 dB attenuation to the system. The condition for 1.25 dB attenuation is that the hybrid must be precisely terminated in 75 ohms at all its ports. It can therefore be concluded that the hybrid may not be precisely terminated in 75 ohms. Another explanation may be the fact that the standard coupling configuration measurement implies the presence of a potential fault in center phase coupling equipment.

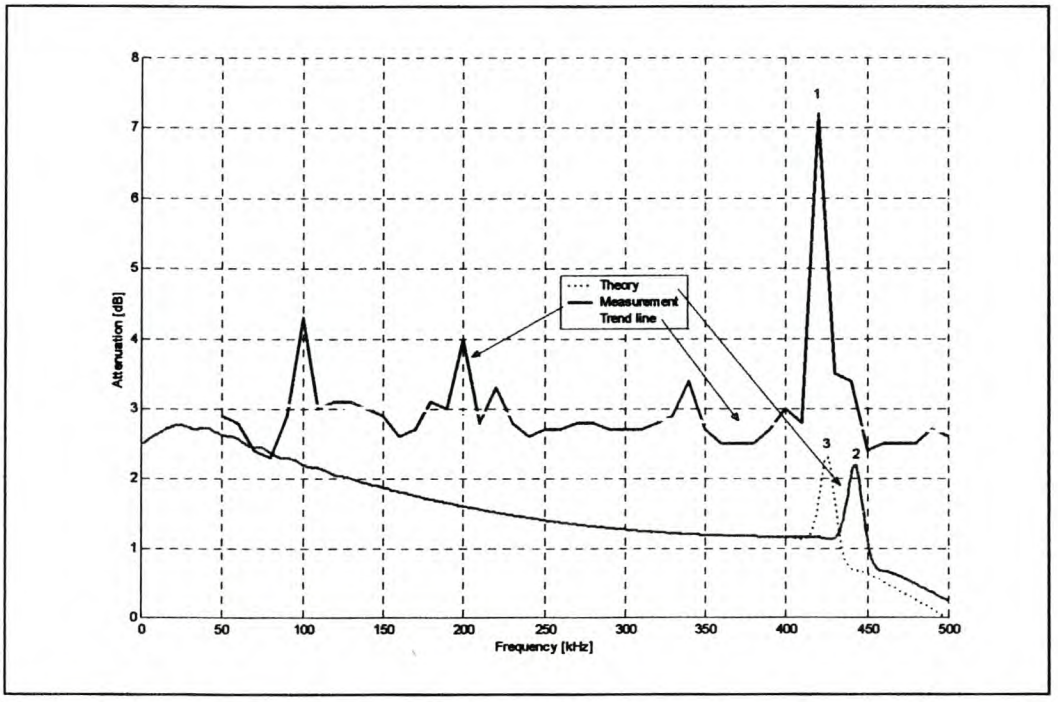

Figure 7.2 Measurement and theory for the additional loss due to the experiment

The resonance effect due to discretely bonded earth wires, explained in Chapter 5, is present in the measured results graph ('1' in Figure 7.2). The sub-module of the simulation program described in Chapter 5 was included in the simulation ('2' and '3' in Figure 7.2). The average distance between towers is 336.7m and 350m is the tower spacing that occurs most frequently according to the histogram (Figure 2.5 in Chapter 2). Point 2 in Figure 7.2 indicates the resonance effect for an average tower spacing of 336.6m and point 3 the tower spacing for 350m.

The trend line of the measurement and the trend of the predictions indicate degrees of attenuation as the frequency increases. Usually the attenuation increases as frequency increases but this trend supports the discussion in Section 6.3.2 that the experimental coupling introduces less loss than the standard coupling configuration if equal amounts of power are coupled.

7.5 Results of the experiment and future research

The attenuation variation of the operational PLC carrier was monitored. Data from the first two weeks of logging are shown in this thesis.

The signal generator at Koeberg power station, described in Chapter 6, was not switched on due to the fact that Eskom and the author speculated that the LT's were faulty. With faulty LT's the extra signal generated could couple strongly on neighbouring PLC systems. The chance was not taken and the generator was only activated after the new tuning units in the LT were installed. Therefore the signal monitored is coupled via the standard Eskom's coupling configuration (1,-1,0) and retrieved via outer phase (1,0,0) coupling configuration. Simulations, shown in Figure 7.3, for this coupling configuration indicates less sensitivity for variation in average phase conductor height variation than the design-coupling configuration.

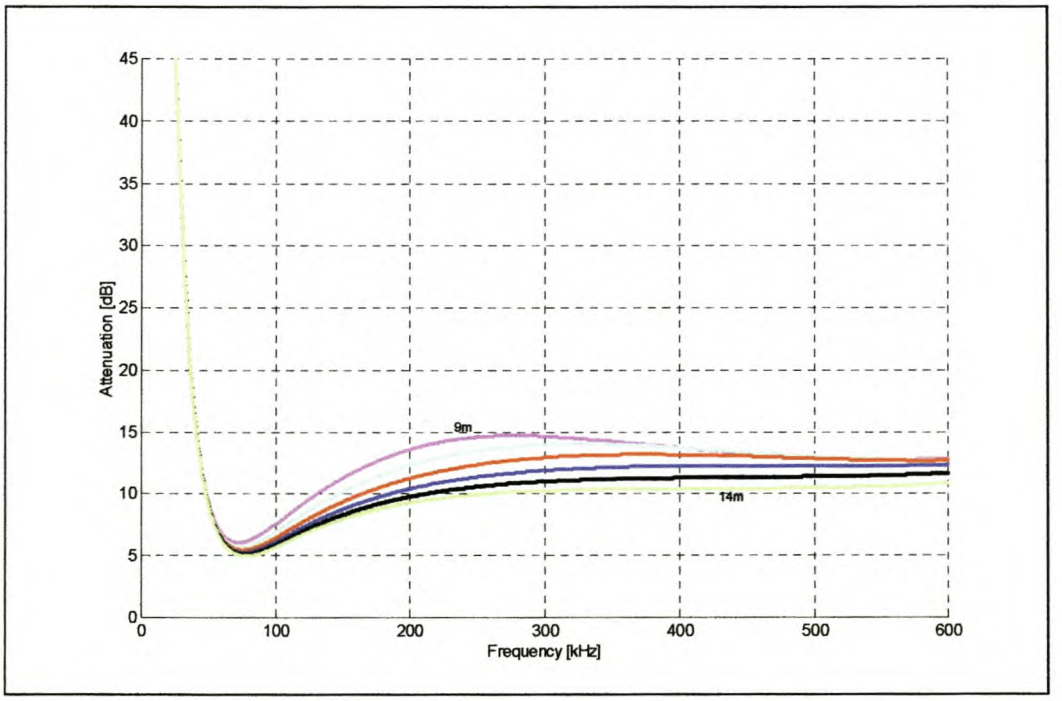

Figure 7.3 Attenuation for (1,-1,0) to (1,0,0) coupling (100 ohm-meter soil resistivity)

The monitoring system as described in Chapter 6 is used to monitor the signal variation.

Figure 7.4 demonstrates the attenuation (30 second data) of the operational carrier (348 - 352 kHz).

After the LT was fixed the generator was switched on, data are shown in Sub-section 7.6

7.5.1 Effects due to the faulty line traps

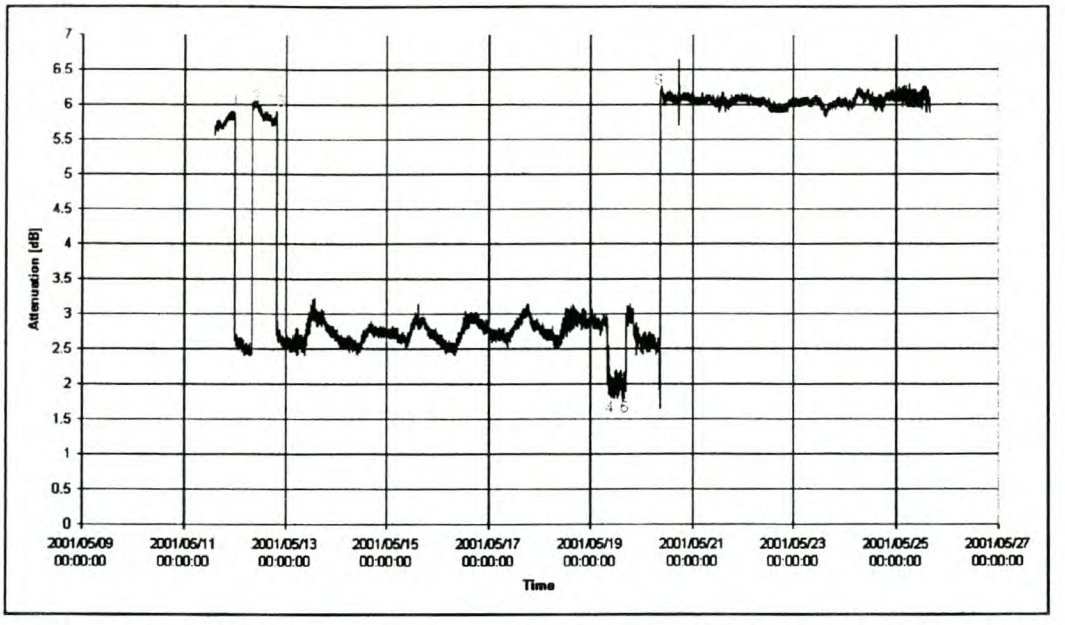

Figure 7.4 Attenuation variation of the operational carrier (30 sec data)

The first prominent effect in Figure 7.4 is the step changes in the attenuation. The times that those changes occurred were (as numbers in Figure 7.4): 1 - 2001/05/12 0:17, 2 – 2001/05/12 8:25, 3 – 200/05/12 19:58, 4 – 2001/05/19 8:25, 5 – 2001/05/19 16:46 and 6 – 2001/05/20 8:46.

The steps occurred on Saturdays and Sundays. Eskom usually does station switching on weekends due to the fewer loads. Data of the switching done at Koeberg power station and Acacia sub-stations were extracted (from the main network). A comparison between data and attenuation steps indicated some correlation. Links (like a manual switch) are not monitored by Eskom's network therefore there is not a 100% correlation.

The impedance of the sub-station influences the attenuation of the PLC received signal. If the impedance of the station is very small then it will be difficult to transmit a signal to the remote station because most of the coupled power will be dissipated in the local station. The Line Trap has the function of providing higher impedance than the transmission line with the aim of realizing transmission to the remote station (Chapter 2). This impedance should be independent of the switching configuration of the station.

It can be conjectured that faulty Tuning Units in Line Traps are responsible for the prominent attenuation steps. At the time of monitoring the data, the Line Traps were still untested and only after the tests it was learnt that 3 of the 4 Line Traps were faulty. The effects introduced due to the faulty Line Traps are now known and the data analysis can be continued, as there are many interesting effects embedded in Figure 7.4.

7.5.2 Effects due to the weather conditions on the PLC attenuation

Weather conditions were monitored by three weather stations (Koeberg, Roodekuil and Milnerton). Two weather stations, Koeberg and Milnerton, are closely located at the ends of the transmission line. Roodekuil is approximately in the center of the transmission line. The averages of the data of the three weather stations are used in the comparisons that follow. The data is quite reliable although 'spikes' like the temperature on the 18/05/2001 do occur. The data can be checked and the 'spikes' can be filtered out but the data displayed in this document is in the "raw" format (i.e. unchanged format).

The ambient temperature

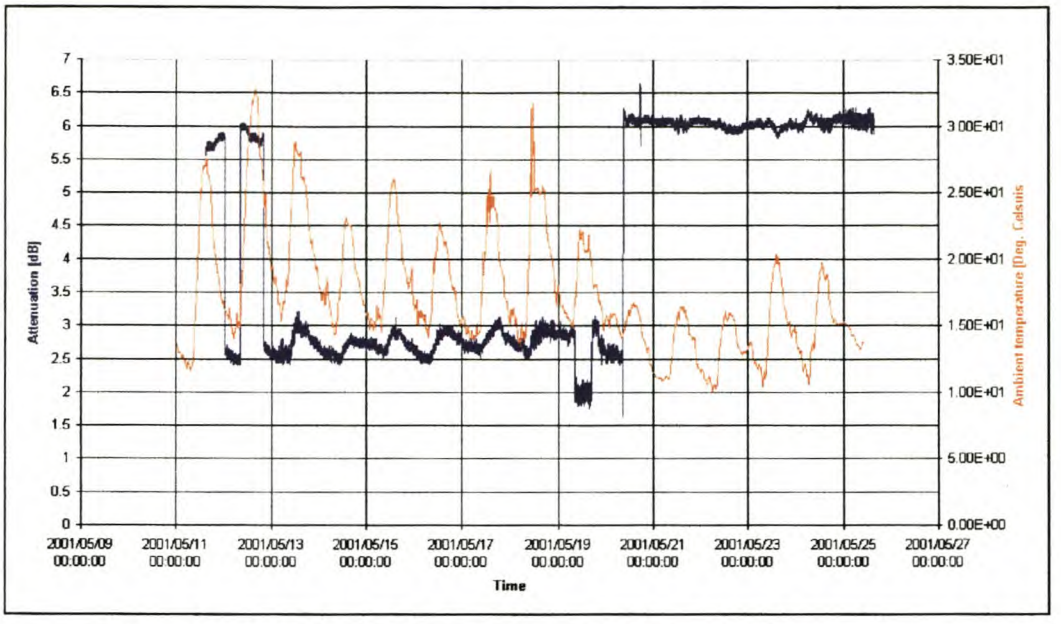

Figure 7.5 PLC signal attenuation and the ambient temperature.

For the first week the average temperature was considerably higher than that of the second week. The attenuation for the first week, ignoring the steps due to the Line Trap, shows an approximately 0.5 dB cyclical variation. For the second week, the variation is not as observable as the first week possibly due to the considerably lower ambient temperature variations.

Simulations (See Chapter 4) indicated that the attenuation of the PLC signal is a function of the average height of the phase conductors. The sag of a transmission line is a function of the conductor temperature [1]. The conductor temperature will change in tandem with the ambient temperature, and therefore a variation in sag will occur. It can be observed that the attenuation variation lags behind the ambient temperature in Figure 7.5. The reason for the lag, is due to the temperature time constant of the transmission line, in other words the transmission line takes time to react to the change in the ambient temperature.

The result is essential for the future of this research as it suggests that there is a measurable attenuation variation due to the changes in the phase conductor sag. The next step in the research will be to correlate the sag with the attenuation variation in order to develop an ampacity control system.

The wind speed

Figure 7.6 shows an interesting and unexpected result when the attenuation and wind speed are plotted on the same axis. The amplitude of the high frequency variation in the attenuation is greater for high wind speeds, clearly seen in Figure 7.6 for the 18/05/2001 and 25/05/2001.

As the wind blows over a transmission line a resonance effect occurs between two dead-end towers. Eskom usually installs dampers on the transmission lines to limit this effect. But the effect is clearly observable in the attenuation, as Figure 7.6 shows and is an indication of how sensitive the attenuation is to random variation in the sag.

This occurrence may be less on longer transmission lines. The Koeberg-Acacia transmission line is relatively short (31 km) and is located near the coastline (Chapter 2) and therefore ideal for the measurement of the influence of wind on the PLC - signal attenuation.

This correlation between wind speed and attenuation variation can be examined in more detail in future research. Information about the average wind speed, as experienced by the whole transmission line, is important for ampacity calculations.

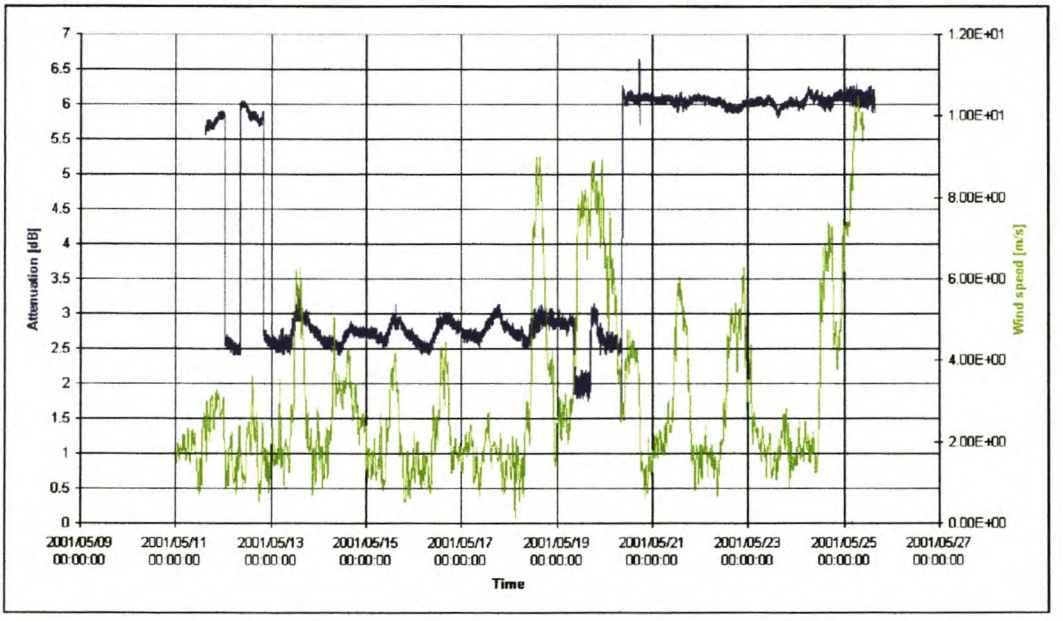

Figure 7.6 PLC signal attenuation and the wind speed

7.5.3 Effects due to the current per conductor on the PLC attenuation

The current did not noticeably influence the attenuation of the PLC-transmission line. This suggests that the current per conductor was not enough to heat the conductors up. If the phase conductor experienced high currents the conductor will heat up and will consequently sag.

Figure 7.7 shows the current per phase and the attenuation of the PLC signal.

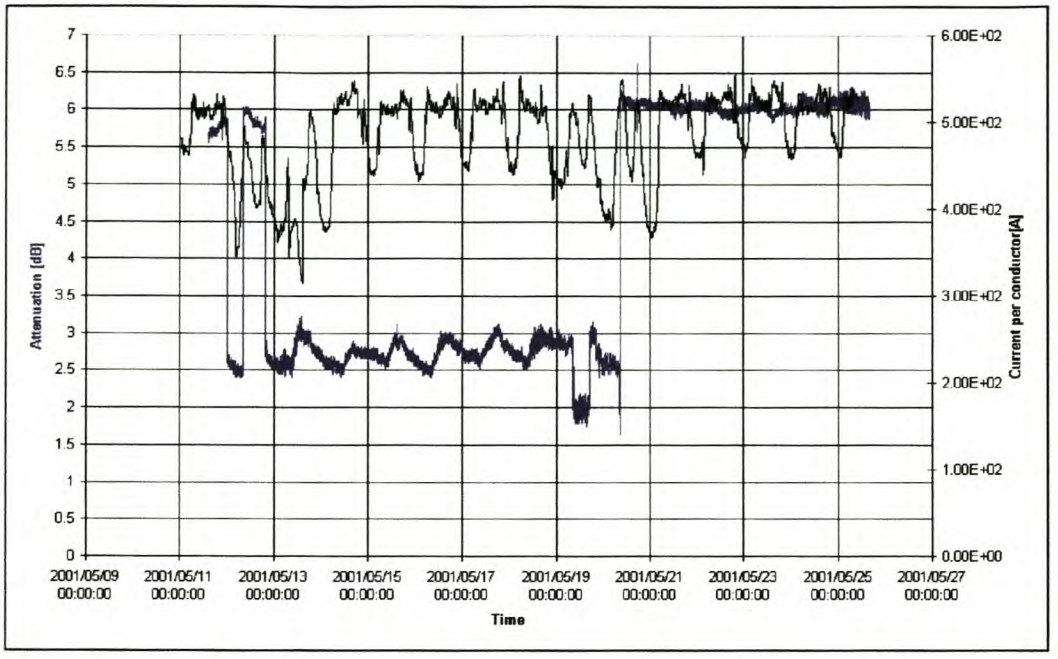

Figure 7.7 PLC attenuation and the current per phase conductor.

7.6 Measured attenuation after the faulty line traps were replaced and correlation with conductor temperature

7.6.1 Introduction

The PLC signal attenuation graphs, shown in the previous section, showed the attenuation of the existing communication signal. At that stage there were three faulty line traps on the Koeberg-Acacia PLC system. After the faulty line traps were identified and replaced the experimental generator, which is conFigured to couple a signal on the outer phase, was activated. The generator was set at a fixed 500 kHz frequency.

7.6.2 Motivation for the development of a conductor temperature simulation program

In the previous section the PLC signal attenuation was plotted with different weather conditions. Figure 7.5 shows indications of some correlation between the PLC signal attenuation and the fluctuation in the ambient temperature. It was conjectured that sag might cause PLC signal attenuation variation due to the fact that ambient temperature indirectly influences sag. In other words: the ambient temperature contributes to the conductor temperature, which consequently influences the sag of the transmission line [2]. There are other parameters, which also add or subtract temperature to the conductor and the purpose of the simulation program is to include those parameters to estimate the conductor temperature.

Thus if close correlation between the conductor temperature and the PLC signal attenuation variation is detected it would be a clear indication that sag is the cause of the signal attenuation fluctuations.

7.6.3 Theory of the conductor temperature simulation program.

The simulation program incorporates four heat sources and three cooling mechanisms [3], as experienced by the transmission line phase conductors. Eqn 7.1 demonstrates the theoretical concept of heat gain and heat loss under thermal equilibrium conditions.

$$\text{Heat gain} = \text{Heat loss}$$
$$P_j + P_m + P_s + P_i = P_c + P_r + P_w \tag{6.18}$$

where

P_j = Joule heating

P_m = Magnetic heating

P_s = Solar heating

P_i = Corona heating

P_c = Convection cooling

P_r = Radiative cooling

P_w = Evaporative cooling

The different heating and cooling parameters in eqn 7.1 are described in [2]. The simulation does not include effects that rain may have on the conductor temperature.

The simulation program calculates the steady state temperature of the conductor according to the measured input parameters.

7.6.4 Input parameters for the simulation program

The input parameters of the simulation program are the actual measured data. None of the parameters were estimated. Figure 7.8 demonstrates the different sources and the time intervals of the collected data.

Due to the difference in the time intervals, the data had to be reworked to a standardized interval. Due to the fact that the simulation model calculates the steady state conductor temperature, 15 min time intervals was chosen.

It was also necessary to convert the wind direction according to the direction of the transmission line. Figure 7.9 shows the direction of the transmission line. The wind direction data measured at Milnerton weather station (near Acacia sub-station) was not changed due to the fact that approximately two thirds of the transmission line is in the North-South direction. The wind direction was compensated for at Koeberg power station i.e. for the other third of the transmission line not running in the North-South direction.

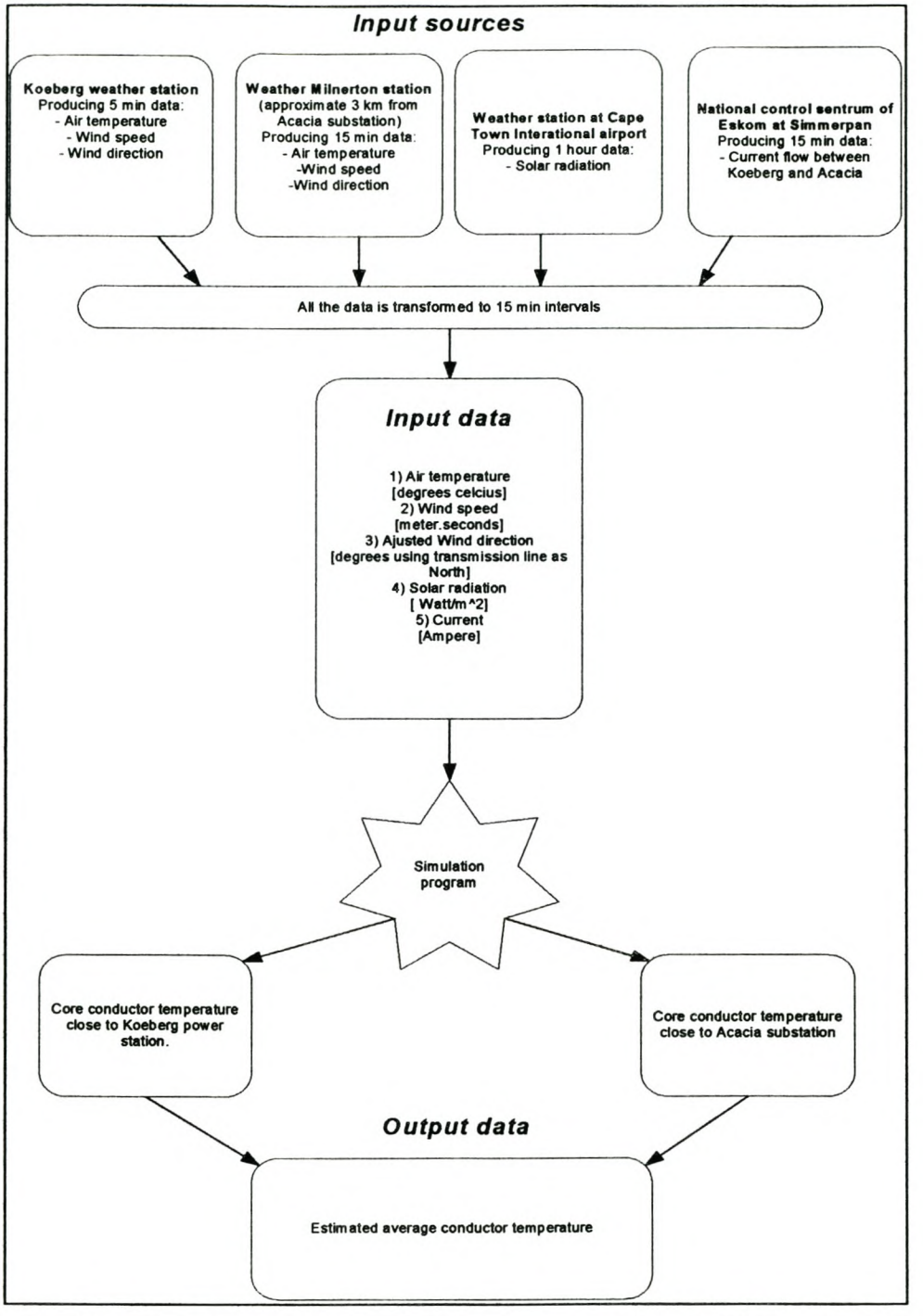

Figure 7.8 Flow diagram of the input– output data for the conductor temperature simulation program

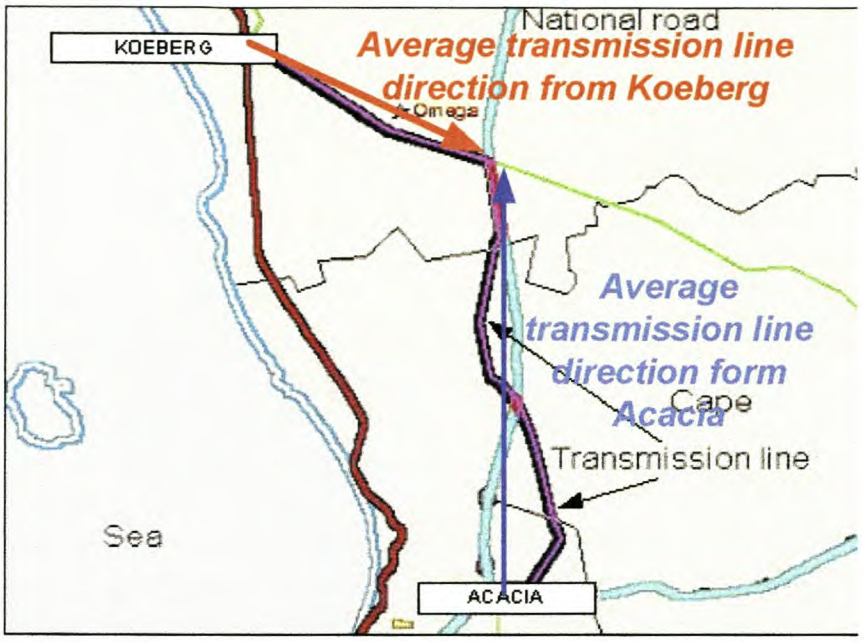

Figure 7.9 Transmission line direction from Koeberg power station and Acacia sub-station

The ambient temperature, wind speed, solar radiation and current for the period logged is shown in Figures 7.10 to 7.12. The data in the graphs are the measured information applied in the simulation program.

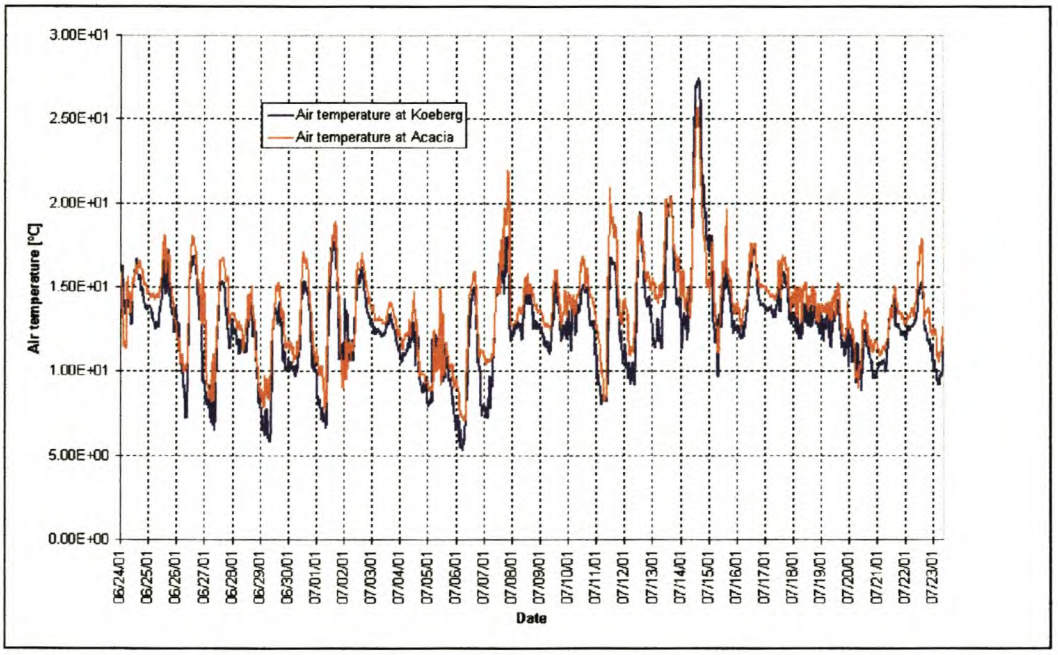

Figure 7.10 Air temperatures at Koeberg power station and Acacia sub-station

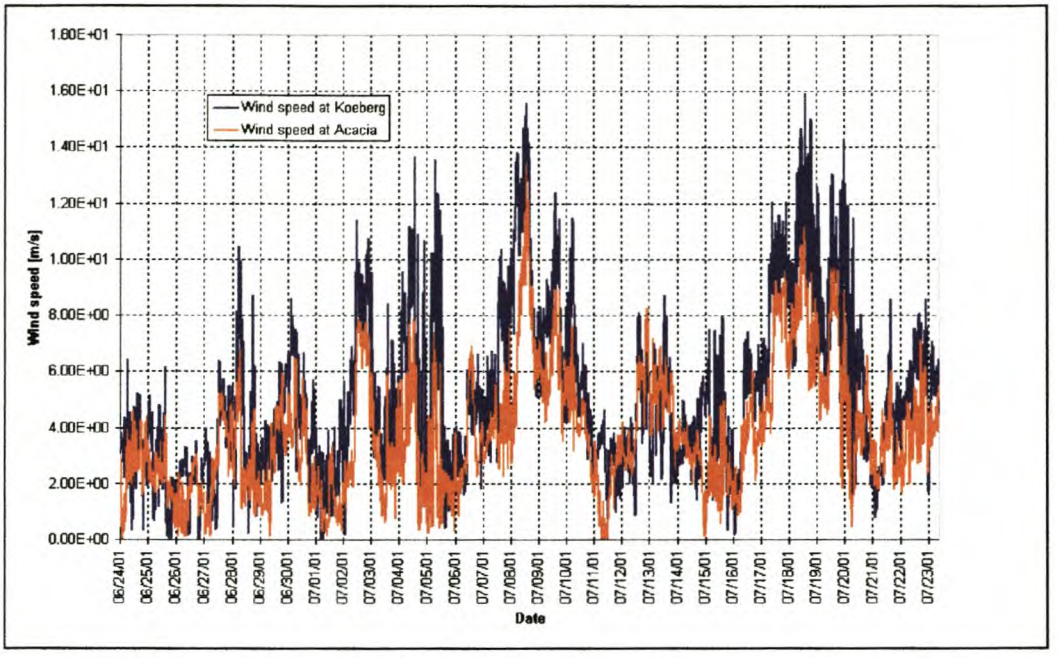

Figure 7.11 Wind speed at Koeberg power station an Acacia sub-station

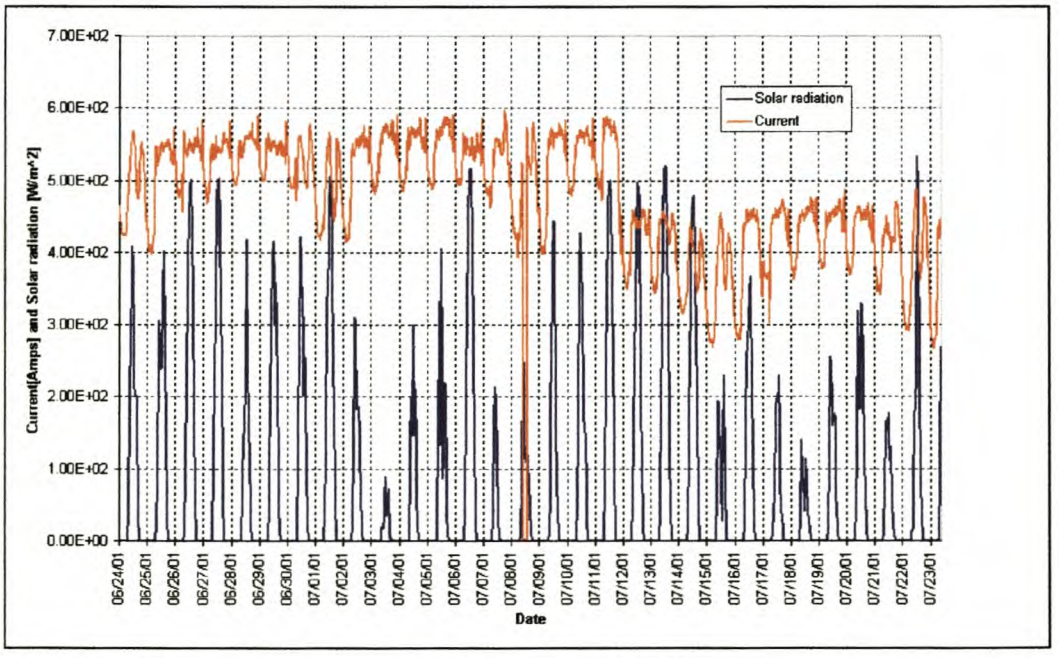

Figure 7.12 Current (between Koeberg power station and Acacia sub-station) and solar radiation (measured at Cape town international air port)

7.6.5 Result of the simulation program

The estimated core conductor temperature produced by the simulation program is shown in Figure 7.13.

The simulation program calculates the steady stated core temperature of the conductor, therefore it needs to be noted that the measured parameters at time *'T'* was used to

calculate the conductor temperature at time '*T*'. The two-conductor temperature estimates, at Koeberg and Acacia separately, are approximately in the same region throughout the time frame shown (Figure 7.13).

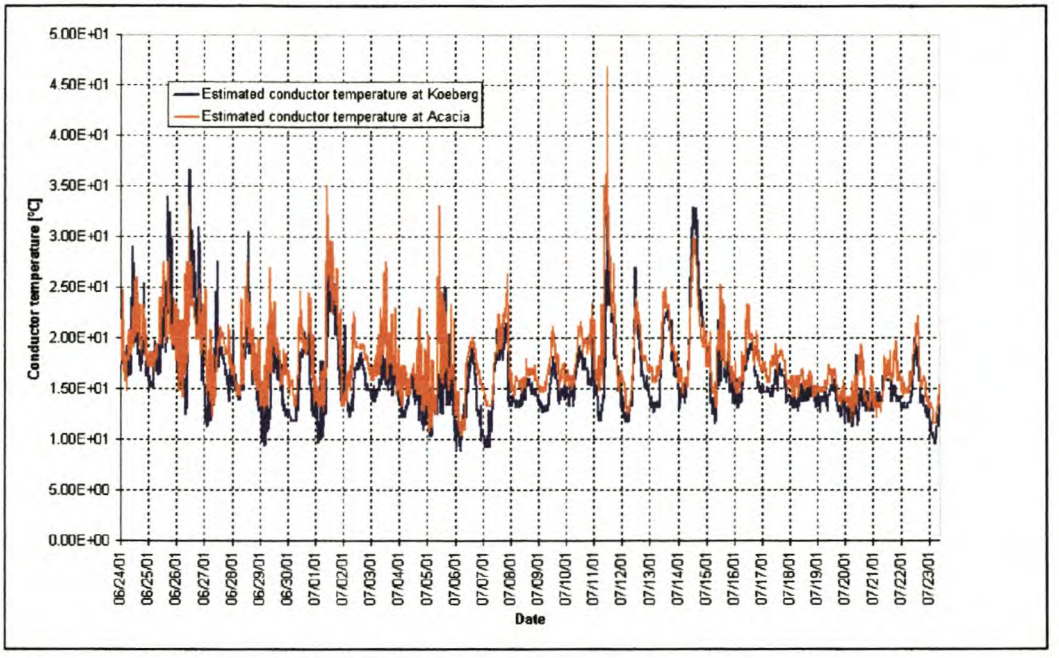

Figure 7.13 Estimated conductor temperature at Koeberg power station and Acacia sub-station

Calculating the average temperature of the conductor the following ratio is used as shown in eqn 7.2.

$$CT_{average} = \left(\frac{1}{3}\right) CT_{Koeberg} + \left(\frac{2}{3}\right) CT_{Acacia} \tag{6.19}$$

where

CT = Conductor Temperature

The reason for this ratio is due to the fact that the wind direction plays a prominent role in the conductor cooling. $\frac{2}{3}$ of the transmission line is approximately in the north to south direction and $\frac{1}{3}$ is in the south east direction as showed in Figure 2.

An extreme peak can be identified on the 11th of July. The peak highlights the fact that this is not a measured conductor temperature but an estimate based on the actual measurements of the transmission line conditions. The wind speed was very slow on the 11th July, 0.042 m/s, and the direction was parallel to the transmission line. The wind did not cause noticeable cooling of the transmission line. The transmission line direction is taken as an average north to south form Acacia sub-station. A wind angle of close to 90 degrees is interpreted by the simulation program as representing nil cooling for two thirds of the transmission line. This approximation is obviously not absolutely correct.

The amplitude of the simulated peak is unlikely to be the same as that of the actual amplitude, but the simulation program succeeded in indicating that the transmission line conductor experienced heat gain. From a totally independent measurement of PLC attenuation a dip is also identified during the same time (Figure 7.15). Using the conductor temperature simulation program, the peak in the PLC attenuation band can now be explained. Heat gain of the conductor causes the conductor to sag [2]. The sag in its turn introduces a change of PLC modal characteristic impedance, which then leads to attenuation variation. Sub section 7.6.6 continues this discussion on dips occurring in the PLC attenuation band.

Figure 7.14 demonstrates the average conductor temperature thus combining the two graphs in Figure 7.13 with the ratio given in eqn 7.2.

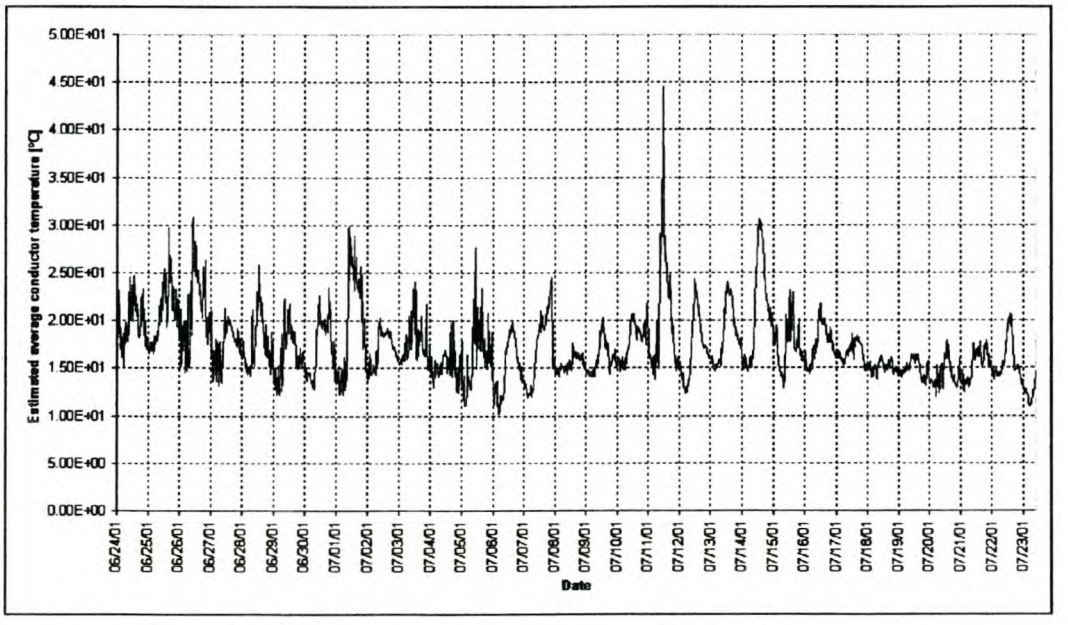

Figure 7.14 Estimated average core conductor temperature

7.6.6 Correlation between the conductor temperature and the PLC signal attenuation.

Figure 7.15 shows the attenuation fluctuations of the PLC signal (at 500 kHz) coupled via the experimental coupling configuration.

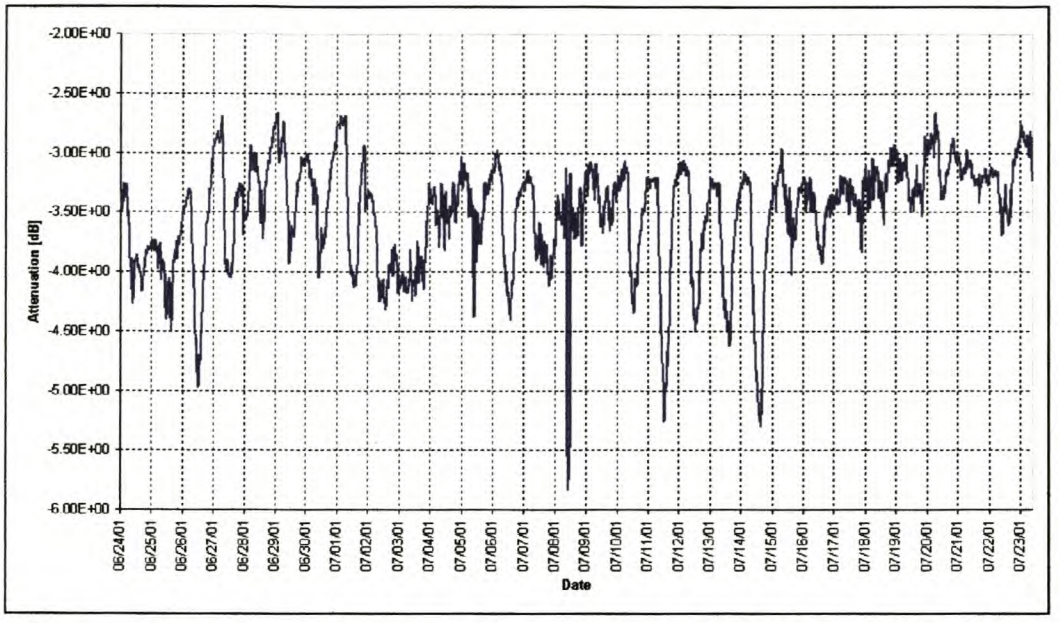

Figure 7.15 Measured attenuation of an PLC signal at 500 kHz coupled via the outer phase

Fluctuations of more than 2 dB can be seen in Figure 7.15. From the PLC signal attenuation, four dips in the data can be identified (marked 1 to 4 in Figure 7.16). Figure 7.16 is a combination of the Figures 7.14 and 7.15.

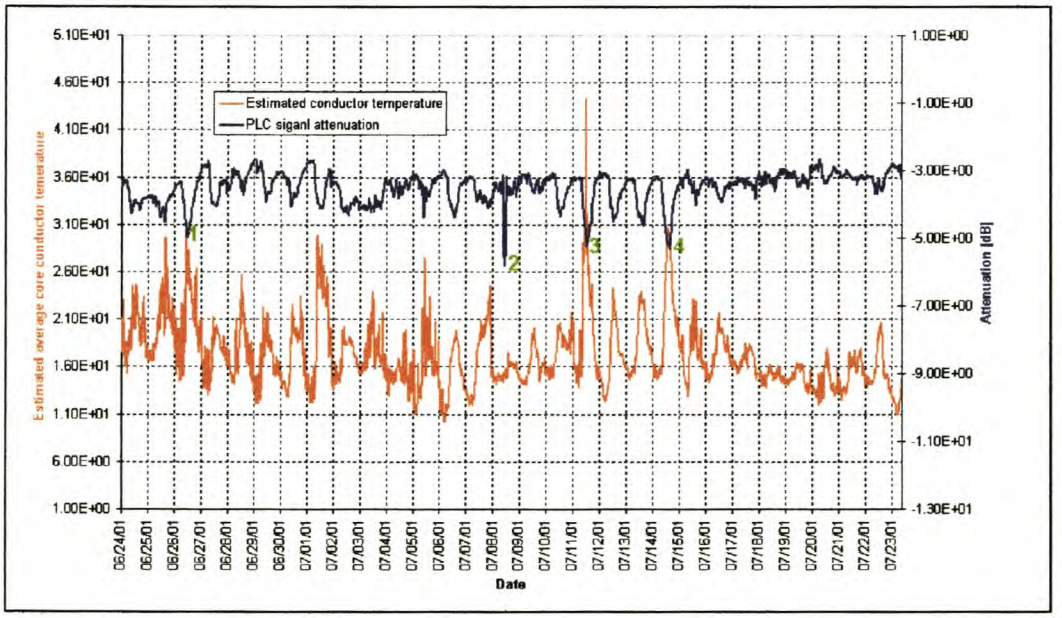

Figure 7.16 Estimated conductor temperature and the PLC signal attenuation

Three of the dips (1,3 and 4 in Figure 7.16) correlate strongly with the temperature peaks in the measured data. Dip number two is due to the fact that the transmission line was isolated on the 8th July and that resulted in a change in the impedance at the termination end of the PLC signal path. The power cut explains the sudden change in the attenuation. From Figure 7.12 it is evident that there was a current dip (to zero ampere) on the 8th July. This confirms the isolation of the transmission line on the 8th.

Using the standard correlation algorithms, as in Microsoft Excel and Matlab, the correlation of the two sets of data, as shown in Figure 7.16 is equal to -0.7. This negative correlation value means that the peaks correlate with the dips.

The 14th July is identified as the day with the highest measured air temperature (Figure 7.10). Figure 7.17 shows the average estimated conductor temperature and the measured attenuation. The correlation for only this specific day's data is equal to -0.96.

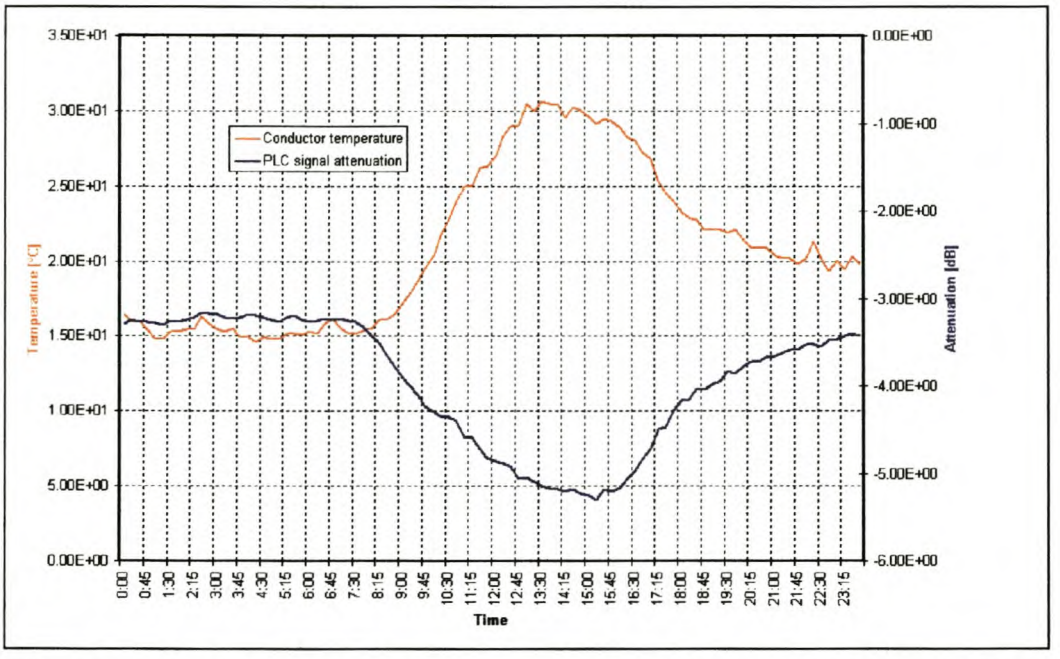

Figure 7.17 Estimated conductor temperature and PLC signal attenuation for the 14th Juny.

This is an inspiring result, which suggests that the sag (directly influenced by the conductor temperature) relates strongly to the PLC signal attenuation. The next logical step is to plot the correlation between attenuation and conductor temperature for each day (Figure 7.18) to see if the correlation is consistent.

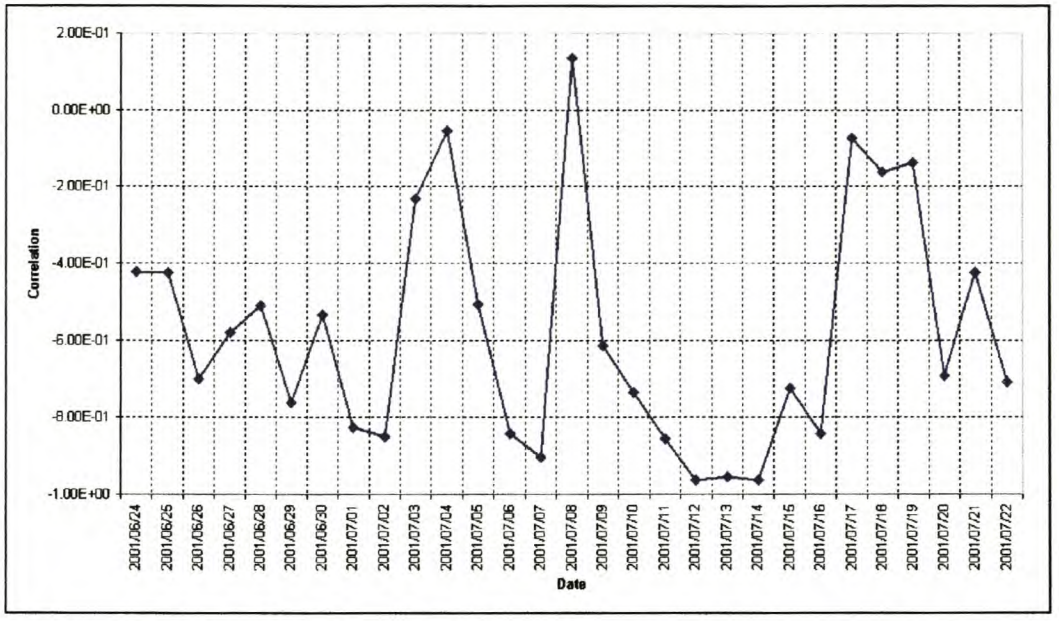

Figure 7.18 The correlation from day to day between conductor temperature and PLC signal attenuation.

From Figure 7.18 it is clear that the 12th, 13th and the 14th of July gave exceptionally good correlation values between conductor temperature and PLC signal attenuation. It must be investigated why the correlation was not so good in regions other than the 12th to 14th of July. After a detailed investigation of the measured information one prominent effect came to the fore, namely rain.

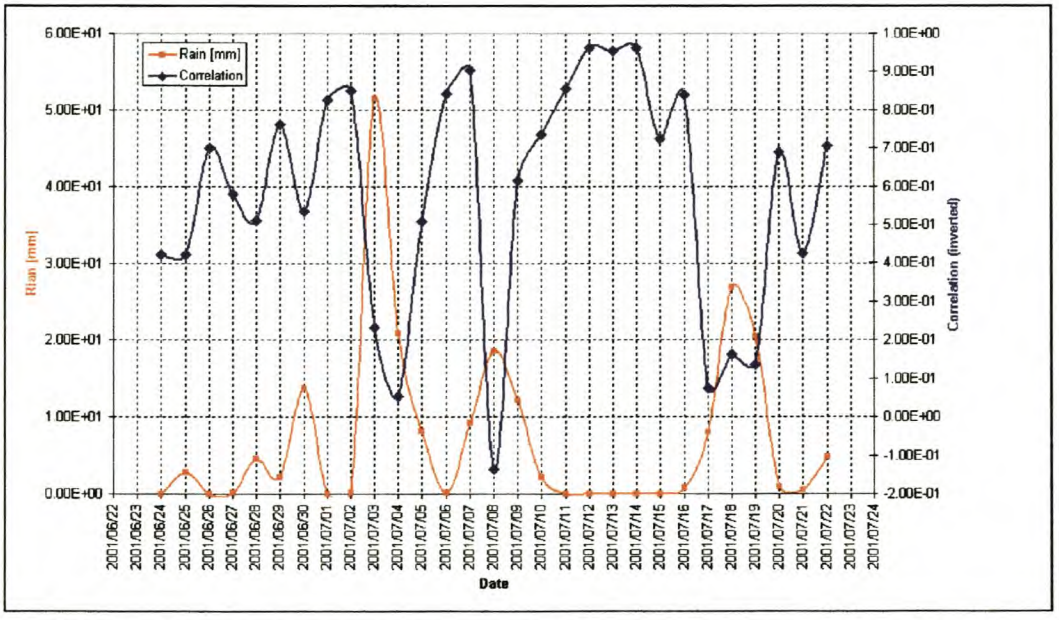

Figure 7.19 Correlation (between PLC signal attenuation and conductor temperature) and rainfall in mm.

From Figure 7.19 it is evident that the best correlations occurred during periods with no rain. This result may suggest three possibilities. Firstly that the simulation model that estimates the conductor temperature is not valid in rain because the cooling effect of the water is not included in the model, therefore the predicted conductor temperature becomes unreliable. Secondly that the rain adds a vertical force to the conductor and that could increase the sag. Thirdly that the soil resistivity may change due to the rain and that might influence the attenuation characteristics. The following discussion will consider the third reason.

A typical penetration depth of a PLC signal into the ground is calculated with eqn 7.3.

$$\delta = \sqrt{\frac{\rho}{\pi f \mu}} \tag{6.20}$$

where

δ = Penetration depth in meter
ρ = Resistivity in ohm meter
μ = Permeability in henry/meter
f = Frequency in Hz

The soil resistivity is taken as 100 ohm meter and the frequency as 500 kHz. Using eqn 7.3 the penetration depth is calculated as 7.12m.

Dr M De Wet [4] was involved in the process of drilling boreholes at Koeberg power station. During a discussion between the author, Prof JH Cloete and Dr M De Wet on 26 October 2001 the following information about soil characteristics was gathered. At Koeberg power station the first 19m of the ground is sand where the borehole was drilled. The soil type remains approximately the same from Koeberg to Acacia sub-station. The water from the rain tends to filter quickly through the sand to the water table. Therefore the level of the water table is very sensitive for the amount rain fallen.

The PLC signal (at 500 kHz) penetrates a typical 7.1 m in the ground. It can be speculated that most of the soil's characteristics, as experienced by the PLC signal, is sand for the entire route of the Koeberg-Acacia transmission line. The water filters quickly through the sand and that, together with the dissolving salts, changes the electrical characteristics of the soil. It is concluded that the ground resistivity may change substantially during periods of rain.

Figures 4.6 to 4.8 demonstrate the predicted change in PLC attenuation for different soil resistivities using the experimental outer phase coupling configuration. Focusing on the 11m average phase-conductor-height graphs in those Figures it is noticed that the simulated attenuation is 24 dB for 100 ohm-meter, 20.5 dB for 300 ohm-meter and 17.5 dB for 500 ohm-meter soil resistivity. Consequently the effect of varying soil resistivity would most likely introduce an offset effect to the day night cycle attenuation fluctuations (in other words it would let the signal drift according to the soil resistivity change). In order to examine this hypothesis the PLC signal attenuation is filtered by a low pass filter (using the 'filtfilt' function in Matlab). A second order Butterworth filter is used with a 3 dB cut of frequency of 4.44×10^{-6} ($\frac{1}{f} = 2.604$ days). The filtered attenuation and rainfall is shown in Figure 12. The rainfall graph in Figure 7.20 represents accumulated rain in 5 min intervals where Figure 7.19 showed accumulated rain for each day.

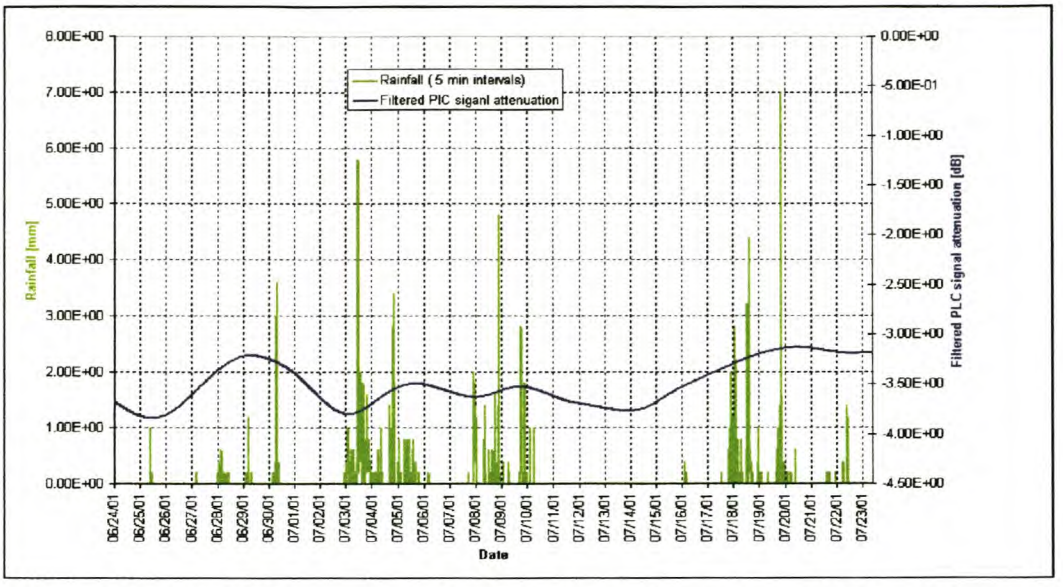

Figure 7.20 Rainfall (accumulated rain for 5 min intervals) and filtered (second order butterworth low pass filter with 1/fc = 2.6 days) PLC signal attenuation variation

In Figure 7.20 it is apparent that there is no definite correlation between the rainfall and mean filtered attenuation variation. However Figure 7.21 demonstrates a more definite correlation, of -0.72, between the filtered conductor temperature and the filtered PLC signal attenuation variation. This supports the conjecture that the offset variation of the PLC signal fluctuations is most likely due to the conductor temperature and not due to changes in the soil resistivity.

The effect expected from varying soil resistivity is not prominently present in the measured PLC signal attenuation. The rain did not influence the offset (Figure 7.21) of the attenuation noticeably thus the rain most probably only introduced a high frequency noise into the system.

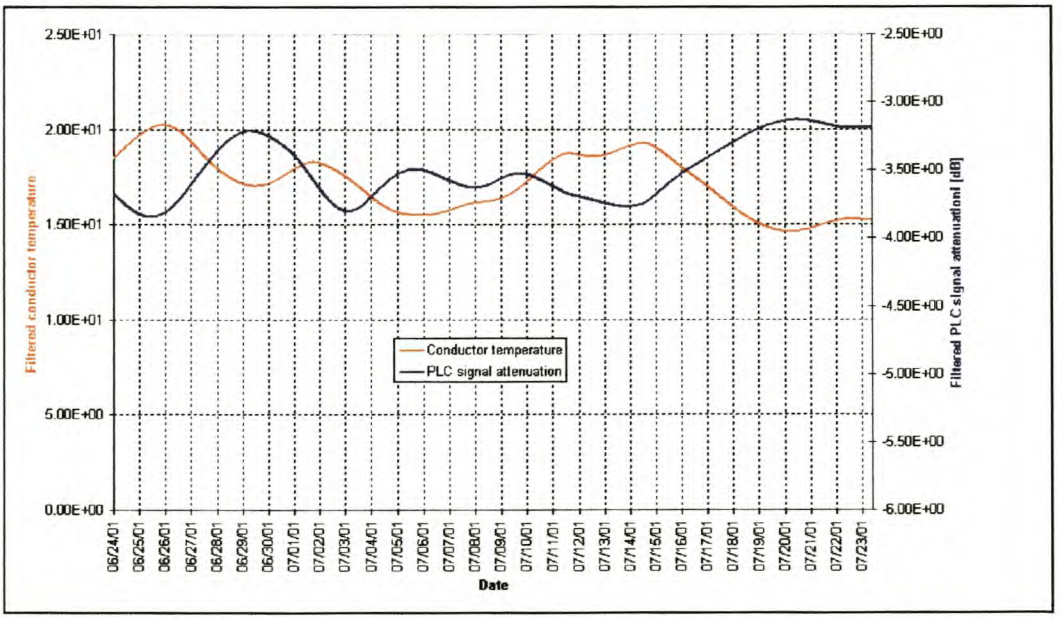

Figure 7.21 Filtered (second order butterworth low pass filter with 1/fc = 2.6 days) PLC signal attenuation and filtered conductor temperature

A band-pass filter (second order butterworth, 1/f1 = 2.0833 days and 1/f2 = 10 hours) is used to filter the two data sets in Figure 7.16. The band-pass filter allows only the day-night cycle fluctuations through. Consequently filtering the high frequency noise out and the offset shown in Figure 7.21. The filtered data is shown in Figure 7.22. A surprisingly good correlation of –0.85 is evident between the two sets of data (the conductor temperature was inverted in order to observe the correlation better). The correlation improves when bigger fluctuations occur in the data.

With this result it can be concluded that there is not only a theoretically predictable correlation between sag and PLC signal attenuation, but also a strong measured correlation between PLC signal attenuation and conductor temperature. The conclusion is inescapable: PLC signal attenuation is a predictor of conductor temperature and sag.

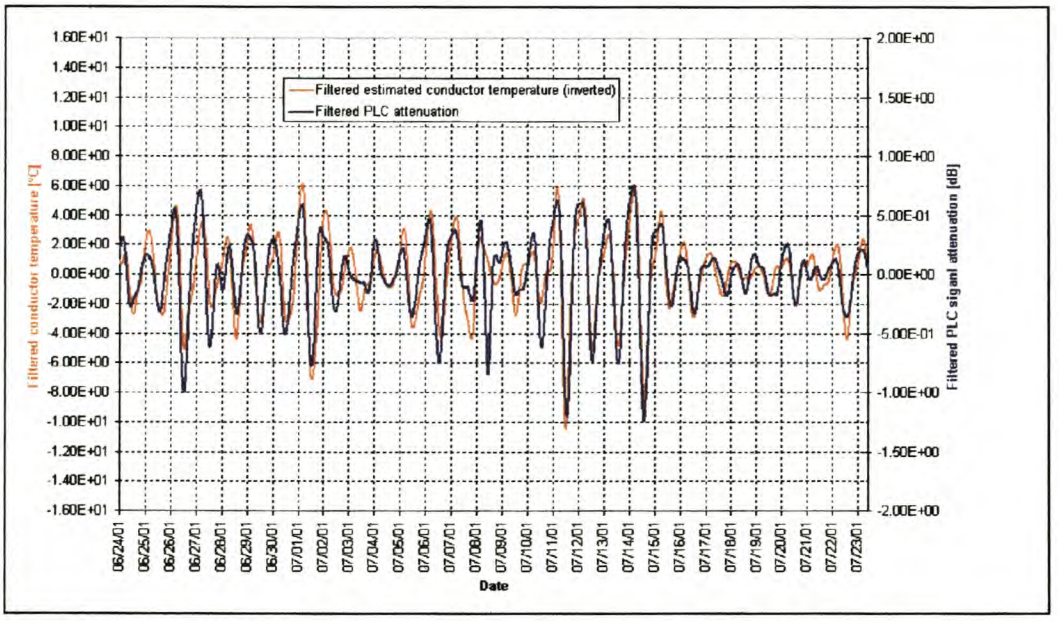

Figure 7.22 Filtered, passing only the day-night fluctuations, estimated conductor temperature and PLC signal attenuation.

7.6.7 Conclusion of PLC and conductor temperature analysis

It is became clear that measurable PLC signal attenuation fluctuations are observable on the PLC system through the use of an outer –phase-to- outer -phase coupling mechanism.

A simulation program was written and tested to estimate conductor temperature from measured weather and line conditions.

The measured attenuation of the experimental PLC signal was correlated against the estimated conductor temperature. Good correlation (Figure 7.19) can be observed during periods of no rain between the PLC attenuation fluctuations and the estimated conductor temperature.

The first layer of soil is sand for the length of the Koeberg-Acacia transmission line and is likely to be deeper than 15m throughout the line [3]. Rain water filters quickly through sand and therefore it can be expected to change the electrical properties of the sand as experienced by the PLC signal. During the winter month tests, a vast volume of rain had fallen (approximately 200 mm). This created excellent test conditions to examine if the PLC signal attenuation is rain sensitive. Due to the non-day-night cycle of rain the attenuation fluctuation signal was filtered by a low pass filter. The filtered data correlated with the filtered conductor temperature but not with the rainfall. It can thus

be postulated that the PLC signal attenuation is not subjected to major offset changes due to rain.

By using a band pass filter the high frequency noise effect was filtered out. This noise was mostly likely introduced by rain and wind. The low frequency offset was also filtered out in order to put the emphasis on the day-night fluctuations. Strong correlation (-0.85) was observed for the whole period after filtering between PLC signal attenuation and conductor temperature. See Figure 7.22.

7.7 Conclusion

In this Chapter the simulation program (described in Chapter 3) is tested in a practical field situation. Several tests were done to identify and repair faulty equipment in the operational PLC system. In Chapter 4 the simulation program is compared with Prof L.M. Wedepohl's program and in both cases the tests indicate promising results.

The additional loss predictions and measurements are shown. The resonance effect due to the discretely bonded ground conductors is noticeable in the measurements. The high attenuation of the standard coupling configuration and the presence of the peak at 200 kHz indicates that there may still be a fault on the centre coupling mechanism on the Koeberg – Acacia PLC system.

The operational carrier on the PLC system was monitored via a spectrum analyzer. The measurement shows correlation between ambient temperature and PLC signal attenuation. Correlation between amplitude of high frequency attenuation variation and wind speeds is also evident.

After the line traps were fixed data from the experiment was logged for 28 days. A simulation program was written in order to utilize a correlation analysis between conductor temperature and PLC signal attenuation variation. After filtering the data with a band pass filter, thereby putting the emphasis on the day-night fluctuations, an extremely good correlation of 85% was detected between the conductor temperature and PLC signal attenuation. From the analysis is can be concluded that rain introduces a high frequency noise component to the system.

The results may be exploited further in order the develop an PLC ampacity system. The next step in the research will be to correlate the PLC signal variation directly to sag variation.

7.8 Reference

[1] **M.W. Davis**, "A new thermal rating approach: The real time thermal rating system for strategic overhead conductor transmission lines PART 1", Transact. on Power Apparatus and Systems, Vol. PAS-96, No. 3, May/June 1977, pp. 803 – 809.
[2] **Southwire Company**, Overhead Conductor Manual, First edition.
[3] **Cigre Work Group 22.12** (Chairman **R. Stephen**, South Africa), "The thermal behavior of overhead conductors", Électron No 144, Ocktober 1992, pp. 107 – 125.
[4] **Dr M De Wet,** Lecturer at Civil Engineering Department, Stellenbosch University, private conversation on 28 October 2001.

Chapter 8

Conclusion and recommendations

Specialized skills and knowledge about PLC systems was gained. This research introduced a new field, i.e. the use of PLC signal attenuation to monitor OHTL sag. It has contributed substantially to any future studies that will be done in this new direction.

Theoretical knowledge and an in-depth understanding was gained as the PLC simulation program developed. A simulation program, with the ability to simulate end-to-end attenuation and including the coupling equipment, was thoroughly tested against Prof Wedepohl's simulation program. A close correlation between the two simulation approaches was revealed.

Practical 'hands on' skills were developed as numerous field measurements were conducted in live and isolated 400 kV transmission line conditions. From the results it is clear that the theory and the practical measurements correlate closely for the experimental (1,0,0) coupling configuration. Measurements of the standard coupling (1,-1,0) configuration reveals an unexplained peak and this led to speculation that there might still be a fault on the center phase coupling circuitry. The same peak presented itself in the attenuation measurements of the signals coupled via the outer phase (1,0,0) before the installation of the new tuning units.

Simulations of PLC signal attenuation (using the De Villiers program) for different types of ground conductor properties and soil resistivities were done. The simulations indicated that mode 2 and mode 3 propagations are influenced by the different ground conductor and soil resistivities. It can also be concluded that mode 1 is not influenced extensively by the soil resistivity or by the ground conductor properties.

An experiment was developed to monitor PLC signal attenuation over a long period of time (2 weeks) and was installed at Koeberg power station and Acacia sub-station. The logged data showed measurable PLC signal attenuation variation. The signal generated (at Koeberg) by the operational carrier was logged (at Acacia) with the faulty line traps in the system. The day – night cycle attenuation variation shows indications of correlation with the ambient temperature changes.

After the three faulty line traps were replaced data from the experiment was logged for 28 days. A simulation program was written in order to utilize a correlation analysis between conductor temperature and PLC signal attenuation variation. After filtering the data with a band pass filter, thereby putting the emphasis on the day-night fluctuations, an extremely good correlation of 85% was observed between the conductor temperature and PLC signal attenuation. From the analysis it is clear that even higher correlations was present during periods with extreme conductor temperature fluctuations as the 14th July (96% correlation).

This result is extremely important, as the core function of the proposed application emerging from this study, namely ampacity control, is to reliably monitor excessive sag variations.

This study established that the PLC signal attenuation variations are accurately measurable at levels of ± 0.1 dB.

Future research must be conducted to establish the envelope of operational HVTL and PLC system parameters within which reliable correlation can be expected between PLC signal attenuation and the sag of the transmission line. Although a very successful correlation analysis was conducted it must be noted that the conductor temperature is not the only parameter influencing sag. For an example: a constant wind can physically push the transmission line conductors to the side, consequently influencing the sag.

The next step in the study field is to develop an algorithm to relate PLC attenuation fluctuation directly with sag. The result of the estimated sag from the PLC signal attenuations can then be used to predict the ampacity of the transmission line in real time. A thorough risk analysis must also be done applying different conditions and configurations to calculate the confidence level of this method. Existing ampacity control methods may be used in tandem with the proposed method in order to reduce the overall risks involved in ampacity control.

In conclusion: the real-time knowledge of actual average sag, calculated from the PLC signal attenuation, can be used in a dynamic ampacity control system. This will have a dramatically positive influence on the cost effectiveness of energy transmission on HVTL systems.

Appendix A

Provisional patent

D. M. Kisch Inc, Sandton

Form P.6

REPUBLIC OF SOUTH AFRICA

PATENTS ACT, 1978

PROVISIONAL SPECIFICATION

(Section 30 (1) - Regulation 27)

OFFICIAL APPLICATION NO.			LODGING DATE		DMK REFERENCE
21	01	2001/2258	22	19 March, 2001	P21404ZA00

FULL NAME(S) OF APPLICANT(S)	
71	UNIVERSITY OF STELLENBOSCH

FULL NAME(S) OF INVENTOR(S)	
72	CLOETE, Johannes Hendrik DE VILLIERS, Wernich

TITLE OF INVENTION	
54	AMPACITY AND SAG MONITORING OF OVERHEAD POWER TRANSMISSION LINES

INTRODUCTION AND BACKGROUND

THIS invention relates to overhead electrical power transmission lines and more particularly to ampacity and sag monitoring and control of such lines.

Regulations require that transmission lines be operated safely at all times. An important safety consideration is the provision of adequate and mandatory clearance underneath the lines. Hence, one of the most important limitations on line ampacity is the need to ensure that sagging does not exceed a maximum design value under all operating conditions.

Various methods of line ampacity control are known, ranging from a conservative approach to more liberal line sag models and clearance warning methods. The former methods prescribe constant capacity based on conservative consumptions for parameters such as ambient temperature and wind speed for example, which would allow for conservative and acceptable safety margins. In the latter methods, the utility suppliers are adapting line ratings to actual weather conditions, thus controlling power lines more dynamically.

An example of the latter methods, is the temperature-sag model. A line tension monitoring system comprising tension monitors for each ruling span is utilized on the line, to determine from tension measurements the sag and rate of sag change. The main disadvantage of this system is that the

tension monitors required for each ruling span make the system expensive, time consuming to install and difficult and time consuming to maintain.

OBJECT OF THE INVENTION

Accordingly it is an object of the present invention to provide an ampacity and sag monitoring and control method and system with which the applicant believes the aforementioned disadvantages may at least be alleviated.

SUMMARY OF THE INVENTION

According to the invention there is provided a method of monitoring sag in a conductor comprising the steps of: establishing a relationship between propagation effects of a signal on the conductor and sag of the conductor; monitoring for the propagation effects; and determining resulting sag in the line.

The effects may be modal cancellation of fields associated with the signal and propagating along the conductor. It has been found that there is a relationships between a peak modal cancellation frequency and average sag of the conductor.

The method may further include the step of generating and coupling to the conductor a monitoring signal such that fields associated with the

monitoring signal propagate along the conductor in a plurality of modes, and determining a peak modal cancellation frequency for the monitoring signal.

The method still further includes the step of utilizing the peak modal cancellation frequency and said relationship to determine the resulting sag.

Also included within the scope of the present invention is a method of ampacity control for a transmission line, the method comprising the steps of:

- determining a conservative ampacity rating value;
- determining a maximum dynamic ampacity rating value;
- intermittently utilizing line sag measurement data based on propagation effects of a signal on a conductor of the line due to sagging, to confirm a safe operational rating between the conservative value and the maximum dynamic value.

The method may further include the step of generating and coupling to the line a monitoring signal such that fields associated with the monitoring signal propagate along the line in a plurality of modes, and determining a peak modal cancellation frequency for the monitoring signal.

The method may also include the step of generating an early warning signal if the operational rating approaches the maximum dynamic ampacity rating value.

Also included within the scope of the present invention is a monitoring system for sag of an overhead power transmission line, the system comprising:

- monitoring signal generating means;
- means for coupling the monitoring signal to the line;
- means for detecting a peak modal cancellation frequency of the signal; and
- means for relating the peak modal cancellation to sag of the line according to a predetermined relationship.

The invention also includes within its scope an ampacity monitoring and/or control system for an overhead power transmission line as herein defined and described.

BRIEF DESCRIPTION OF THE ACCOMPANYING DIAGRAMS

The invention will now further be described, by way of example only, with reference to the accompanying diagrams wherein:

figure 1 is a diagrammatic representation of a power line supported by a plurality of towers;

figure 2 is a block diagram of a power transmission system including a data communication system and a monitoring and control system according to the invention;

figure 3 is a graph of attenuation against frequency for various average conductor distances from ground, indicating a shift in peak modal cancellation frequency with changing average distance; and

figure 4 is a diagram illustrating an ampacity control method according to the invention.

DESCRIPTION OF A PREFERRED EMBODIMENT OF THE INVENTION

A system for monitoring and controlling ampacity and sag of an overhead power transmission line 10 shown in figure 1 is generally designated by the reference numeral 12 in figure 2.

As shown in figure 1, typically part of the line 10 is supported between first and second dead-end structures 14.1 and 14.2. It is further supported by spaced suspension structures 16.1 to 16.3. Sag of the line or a conductor in the line is defined as a difference 18 in height of the line or conductor on a straight line 20 between adjacent towers, if the towers are at the same height 22.

In the example of figure 2, the transmission line 10 is shown to extend between a power source controller 24 and a load 26. The power source controller 24 is operative to connect any one or more of power sources 28.1 to 28.n to the load via the transmission line depending on ampacity data received from the ampactiy monitoring system 12 as hereinafter described.

Also connected to the transmission line 10 is a known and convention power line carrier (PLC) data communication system 30 utilizing carriers in the 50 kHz – 500 kHz band. The data communication system comprises a first PLC transceiver 32 and first PLC interface 34 connected to the line 10 at one end thereof and a second PLC transceiver 36 and second PLC interface 38 connected to the other end thereof. The data communication system enables bi-directional data communications between the source 24 and the load 26 utilizing carrier frequencies coupled to the line such as to ensure as little as possible modal attenuation. Typical carrier frequencies are shown at 40 in figure 4.

One basic example of the monitoring system 12 comprises a monitoring signal generator 42 connected between the first PLC transceiver 32 and PLC interface 34. It further comprises a spectrum analyzer 44 connected between the second PLC transceiver 38 and interface 36. The spectrum analyzer 44 is connected to a logging computer 46 and the logging

computer is connected to a control centre 48 which also controls the monitoring signal generator 42. The control centre is further connected via data line 50 to power source controller 24.

It has been found that there is a relationship between sagging 18 of a conductor and a peak modal cancellation frequency of a monitoring signal propagating on the conductor. A typical relation (which will differ from conductor to conductor) is shown in figure 4. For a conductor 23 meters above ground, the peak modal cancellation frequency is shown at 44.1. For a conductor 22 meters, 21 meters, 20 meters, 19 meters and 18 meters above ground, the peak modal cancellation frequencies are shown at 44.2 to 44.6 respectively. The frequency at 44.1 is about 280 kHz and at 44.6 about 160 kHz.

The peak modal cancellation may be determined by causing monitoring signal generator 42 to generate a tone S_{tm} sweeping between 150kHz and 250 kHz in a first time period of say 0.5hr. It will be noticed that the frequency of the monitoring signal is remote from the carrier frequencies 40 used for the aforementioned conventional data communications. The tone is coupled to the line 10 so that associated **E** and **H** fields propagate along the line in a plurality of modes.

The fields mutually destruct one another and peak cancellation is obtained at a frequency which is related to the sag in the line according to a measurable and determinable relationship.

Output signal S_{to} is fed to spectrum analyzer 44 and data relating to the time, frequency and amplitude of the signal S_{to} is periodically (say every 15 seconds) logged by logging computer 46. This data is transmitted to control centre 48.

From the data, the control centre 48 determines and/or tracks the peak modal cancellation frequency 44.6 to 44.1 and from the aforementioned relationship computes data relating to the resulting average sag 18 and rate of sag change for the line, in real time.

The transmission line can then be calibrated into sections via measurements on site and limiting or problem sections can be identified. With the information of the calibrated transmission line and the aforementioned real time average sag of the whole line, the sag of each span can be computed with a certain probability of error.

The method according to the invention of controlling sag or ampacity of a transmission line is illustrated in figure 4. A safe, conservative or static ampacity rating 50, which will hold for all conditions, is determined

according to the known conservative methods referred to in the introduction of this specification. Furthermore, a maximum dynamic ampacity rating 52 is also determined.

By utilizing the aforementioned data relating to real time sag 18 and rate of sag change, the line 10 may be operated in a region towards maximum ampacity rating 52 as shown at 54. A real time warning system based on the aforementioned real time sag, rate of sag change and maximum allowable sag may be used to ensure that the line is operated safely.

It will be appreciated that there are many variations in detail on the method and system according to the invention without departing from the scope and spirit of this disclosure.

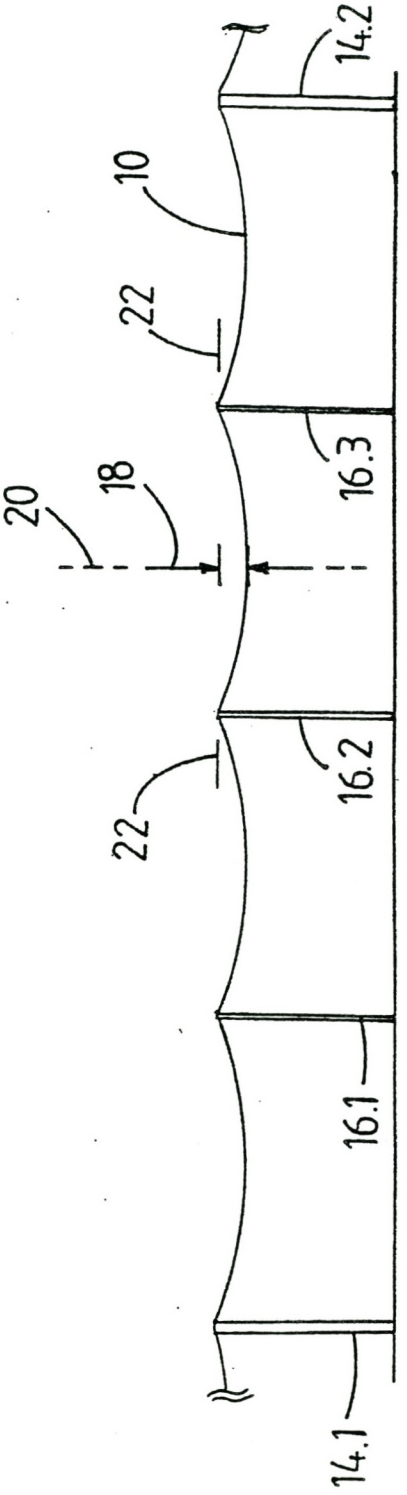

FIGURE 1

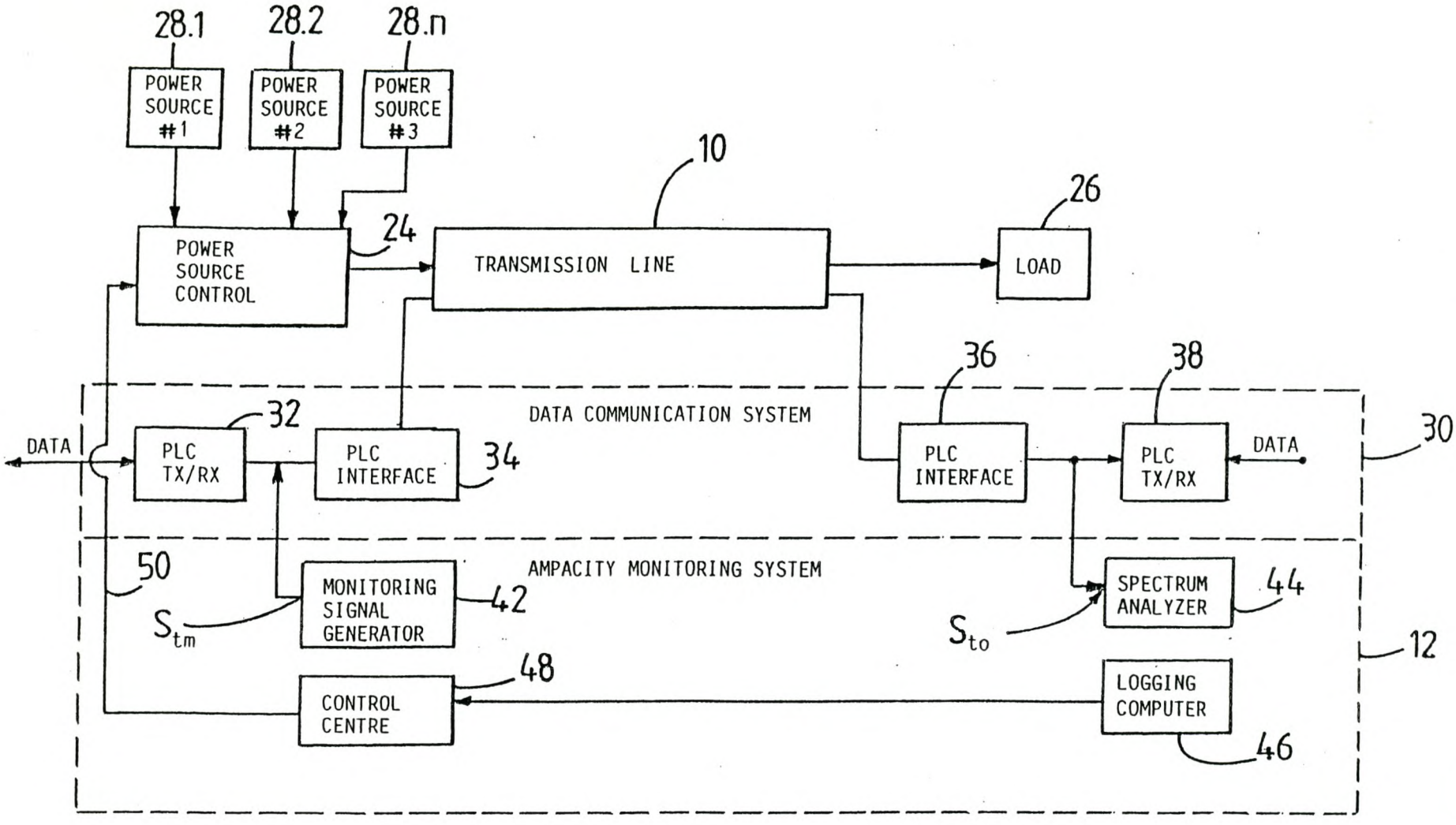

FIGURE 2

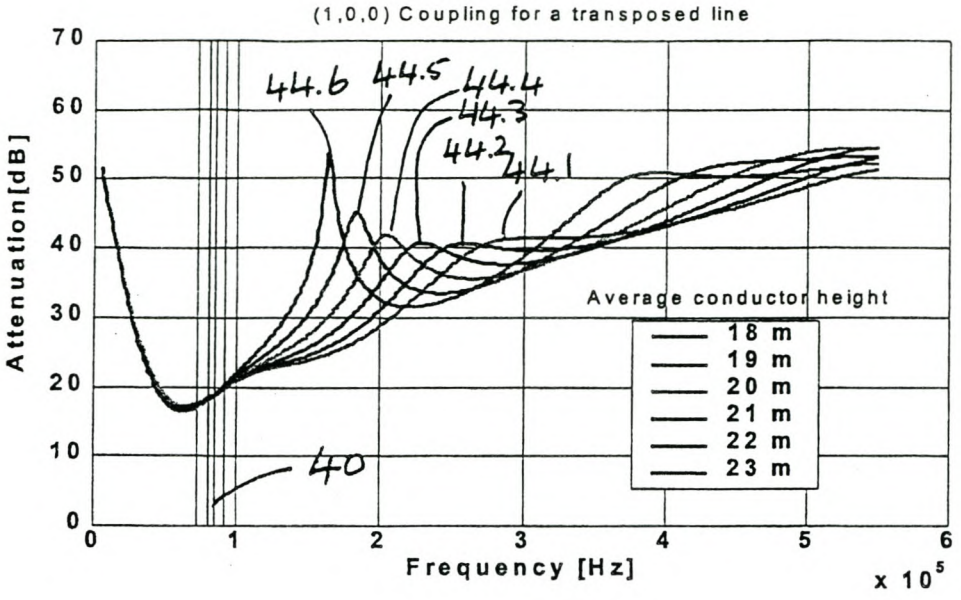

Figure 3

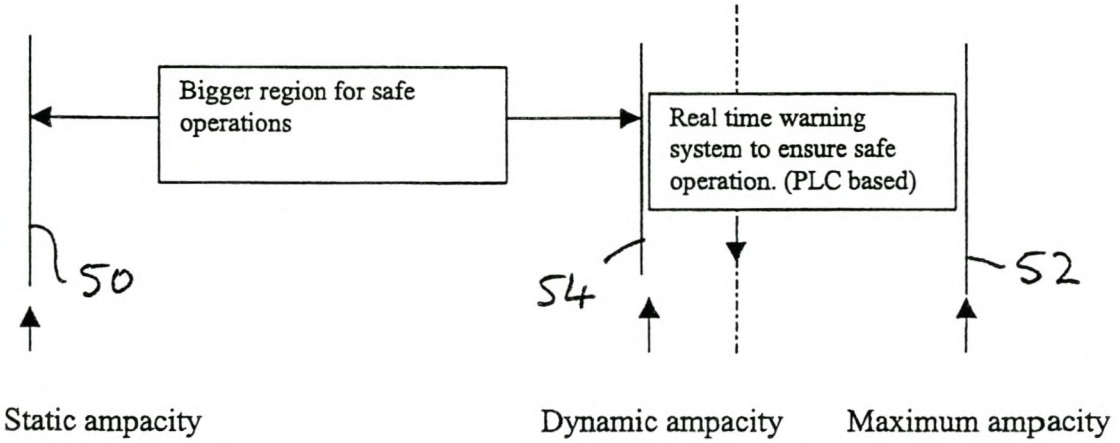

Figure 4

Appendix B

Field measurements

B.1 Installation of the additional symmetrical hybrid on 18 February 2001

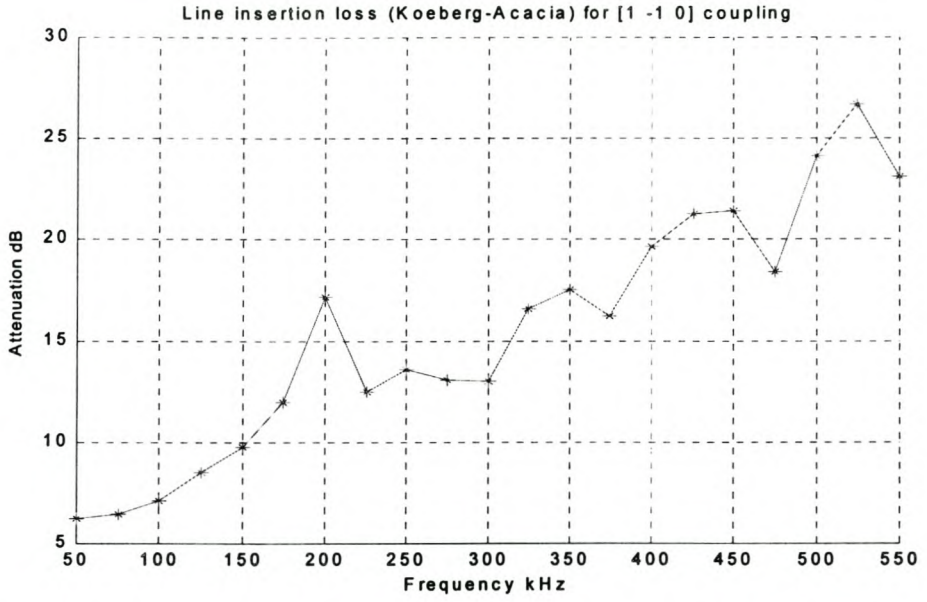

Figure B.1 Attenuation of the transmission line (standard differential coupling between centre and outer –phase).

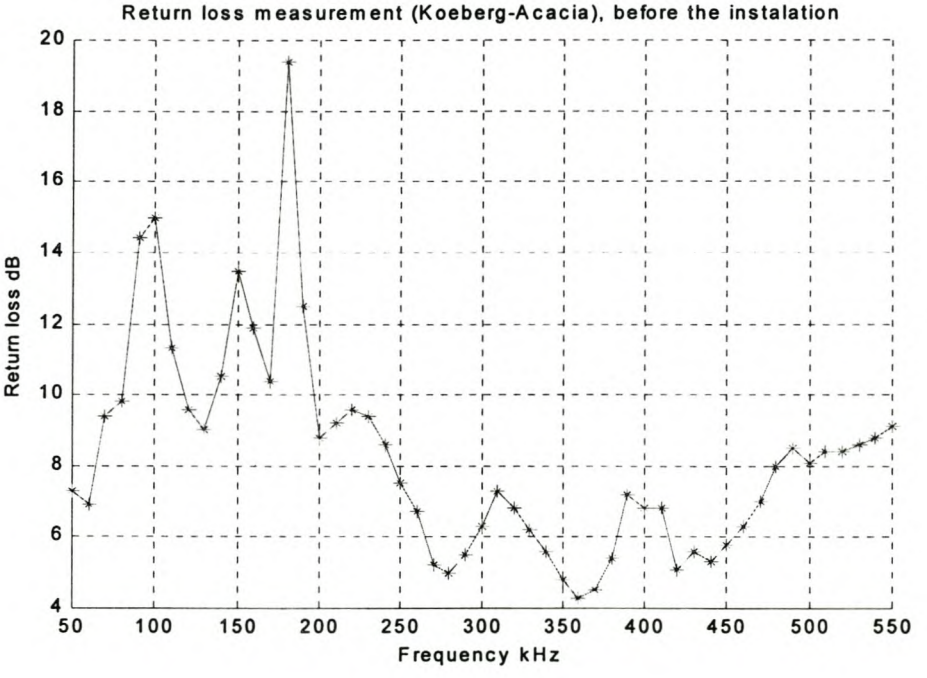

Figure B.2 Return loss for the standard coupling configuration(1,-1,0).

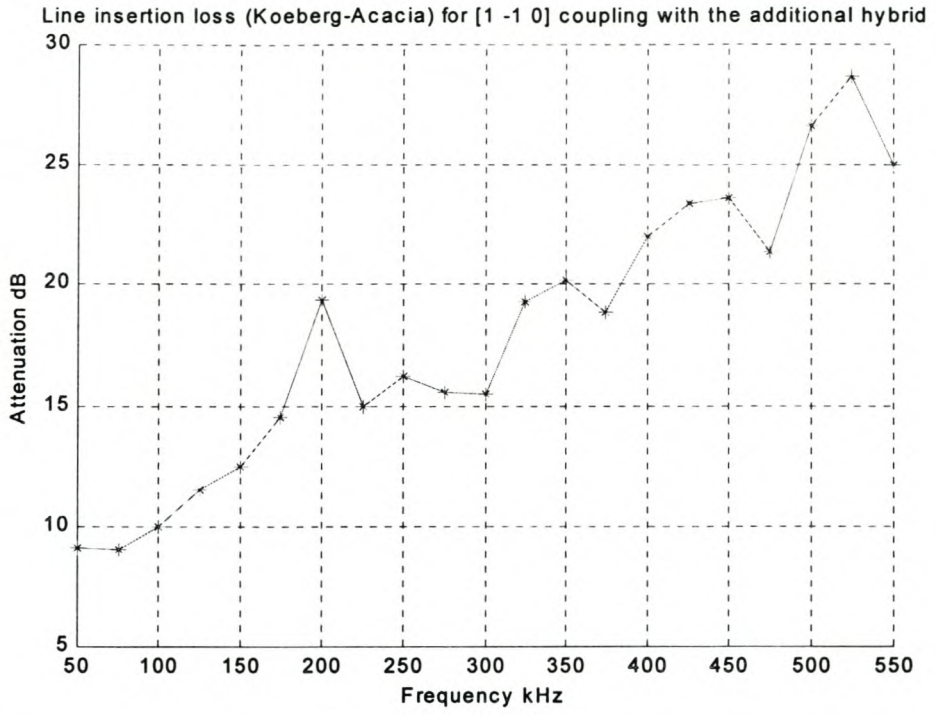

Figure B.3 Attenuation of the standard coupling configuration after the installation of the symmetrical hybrid.

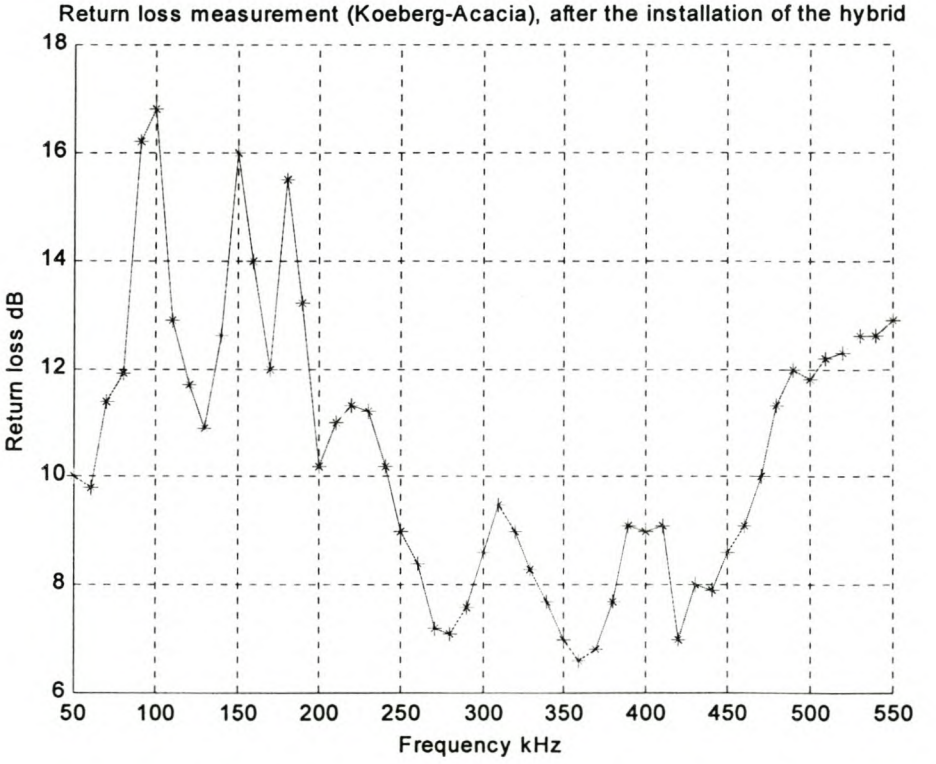

Figure B.4 Return loss for the standard coupling configuration with the additional hybrid installed.

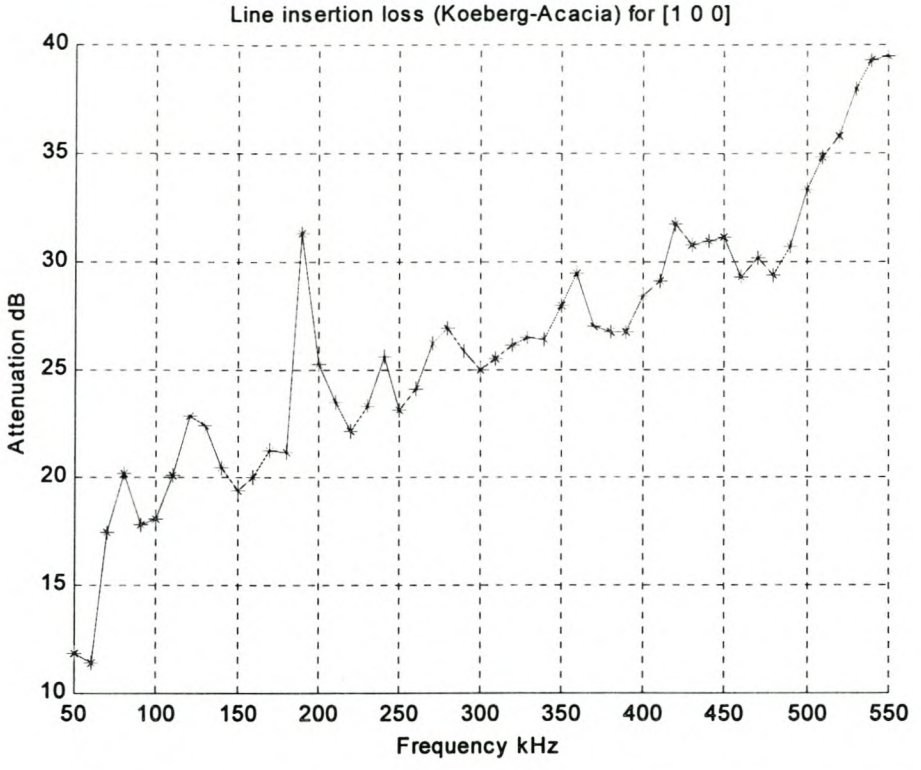

Figure B.5 Insertion-loss for the (1,0,0,) coupling on the outer phase.

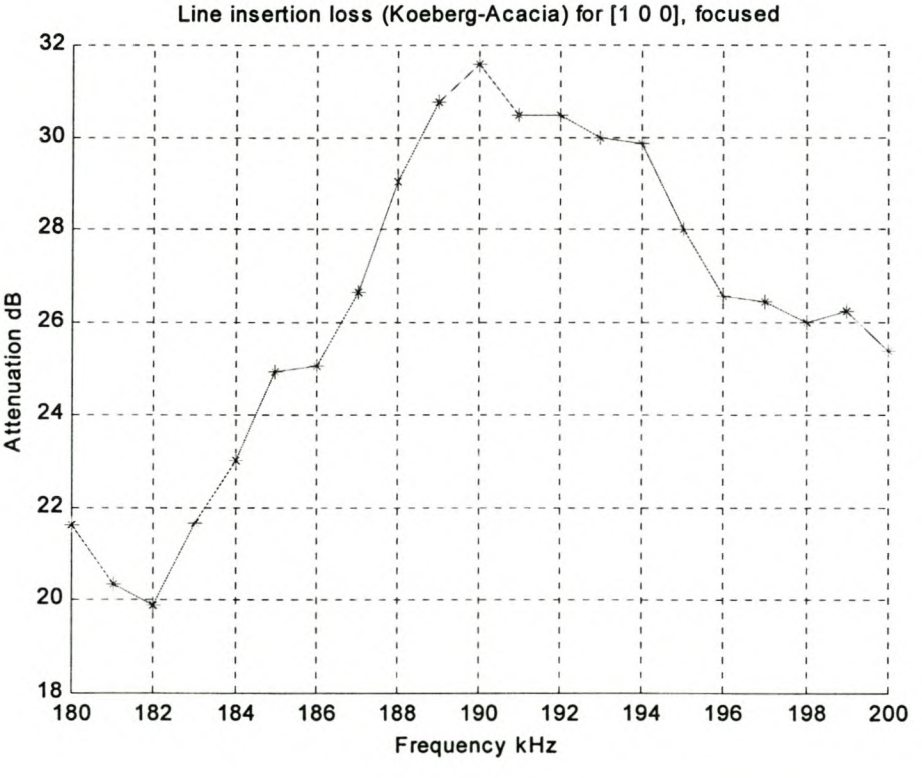

Figure B.6 Focused measurement [180 – 200 kHz] of the insertion-loss for the (1,0,0) coupling on the outer phase.

Figure B.7 Return loss measured at the additional port (of the experiment).

B.2 Measurements while the system was operative (installation of the logging device) on 19 March 2001

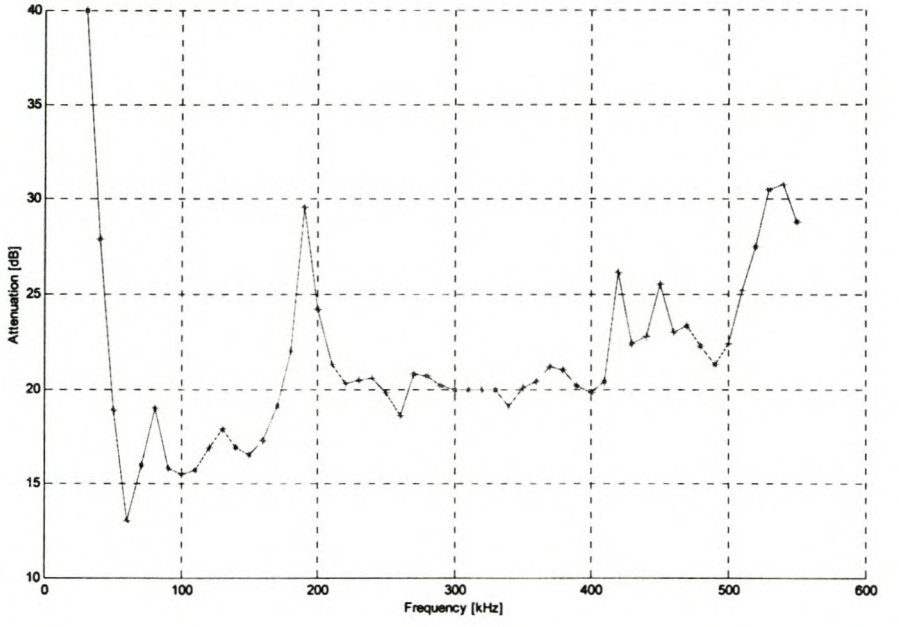

Figure B.8 Attenuation of an outer phase (1,0,0) coupling configuration

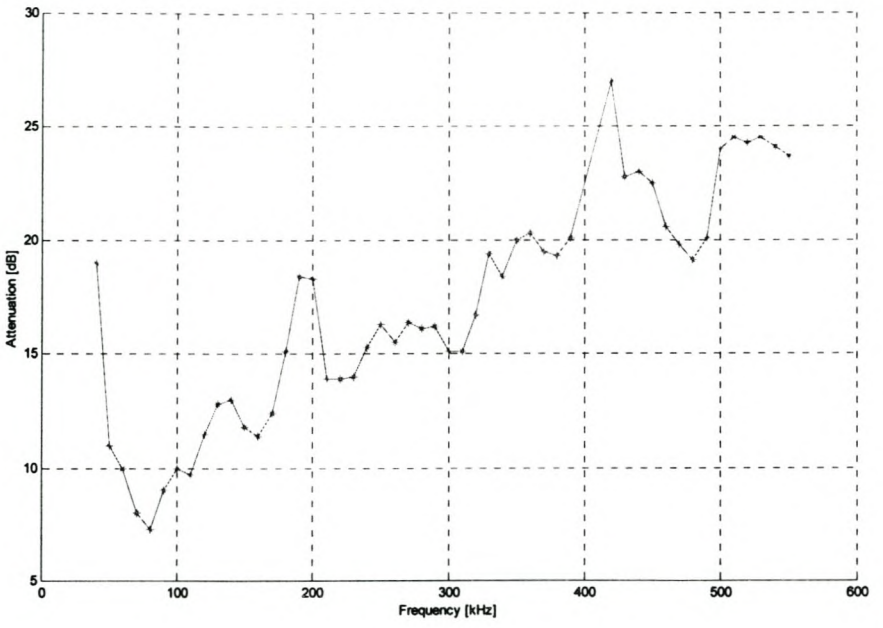

Figure B.9 Attenuation of centre phase coupling (0,1,0) configuration.

B.3 Measurements after new line trap tuning units were installed on 23 June 2001

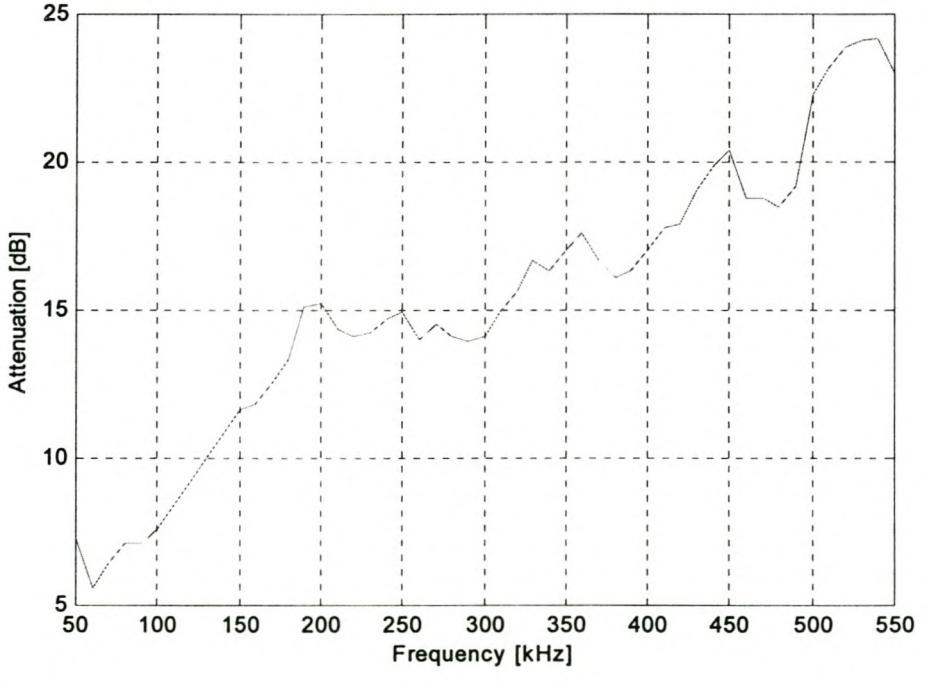

Figure B.10 Attenuation for the standard coupling configuration (1,-1,0) without the experiment (line traps earthed at station side)

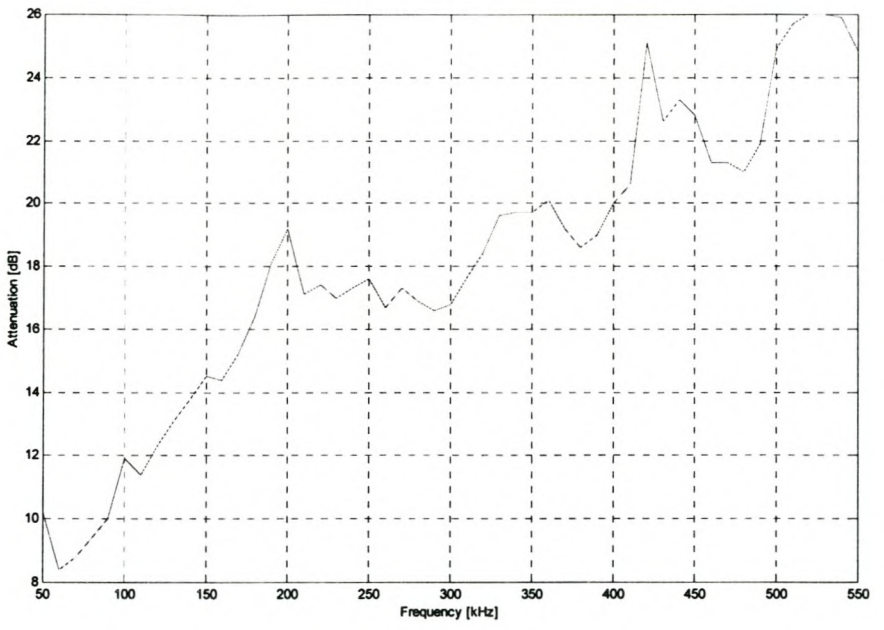

Figure B.11 Attenuation for the non standard coupling configuration (1/2,-1,0) with the experiment (line traps earthed at station side)

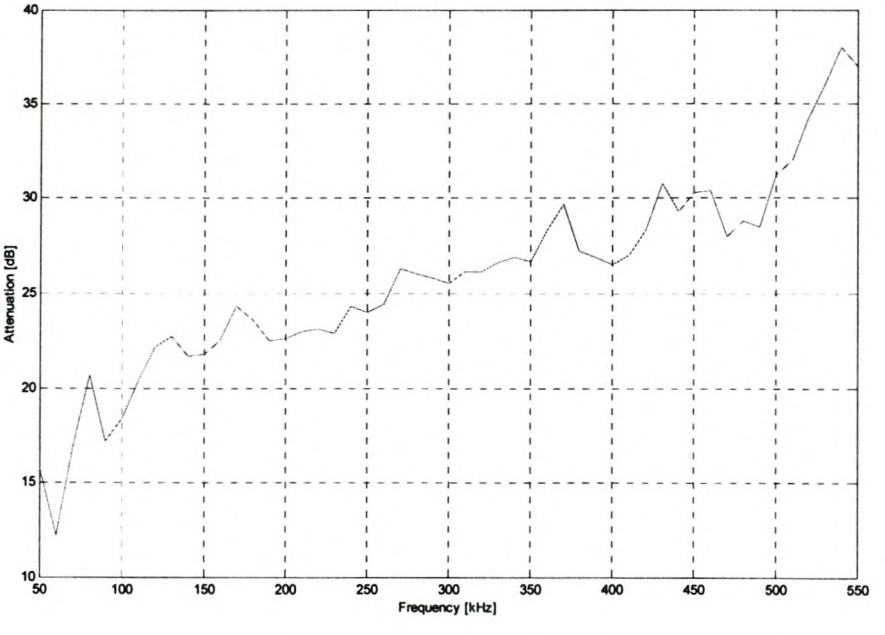

Figure B.12 Attenuation of the outer phase coupling (1,0,0) while the transmission line is earthed (measured at the additional port for the newly installed hybrid)

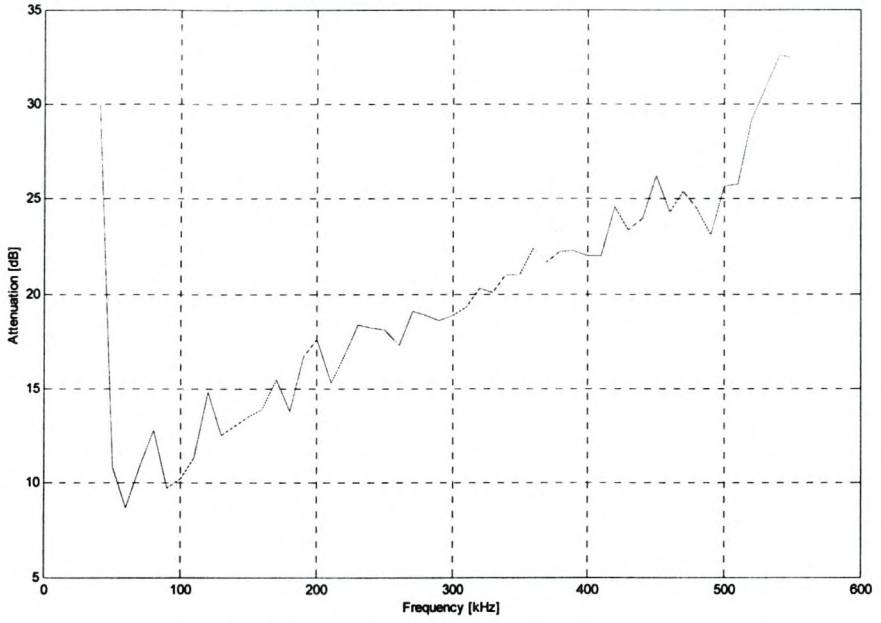

Figure B.13 Attenuation of the outer phase coupling (1,0,0) while the transmission operative (measured at the outer phase coaxial cable.

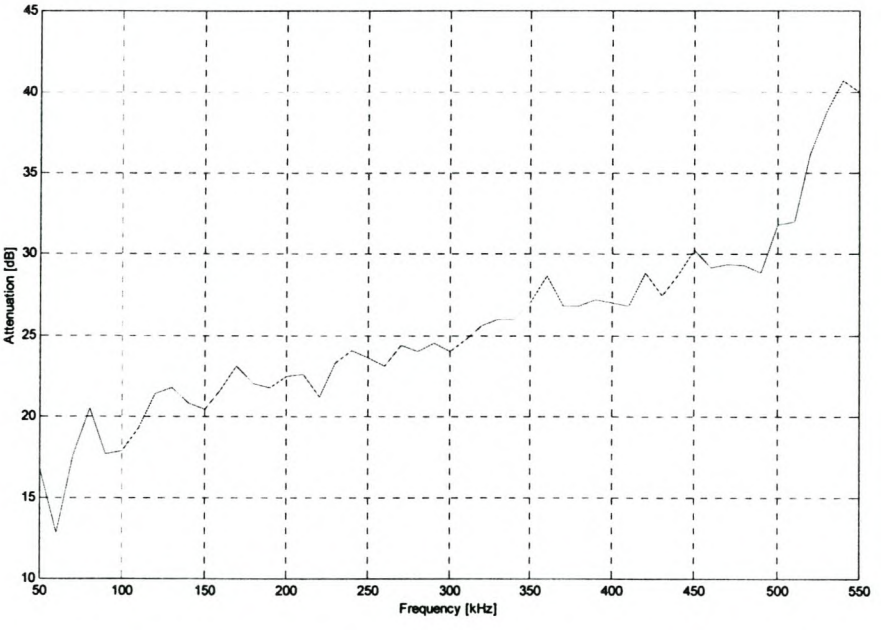

Figure B.14 Attenuation of the outer phase coupling (1,0,0) while the transmission was operative (measured at the additional port of the newly installed hybrid).